TECHNISCHE UNIVERSITÄT WIEN

Many-body feedback cooling

Particle manipulation through far-field wavefront shaping

A thesis presented for the degree of
Master of Science

under supervision of

Univ.Prof. Dr.techn. Stefan Rotter
& **Dr. Nicolas Bachelard**
Institute for Theoretical Physics, E136
TU Wien

by

Markus Kaczvinszki
01425090
066 461 Masterstudium Technische Physik

August 29, 2020

Abstract

In this thesis a new way of cooling dielectric particles with optical forces will be presented. Without tracking particle positions, the collective motion inside a system gets monitored from the far-field by measuring the time evolution of the system's scattering matrix. This information alone enables us to shape the input field, so that its interaction with the particles counteracts or enhances their motion optimally.

We formulate an underlying theory based on a scalar field approximation of the electromagnetic field. The particle positions serve as an optical potential for the field and resulting field configurations generate forces upon the particles in the direction of higher field intensity. The macroscopic kinetic energy change of the particle system is connected with changes in the scattering matrix, encoded in a new linear operator, which provides optimal cooling states through solving a simple eigenvalue problem.

We test the field-matter interactions in simulations using a 2D-multimode waveguide. The influence of randomized as well as of constant input fields on the particle motion will be compared to the strongly damped motion, induced by the optimal cooling states. We characterize our cooling procedure by increasing the particle number, starting with a single particle. We confirm the robustness of our method by testing it on a ten particle system for challenging scenarios, like incomplete far-field information, absorption and complex particle geometries. In addition, simulations with realistic values are made and results are compared with existing cooling approaches in the mesoscopic regime.

Acknowledgements

I want to thank Prof. Dr. Stefan Rotter and Dr. Nicolas Bachelard for entrusting this interesting topic to me and their guidance during the elaboration. I thank Dipl.-Ing. Matthias Kühmayer and Dipl.-Ing. Michael Horodynski for their support. Matthias helped a lot with technical problems, he gave me an introduction to NGSolve and the Ubuntu-terminal. Michael was always up for discussions and open for questions. Furthermore, I want to thank Jakob Hüpfl, he had the initial idea of using the scattering matrix for cooling and already extended the Python code to enable time evolutions of circular particles. More thanks go to my parents for supporting my scientific journey and my younger brother for spell-checking this thesis.

Contents

Introduction

Cooling of particle systems is one of the fundamental tasks of thermodynamics. At small temperatures quantum mechanics starts to play a role, leading to new and sometimes unexpected behaviour of matter. The study of quantum mechanics of macroscopic objects, as well as the study of stochastic processes at small energy (non-equilibrium thermodynamics) are expected to yield new knowledge in physics [1].

While laser cooling of atoms enables the generation of Bose-Einstein condensates [2], there is no comparable useful cooling method in the field of mesoscopic particles. The existing approaches of levitated optomechanics focus primarily on trapping one dielectric particle, in order to use feedback schemes or resonance conditions to slow it down [1][3]. By manipulating objects locally, such current approaches are mainly restricted to single particles, as the multiplexing of traps forms optical bounds hindering the cooling of individual elements in close proximity [4][5].

Yet essential information on the interaction between light fields and matter is contained in the far-field. In complex media the scattering matrix, which connects incoming and outgoing wave states, includes such information. Using wavefront shaping one then can amplify some aspects of the field-matter interaction, with the help of so-called Generalised Wigner-Smith operators [6]. This enables for example micro-manipulation of particles in stationary systems [7].

In this thesis we generalize this concept to dynamic systems, giving rise to the possibility to influence the kinetic energy of a particle ensemble at will and, as such, to iteratively cool multiple dielectric particles. The collective motion inside the system is captured through the changes of the scattering matrix with time. Based on this far-field information our method yields the (differential) macroscopic kinetic energy change an arbitrary asymptotic far-field input applies on the particle system. In particular, here we find optimal cooling fields by solving a simple eigenvalue problem and by injecting them into the system, these fields provide iterative cooling of multiple degrees of freedom.

Based on a semi-classical description we put forward a theoretical framework and verify it in numerical simulations. We study non-relativistic motion of particles under the influence of randomized fields as well as of constant field inputs and compare it to the strongly damped motion, which the optimal cooling fields apply. Moreover, we simulate our light cooling procedure in realistic conditions and test its robustness in challenging scenarios, like incomplete far-field information, absorption and complex particle geometries.

Chapter 1

Field-Matter-Equations

In this chapter we restate the fundamental relations for the electric field and its interaction with dielectric matter. This knowledge of the underlying physics is required, before we can try to optimize the field for a micro-manipulation of particles. We simplify Maxwell's equations to a single scalar field equation, the Helmholtz equation. This simplification allows us to take a look on the force and energy density of the electromagnetic field for a system of dielectric particles, in order to formulate Newton's equations (equations of motion) for these particles.

1.1 Maxwell's equations for dielectric particles

Our starting points are Maxwell's equations for a system containing dielectric materials (scattering particles). An electric field can be generated from the outside of our system and injected through the boundary regions. However, we consider, that there are no free moving charges inside the system. Only the (induced) polarization charges, bounded in the dielectrica, are able to interact and change the electric field. The equations read

$$\partial_i D^i = 0, \tag{1.1}$$
$$\partial_i B^i = 0, \tag{1.2}$$
$$\epsilon_{ijk}\partial_j E^k + \partial_t B^i = 0, \tag{1.3}$$
$$\epsilon_{ijk}\partial_j B^k - \mu_0 \partial_t D^i = 0, \tag{1.4}$$

for linear matter with

$$D^i = \epsilon E^i = \epsilon_0 \epsilon_R E^i, \quad H^i = \frac{1}{\mu} B^i = \frac{1}{\mu_0} B^i. \tag{1.5}$$

As a short remembrance for the used index-notation, ϵ_{ijk} is the Levi-Civita-Symbol (for the cross product), ∂_j the position-derivative (vector) and ∂_t the time-derivative operator.

Furthermore, here E^i is the electric field, B^i the magnetic field, ϵ_0 the dielectric constant, ϵ_R the dielectric function (relative permittivity) of our system and μ_0 is the vacuum permeability. We restrict ourselves to dielectric particles with constant refractive index n_s, leading to a piecewise constant dielectric function (one in vacuum and constant in matter). Nevertheless, a procedure with magnetic particles is also possible and will be presented shortly in the appendix A.1.

1.2 Helmholtz equation

For special conditions we derive a simplified equation for the electric field from Maxwell's equations. The resulting Helmholtz equation [8] is a simple wave equation, which can be derived using the following steps and assumptions.

We build the rotor of equation (1.3) and insert the time derivative of eq. (1.4) to get

$$\delta_{ij}^{lm}\partial_j\partial_l E^m + \mu_0\partial_t\partial_t D^i = 0, \tag{1.6}$$

$$\partial_j\partial_i E^j - \partial_j\partial_j E^i + \mu_0\partial_t^2 D^i = 0. \tag{1.7}$$

An expression for the divergence of the E-field is included in eq. (1.1),

$$\partial_j E^j = -\partial_j \ln(\epsilon) E^j. \tag{1.8}$$

Equation (1.7) is therefore writeable as

$$-\partial_i(\partial_j \ln(\epsilon) E^j) - \partial_j\partial_j E^i + \mu_0\partial_t^2(\epsilon E^i) = 0, \tag{1.9}$$

$$\left[-\partial_i\partial_j \ln(\epsilon_R) - \partial_j \ln(\epsilon_R)\partial_i - \partial_m\partial_m\delta_{ij} + \frac{1}{c^2}\left(\partial_t^2\epsilon_R + 2\partial_t\epsilon_R\partial_t + \epsilon_R\partial_t^2\right)\delta_{ij}\right] E^j = 0. \tag{1.10}$$

We want to strongly simplify this equation by making further assumptions. We consider, that the time-dependence of the field is well described by a harmonic oscillation (i.e. nearly constant frequency, quasi-static behaviour). Furthermore the polarisation of the field shall play no role, thus we consider a 2D-like model, where only the transverse electric field is important. Such a model is for example valid in a thin waveguide (where one of its dimensions is much smaller than the others, this scenario will also be used for simulations later).

The electric field shall point in z-direction. We include the harmonic oscillation using the complex notation. Then the physical field is the real part of our complex E-vector,

$$E^i = \psi e^{-iwt} e_z^i, \tag{1.11}$$

where w is the oscillation frequency in radians and e_z^i is the unit-vector in z-direction.

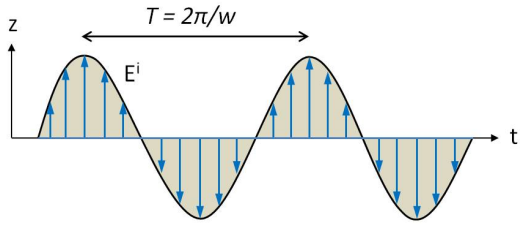

(a) Linear polarized E-field in z-direction for a harmonic oscillation.

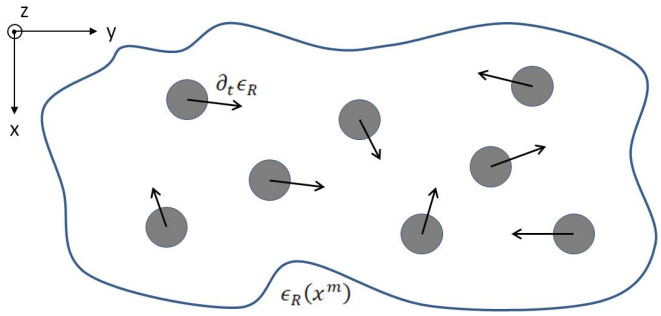

(b) Scattering landscape, defined by the piecewise-constant dielectric function ϵ_R.

Figure 1.1: System described by the Helmholtz equation. For stationary conditions the E-field follows a harmonic oscillation and the particles do not move. A slow movement of particles $\partial_t \epsilon_R$, leads to changes in E^i, that are only significant at a timescale $\Delta t \gg 2\pi/w$.

The dielectric function shall not change in E-field direction,

$$\partial_j \ln(\epsilon) E^j = \partial_z \ln(\epsilon(x,y))\psi = 0, \tag{1.12}$$

therefore the E-field is parallel to all boundaries and ψ is a continuous function. The resulting modified Helmholtz-equation is

$$\left[\Delta + \epsilon_R k^2\right] \psi = \left(\frac{1}{c^2} \partial_t^2 \epsilon_R - 2i \partial_t \epsilon_R \frac{k}{c} \right) \psi, \tag{1.13}$$

with $w = kc$, the vacuum wavenumber k, speed of light c and the Laplace-operator Δ.

The right side of eq. (1.13) can be neglected, if the movement of the dielectric particles is small. Correspondingly, we assume that the particle velocities have to be much smaller than the speed of light. Since the dielectric function is non-continuous, such a description might only be reasonable for a finite area. The stationary, scalar Helmholtz equation describes the field amplitude and reads

$$\left[\Delta + \epsilon_R k^2\right] \psi = 0. \tag{1.14}$$

The particles (in the otherwise empty space) modulate the scattering landscape $U = \epsilon_R k^2$, see figure 1.1. Regarding the field ψ, the scattering landscape acts like a (non-continuous) potential. In the case of moving particles the dielectric function $\epsilon_R = \epsilon_R(x^m, x_s^m(t))$ is time-dependent and the Helmholtz equation still holds for quasi-stationary conditions. That means the field configuration adjusts itself nearly instantaneously to the change of the dielectric function, so that the stationary Helmholtz equation can be solved at any given point in time. Here x^m are the global coordinates of our system and x_s^m describes the position of the particles.

Note that an absorption of the field inside matter can be included through a non-vanishing imaginary part of ϵ_R (exponential decrease of the amplitude). However, since absorption reduces the effectiveness of our cooling method strongly, it will be neglected for most parts of this work. In addition, it is common to describe eq. (1.14) using the refractive index n, as defined as $\epsilon_R = n^2$. In this context, the Helmholtz equation is a wave equation, with a position-dependent wavenumber $k_{\text{mat}} = nk$ (in matter the speed of light is reduced $c_{\text{mat}} = c/n$).

The B-field can be calculated easily from the electric field using eq. (1.3) and its harmonic oscillation in time,

$$B^i = -\frac{i}{w}\epsilon_{ijk}\partial_j E^k. \tag{1.15}$$

The physical magnetic field is once again the real part of our complex B-vector. As it is characterized by the imaginary part of E^i, the complex-valued scalar field ψ inherits the whole static electromagnetism of our simplified system.

1.3 Force and energy density of the EM-field

By the force and energy density of the electromagnetic field we simply understand the amount of force or energy the field can generate on a charge at any given point in space. While a general equation can be formulated with tensors (Maxwell-stress-tensor and Energy-momentum-tensor) [9][10], we will evaluate the correct relations for our case from the fundamental Lorentz-force formula.

We assume, that the force on a dielectric is generated by the force of the electric field, applied on the polarisation-charges inside the neutral particles. Besides collisions of scatterers the Lorentz-force acts on the particles,

$$F^i = q(E^i + \epsilon_{ijk}v^j B^k). \tag{1.16}$$

At a local examination (per volume) the Lorentz-force-density reads

$$f^i = \rho E^i + \epsilon_{ijk}j^j B^k. \tag{1.17}$$

We split the charge density ρ and the current flux density j^i as usual in free and bounded parts. The force acting on the dielectrica (bounded charges) is therefore

$$\begin{aligned}
f^i &= -\partial_j P^j E^i + \epsilon_{ijk}\partial_t P^j B^k && (1.18)\\
&= -\chi\partial_j E^j E^i - \partial_j \chi E^j E^i + \chi\epsilon_{ijk}\partial_t E^j B^k + \partial_t\chi\epsilon_{ijk}E^j B^k && (1.19)\\
&= -\chi\partial_j E^j E^i - \partial_j \chi E^j E^i + \chi\partial_t\left(\epsilon_{ijk}E^j B^k\right) - \chi\epsilon_{ijk}E^j\partial_t B^k + \partial_t\chi\epsilon_{ijk}E^j B^k && (1.20)\\
&= -\partial_j\chi E^j E^i - \chi\partial_j\left(E^j E^i\right) + \frac{\chi}{2}\partial_i\left(E^j E^j\right) + \chi\partial_t\left(\epsilon_{ijk}E^j B^k\right) + \partial_t\chi\epsilon_{ijk}E^j B^k. && (1.21)
\end{aligned}$$

Here, $P^i = \epsilon_0 \chi E^i = \epsilon_0(\epsilon_R - 1)E^i$ is the polarisation (dipole density). During the derivation we used Maxwell's equations, see section 1.1, and we worked in units of ϵ_0. Since the susceptibility χ is piecewise constant, we can make further simplifications for a finite volume (χ behaves like a Heaviside function $H(x^m - x_s^m)$). We integrate over the scattering area (area that contains the particles), and see that the first two terms erase each other in this context (see also appendix A.3),

$$\int_M -\partial_j \chi E^j E^i d^3x = \int_M \chi \partial_j \left(E^j E^i\right) d^3x. \tag{1.22}$$

Furthermore, for our quasi-stationary conditions the terms with a time derivative can be safely neglected. For example with the usage of eq. (1.15), the last term in eq. (1.21) (with the Poynting-vector $S^i = \epsilon_{ijk} E^j B^k / \mu_0$) is proportional to v/c, where v is the velocity of the according particle. Thus the force density applied on the scatterers is given by a typical gradient field (characterized through E^2),

$$f^i = \frac{\chi}{2} \partial_i \left(E^j E^j\right) = -\frac{1}{2} \partial_i \chi E^j E^j = \frac{1}{2} \frac{\partial \epsilon_R}{\partial x_s^i} E^j E^j. \tag{1.23}$$

The gradient ∂_i refers to the global coordinates x^i describing space, x_s^i are the time dependent coordinates of the particles. Figure 1.2a shows the action of f^i on the particles.

We are not interested in the oscillation of the dielectrica, because of the pure oscillation of the E-field. Therefore we build the average value over an oscillation period $\tau = 2\pi/\omega$ (comparable to the description in ref. [10]). Following the complex notation, we note the physical E-field as the real part of our complex E-vector, $E^i = \psi e^{-iwt} e_z^i$.

$$\langle E^2 \rangle_\tau = \frac{1}{\tau} \int_t^{t+\tau} \Re(E^i) \Re(E^i) dt' = \frac{1}{2} |\psi|^2. \tag{1.24}$$

Therefore the mean force (-density) acting on the dielectric particles reads (in SI units)

$$\langle f^i \rangle_\tau \approx \frac{\epsilon_0}{4} (\epsilon_R - 1) \partial_i |\psi|^2 = \frac{\epsilon_0}{4} \frac{\partial \epsilon_R}{\partial x_s^i} |\psi|^2. \tag{1.25}$$

This force will lead to a change of the kinetic energy of the system E_{kin}, which is simply the sum of the kinetic energy of all particles. Since the force of the static field changes only because of the movement of the scatterers, the logical value for the local change in the field energy (energy density e_{kin}) is simply the velocity of the according scatterer times the force on the scatterer. By velocity we mean here a generalized one (the local velocity), including translation and rotation movement.

$$e_{\text{kin}} = f^i dx_s^i = f^i v^i dt, \tag{1.26}$$

$$\left\langle \frac{de_{\text{kin}}}{dt} \right\rangle_\tau = \frac{\epsilon_0}{4} \frac{\partial \epsilon_R}{\partial x_s^i} |\psi|^2 \frac{dx_s^i}{dt} = \frac{\epsilon_0}{4} \frac{d\epsilon_R}{dt} |\psi|^2. \tag{1.27}$$

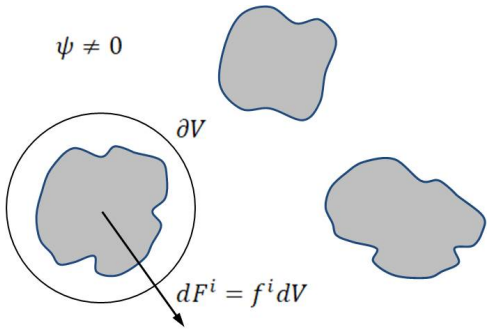

(a) Effects of the field force density f^i. Integration over an area, that contains the respective particle, gives the resulting force F^i on it.

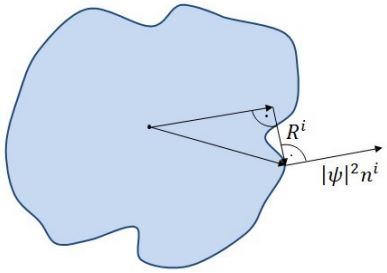

(b) Torque generation on the particle. Normal forces $|\psi|^2 n^i$ on boundary sections, with a non-vanishing lever R^i, contribute to a torque.

Figure 1.2: Interaction between field and particles. The resulting field configuration changes the movement of the enclosed particles.

For our simple case, the particle forces are directed to areas of higher field intensity $|\psi|^2$. One should keep in mind, that the results of this section are only valid for our simplified conditions, if the electric polarisation in the material is well described in the dipole approximation. Otherwise, for example if the electric field gradient is very high, one needs to include higher multipole moments. Furthermore, the polarisation is normally frequency-dependent and the direction of the resulting force also (for some cases particles will experience a repulsive force, leading to an additional minus sign) [11].

1.4 Newton's Equation - field forces

With the knowledge of the last section we can write down the equations of motion for the dielectric particles in the electric field. As mentioned before, we work in an adiabatic regime, thus we averaged over the periodic field oscillations. The movement of an arbitrarily shaped particle can be split into translation and rotation. We calculate the effective force and torque acting on the particles, using the electric force-density f^i, eq. (1.25).

To get the resulting force F^i, we integrate over the particle volume V,

$$F^i = \int_V f^i d^3x = \frac{\epsilon_0}{4}(\epsilon_s - 1) \int_V \partial_i |\psi|^2 d^3x = \frac{\epsilon_0}{4}(\epsilon_s - 1) \int_{\partial V} |\psi|^2 dA^i. \tag{1.28}$$

Only an integral over the particle surface remains, where $dA^i = n^i dA$, with the surface normal vector n^i, ϵ_s is the constant permittivity of the particle. In order to receive the torque M^i, we take the cross-product between lever and force density,

$$M^i = \int_V \epsilon_{ijk} R_j f^k d^3x = \frac{\epsilon_0}{4}(\epsilon_s - 1) \int_V \epsilon_{ijk} R_j \partial_k |\psi^2| d^3x = \frac{\epsilon_0}{4}(\epsilon_s - 1) \int_{\partial V} \epsilon_{ijk} R_j |\psi^2| dA^k. \tag{1.29}$$

The remaining integral goes once again over the particle boundary. As usual for a torque, the cross product connects the surface normal force $|\psi|^2 n^i$ with the lever R^i, see figure 1.2b. The lever is the part of the distance from the center of mass to the boundary (i.e. the respective acting point of the force), that is normal to n^i.

The equations of motion for a dielectric particle in the electric field, in our case represented by the scalar field ψ, read

$$v^i = \frac{dx_s^i}{dt}, \quad m\frac{dv^i}{dt} = \frac{\epsilon_0}{4}(\epsilon_s - 1)\int_{\partial V} |\psi|^2 dA^i, \tag{1.30}$$

$$\omega^i = \frac{d\varphi_s^i}{dt}, \quad I\frac{d\omega^i}{dt} = \frac{\epsilon_0}{4}(\epsilon_s - 1)\int_{\partial V} \epsilon_{ijk} R_j |\psi^2| dA^k, \tag{1.31}$$

with position x_s^i, velocity v^i, angular orientation φ_s^i, angular speed ω^i, mass m and moment of inertia I of the particle. While eq. (1.30) describes the translation movement, eq. (1.31) denotes the evolution of the angular orientation and the angular momentum $L^i = I\omega^i$.

With the wave equation (1.14) for ψ we have a closed system of equations, describing the simplified field-matter-interaction. Besides that, collisions between particles can naturally also occur. Since collisions between arbitrarily shaped particles are difficult to compute, we either choose complex shaped particles and neglect collisions (particles placed far from each other) or we simulate spheres and include hard-body collisions.

In addition, one might include a simplified Brownian motion of the particles through friction. Then, besides the field force F^i, an additional friction force, proportional to the particle speed, is present. For spherical particles and friction we compute the acceleration as

$$\frac{dv^i}{dt} = \frac{F^i}{m} - \gamma v^i, \tag{1.32}$$

where γ is the friction constant. Thereby we neglect a possible minor heating rate through stochastic forces (Langevin force, white noise).

Chapter 2

Scattering problem and Generalised Wigner-Smith operator

In this chapter we take a look on our system in its entirety. While the last chapter's equations describe the differential formalism (microscopic behaviour), we now state relations for the macroscopic behaviour. We define a scattering problem and use the knowledge of input and output fields, to draw conclusions about the scattering particles. Thereby we are able to connect the system's internal changes with changes of the output field, leading to the so-called Generalised Wigner-Smith (GWS) operator [7][12]. This operator builds the fundament for an optimal micro-manipulation of particles, using wavefront shaping.

2.1 Scattering problem

We assume a typical scattering problem. We inject an electric field with fixed wavenumber k into the system from an asymptotic region (channel), so that this input field propagates like a plane wave (or a superposition of plane waves) in direction of the scatterers. After the interaction in the scattering area (with the dielectric particles), we measure the asymptotic output field. The shape of the scattering region M can in principle be arbitrary, as long the scalar Helmholtz equation holds. However for our purpose we need to have (nearly) complete access to the output field. Such a scenario is visualised in figure 2.1.

We define the scattering matrix S, which connects the incoming field with the outgoing field, in a convenient way (S contains basically all accessible far-field information of our system) [8]. For a rectangular channel D (cuboid with Dirichlet boundary conditions) the input field ψ_{in}, for instance for an input in y-direction, can be written with regard to the waveguide mode basis, as

$$\psi_{\text{in}} = \sum_n c_{\text{in}}^n \chi_n(x,z) \frac{e^{ik_{y,n}y}}{\sqrt{k_{y,n}}}. \tag{2.1}$$

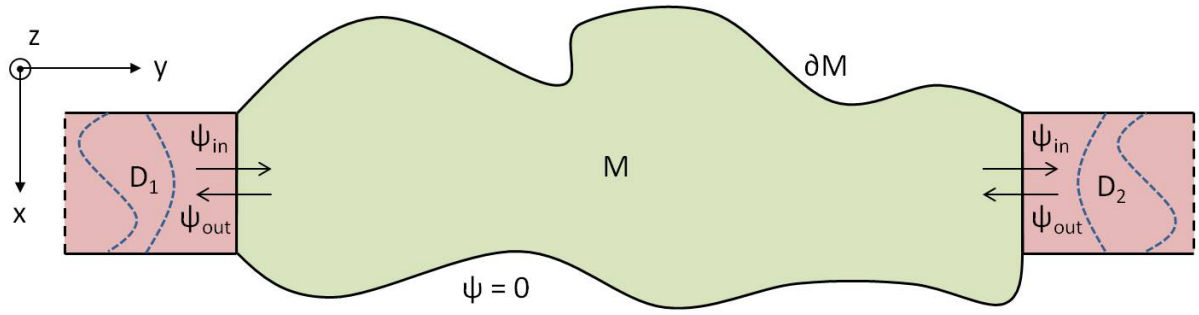

Figure 2.1: Schematic of a generic scattering problem. Trough the channels D_i a field ψ_{in} can be injected into the scattering area M, where the particles are contained. After interaction with the scatterers the output field ψ_{out} can be measured again in the distant channels D_i, where the field consists of plane waves. (The blue lines symbolise the cross-sectional eigenfunctions χ_n.) At all other places of the boundary ∂M the field shall be zero.

The according output field ψ_{out}, regarding the same channel, is

$$\psi_{\text{out}} = \sum_n c^n_{\text{out}} \chi_n(x,z) \frac{e^{-ik_{y,n}y}}{\sqrt{k_{y,n}}}. \tag{2.2}$$

The factor $1/\sqrt{k_{y,n}}$ is included regarding flux normalization, so that the input/output flux (see next section) depends solely on the coefficients c^n.

The transverse field in the asymptotic waveguides satisfies the wave equation (for vacuum conditions), thus for χ_n holds

$$[\partial_x^2 + \partial_z^2 + k^2 - k_{y,n}^2]\chi_n = 0, \tag{2.3}$$

with a chosen orthonormal condition over the channel cross-section A,

$$\int_A \chi_n^* \chi_m dx dz = \delta_{mn}. \tag{2.4}$$

The scattering matrix S, in this basis, shall simply connect the input coefficients c^n_{in} with the output coefficients c^n_{out}, in matrix-vector-notation,

$$\mathbf{c}_{\text{out}} = S\mathbf{c}_{\text{in}}. \tag{2.5}$$

For more than one channel the coefficient vector $\mathbf{c}$ sequentially includes the coefficient vectors of all channels. It is important, that S inherits as much information of the system as possible. Therefore we assume, that any part of the boundary of our scattering system is either connected to a channel or characterized by Dirichlet boundary conditions (i.e. vanishing field amplitude ψ). For the simplified scenario in our simulations, see section 3.3.

2.2 Flux conservation

We define a flux of the field ψ in analogy to the flux in quantum mechanics. For a quick derivation of the flux conservation one multiplies the Helmholtz equation (1.14) with ψ^* and integrates over the volume of the scattering system M. We evaluate the imaginary part and get after partial integration,

$$\frac{1}{2i}\int_M \partial_i \left[\psi^* \partial_i \psi - \psi \partial_i \psi^*\right] d^3x = \frac{1}{2i}\int_{\partial M} \psi^* \partial_i \psi - \psi \partial_i \psi^* dA^i = 0, \tag{2.6}$$

where ∂M denotes the boundary of the system. With respect to our scattering problem, see figure 2.1, this essentially equals to an integration over the channel cross-sections. Therefore it can be calculated with the field resulting in the channels $\psi = \psi_{\text{in}} + \psi_{\text{out}}$, leading to a relation for the coefficients,

$$\sum_n |c^n_{\text{out}}|^2 - |c^n_{\text{in}}|^2 = \mathbf{c}^\dagger_{\text{in}}(S^\dagger S - 1)\mathbf{c}_{\text{in}} = 0. \tag{2.7}$$

Here the sum over n indicates the sum over all basis coefficients regarding all channels D_n. One can see, in a system without losses, the scattering matrix is a unitary operator $S^{-1} = S^\dagger$. However, for a time dependent system this is only approximately the case, because the interaction between field and particles leads to internal gains or losses. For example, if we take eq. (1.13) instead of the stationary Helmholtz eq. (1.14), we get

$$\frac{1}{2i}\int_{\partial M} \psi^* \partial_i \psi - \psi \partial_i \psi^* dA^i = -\frac{2k}{c}\int_M \partial_t \epsilon_R |\psi|^2 d^3x, \tag{2.8}$$

$$\mathbf{c}^\dagger_{\text{in}}(S^\dagger S - 1)\mathbf{c}_{\text{in}} = -\frac{2k}{c}\int_M \partial_t \epsilon_R |\psi|^2 d^3x = -\frac{8k}{c\epsilon_0}\partial_t E_{\text{kin}}. \tag{2.9}$$

The flux into the system does not exactly equate to the outgoing flux. The according difference is proportional to the change of the kinetic energy of the system, eq. (1.27). It is normally very small, so that we can further assume that S is unitary for ideal conditions (in our adiabatic regime). In achievable scenarios these gains or losses will probably be overshadowed by other losses, like a restricted access to the output or absorption (information loss). Thankfully we found a more robust estimation of $\partial_t E_{\text{kin}}$, encoded in the change of the scattering matrix with time, see next section.

Now we want to connect the flux of ψ with a more seizable quantity, namely the electromagnetic energy-flux-density as represented by the Poynting vector S^i. With the equations for the electric and magnetic field (1.11) and (1.15), we obtain

$$S^i = \frac{1}{\mu_0}\epsilon_{ijk} E^j B^k = \frac{c\epsilon_0}{ik}[E^j \partial_i E^j - E^j \partial_j E^i]. \tag{2.10}$$

Averaging over the oscillation period $\tau = 2\pi/w$ and taking the complex notation of E^i and B^i into account, leads to

$$\langle S^i \rangle_\tau = \frac{1}{\tau} \int_t^{t+\tau} \frac{c\epsilon_0}{k} [\Re(E^j)\partial_i \Im(E^j) - \Re(E^j)\partial_j \Im(E^i)] dt' \tag{2.11}$$

$$= \frac{1}{4i} \frac{c\epsilon_0}{k} [(\psi^* \partial_i \psi - \psi \partial_i \psi^*) - (\psi^* \partial_z \psi - \psi \partial_z \psi^*) e_z^i]. \tag{2.12}$$

As usual no power will be transmitted in E-field direction. According to our 2D-like model, the E-vector shall be parallel to all boundaries (to avoid changes of its direction) and therefore the cross-section between system boundary and channel is needed to be normal to the z-direction (i.e. no channel output in E-field direction).

We integrate over the channel cross-section(s) A, in order to get the difference between input and output power P,

$$P_{\text{out}} - P_{\text{in}} = -\int_A \langle S^i \rangle_\tau dA^i = -\frac{c\epsilon_0}{k} \frac{1}{4i} \int_A (\psi^* \partial_i \psi - \psi \partial_i \psi^*) dA^i \tag{2.13}$$

$$= \frac{c\epsilon_0}{k} \frac{1}{4i} \int_{\partial M} (\psi^* \partial_i \psi - \psi \partial_i \psi^*) dA^i = \frac{c\epsilon_0}{2k} \mathbf{c}_{\text{in}}^\dagger (S^\dagger S - 1) \mathbf{c}_{\text{in}}, \tag{2.14}$$

where we considered, that the channel normal vector shows in the opposite direction as the surface normal vector of our system (regarding the cross-section area). The comparison with eq. (2.7) or rather (2.9) shows, that the flux conservation denotes in principle the conservation of energy. Some energy of the input field will be transferred to the particles or the other way around, however this amount is very small compared to the field energy.

2.3 Generalised Wigner-Smith relation

The GWS-intensity-relation (presented in the following) is the fundamental equation of our interest and makes micro-manipulation of dielectric particles based on the systems scattering matrix possible. A straight-forward derivation of it [12] is similar to the one of flux conservation and contains the following steps, here shown in detail (a different derivation is presented in ref. [7]).

We start by differentiating the Helmholtz equation with respect to an arbitrary system parameter α,

$$[\Delta + U] \frac{d\psi}{d\alpha} + \frac{dU}{d\alpha} \psi = 0, \quad U(\vec{r}) = \epsilon_R(\vec{r}) k^2. \tag{2.15}$$

We multiply with ψ^* and integrate over the volume of the system M (scattering area). After a partial integration we obtain

$$\int_M \partial_i\psi^*\partial_i\psi_\alpha d^3x = \int_{\partial M} \psi^*\partial_i\psi_\alpha dA^i + \int_M \psi^* U\psi_\alpha + \psi^* U_\alpha \psi d^3x, \tag{2.16}$$

with the short cuts $\psi_\alpha = \frac{d\psi}{d\alpha}$ and $U_\alpha = \frac{dU}{d\alpha}$.

Not to forget, besides its derivative, the Helmholtz equation still holds on its own, giving a second constraint. In order to get the left term in eq. (2.16), we multiply the Helmholtz equation with ψ^*_α, complex conjugate and integrate over M,

$$\frac{d\psi}{d\alpha}[\Delta + U^*]\psi^* = 0, \tag{2.17}$$

$$\int_M \partial_i\psi^*\partial_i\psi_\alpha d^3x = \int_{\partial M} \psi_\alpha\partial_i\psi^* dA^i + \int_M \psi_\alpha U^*\psi^* d^3x. \tag{2.18}$$

We insert eq. (2.16) into eq. (2.18) (subtraction), resulting in

$$\int_M \psi^* U_\alpha \psi d^3x = \int_{\partial M} \psi_\alpha\partial_i\psi^* - \psi^*\partial_i\psi_\alpha dA^i + \int_M \psi^*(U^* - U)\psi_\alpha d^3x. \tag{2.19}$$

For a real-valued dielectric function ϵ_R (lossless system) the scattering landscape U is also real and the last term is zero. The other term on the right side includes the derivatives of ψ and has a similar form like the flux, therefore we can easily evaluate it at the boundary ∂M (using the waveguide mode basis in the channels),

$$\int_M U_\alpha|\psi|^2 d^3x = \int_{\partial M} \psi_\alpha\partial_i\psi^* - \psi^*\partial_i\psi_\alpha dA^i \tag{2.20}$$

$$= 2i\sum_n c_n^* \frac{dc_n}{d\alpha} - (Sc)_n^* \frac{d(Sc)_n}{d\alpha} \tag{2.21}$$

$$= -2i\sum_n (Sc)_n^* \left(\frac{dS}{d\alpha}c\right)_n = -2i\mathbf{c}^\dagger S^\dagger \frac{dS}{d\alpha}\mathbf{c}. \tag{2.22}$$

The sum over n denotes the sum over all basis coefficients $c^n = c^n_{\text{in}}$ regarding all channels. It is remarkable, that for $S^\dagger S = 1$ the relation is also valid for α-dependent input coefficients. We define the Generalised Wigner-Smith operator [6][7] (short GWS-operator) with respect to the parameter α as

$$Q_\alpha := -iS^{-1}\frac{dS}{d\alpha}. \tag{2.23}$$

Therefore, for a (nearly) unitary scattering matrix, the GWS-intensity-relations reads

$$\mathbf{c}^\dagger Q_\alpha \mathbf{c} = \frac{1}{2}\int_M \frac{d}{d\alpha}\left(\epsilon_R k^2\right)|\psi|^2(\mathbf{c})d^3x. \tag{2.24}$$

Eq. (2.24) connects changes in the outgoing field with changes in the scattering system. Possible options for α are for example the frequency $w = ck$ [13][14], the position of particles [6] or even the refractive-index of the particles [7]. For our case the scatterers are moving and changes in their positions can be naturally described with time t as the parameter.

For $\alpha = t$ we obtain the main relation of our interest. According to eq. (1.27) we get

$$\mathbf{c}^\dagger Q_t \mathbf{c} = \frac{k^2}{2}\int_M \frac{d\epsilon_R}{dt}|\psi|^2 d^3x = \frac{2k^2}{\epsilon_0}\frac{d}{dt}E_{\text{kin}}. \tag{2.25}$$

The kinetic operator (or maybe GWS-time-operator) Q_t is directly connected with the change of the systems kinetic energy, caused by the interaction between electric field and dielectric particles.

2.4 GWS-Eigenvalue method

The GWS-intensity-relations (2.24) describe important quantities of the interaction between electromagnetic field and particles. In this section we show how one can modify these quantities using specially designed input fields. The underlying principle is simple and uses the information saved in the systems scattering matrix and its derivative.

For a system without losses we remember that the scattering matrix S is unitary and therefore the GWS-operator Q_α is a Hermitian operator, i.e., its eigenvalues are real and its eigenvectors $\mathbf{u}_i$ are linearly independent.

We now consider these eigenvectors as possible input states and see that the corresponding eigenvalues $\lambda_i = \mathbf{u}_i^\dagger Q_\alpha \mathbf{u}_i$ are directly proportional to the according quantity, shown on the right hand side of (2.24). Thus simply choosing an input state proportional to the eigenvector with the minimal (negative) or maximal eigenvalue of Q_α will result in an extremum of the system quantity.

We will explain the method now directly with an example. We choose α to be the coordinate x_s^i (center of mass) of one particle in a static system. Then the GWS-relation actually provides the electromagnetic force, eq. (1.28), on this particle for any given input field [7],

$$\mathbf{c}^\dagger Q_s \mathbf{c} = \frac{k^2}{2}\int_M \frac{d\epsilon_R}{dx_s}|\psi|^2 d^3x = \frac{2k^2}{\epsilon_0}F^i e_s^i. \tag{2.26}$$

We change the position of the particle slightly by moving it in a desired direction e_s^i, in order to calculate the difference in S, for an estimation of Q_s. Then we solve the eigenvalue problem $Q_s \mathbf{u}_i = \lambda_s \mathbf{u}_i$ and inject an input field into the system, which is proportional to the preferred eigenvector, $\mathbf{c} \propto \mathbf{u}_i$.

The eigenvector to the highest (or smallest) eigenvalue will lead to a maximal force in (or against) the direction e_s^i. This does not necessary means, that the force will point in the desired direction, however since the field intensity at the particle boundary is limited, the force in other directions (normal to e_s^i) is usually small.

Therefore one is able to manipulate the field in the near field, only with the asymptotic far-field information encoded in the GWS-operator. This works also for time itself as parameter $\alpha = t$, at least for adiabatic conditions, and builds the basis of our cooling procedure.

Chapter 3

Light cooling procedure and its implementation

In this chapter an accurate description of our light cooling procedure will be given. At first we want to share, how we came to the idea, that an optimal manipulation of many particles is even possible. Then we describe the iterative cooling mechanism and demonstrate it with numerical simulations. Lastly we specify the experimental set-up of a two-dimensional waveguide for the computations. We characterize the system in terms of contained particles and input control.

3.1 From the micro-manipulation of a single particle to many-body energy manipulation

Here we emphasize the generalization from an optimal tackling of one particle, as shown in last section's example, to the intended many particle cooling method. Moreover we provide a better understanding of the GWS-time-operator in eq. (2.25) and of its eigenvalues.

Our starting point is a static system containing dielectric scatterers. For such a scenario we already know, that one can generate a field, which applies a maximal force on a chosen particle in a chosen direction [7], using eq. (2.26). However in order to achieve this, we have to move the particle slightly.

The idea is now to consider a natural movement of the particle, in the otherwise static system. Doing this, the position change happens by itself and is automatically linked with the time-dependence of the scattering matrix. In this context (of one moving particle) it makes sense, that an optimization with the GWS-operator with respect to time derivation leads to the same (stationary) field configuration as working with the GWS-operator with respect to particle position derivation (in movement direction) Q_s.

$$Q_t = \frac{dx_s}{dt} Q_x + \frac{dy_s}{dt} Q_y = Q_s v_s. \tag{3.1}$$

Now we can consider a second moving particle and see, that Q_t will certainly inherit the position change of both particles (dS/dt is a total differential). Since the GWS-operator consists of a derivation and due to its role in eq. (2.24), we are able to describe any complex change of the system, by splitting it up in (quasi-independent) small changes.

Thus we can make the generalization to an arbitrary amount of particles [15], with different velocities and angular momenta,

$$Q_t = -iS^{-1}\frac{dS}{dt} = \sum_{n=1}^{N} \frac{dx_n^i}{dt} Q_{x_n^i} + \frac{d\varphi_n^i}{dt} Q_{\varphi_n^i}, \tag{3.2}$$

where φ_n^i denotes the angular orientation of the n-th particle. As rotation is also a form of movement (around a reference point), the operator $Q_{\varphi_n^i}$ is connected to a force-dependent quantity, namely the torque M^i, which the field generates on the particle.

We rewrite the right side of the GWS-time-relation (2.25) for the case of N arbitrarily shaped particles, so that the impact of translation and rotation movement is clearly visible (see also appendix A.4), resulting in

$$\frac{dE_{\text{kin}}}{dt} = \frac{\epsilon_0}{4}(\epsilon_s - 1) \sum_{n=1}^{N} \left[v_n^i \int |\psi|^2 dA_n^i + \omega_n^i \int \epsilon_{ijk} R_j |\psi^2| dA_n^k \right] = \frac{\epsilon_0}{2k^2} \mathbf{c}^\dagger Q_t \mathbf{c}. \tag{3.3}$$

Here, the first summation term corresponds to the translation power $v_n^i F_n^i$ and the second term corresponds to the rotation power $\omega_n^i M_n^i$ of the n-th particle. The integrals reach over the particle surfaces $dA^i = n^i dA$, where n^i denotes the surface normal vector and correspond to the according intern GWS-operators in eq. (3.2).

In particular considering the (normalized) eigenvectors $\mathbf{u}_i$ of Q_t as possible input states $\mathbf{c}_i = |\mathbf{c}|\mathbf{u}_i$, leads to the desired linear connection between kinetic energy change and the eigenvalues θ_i,

$$\frac{d}{dt} E_{\text{kin}}(\mathbf{c}_i) = \frac{\epsilon_0 |\mathbf{c}|^2}{2k^2} \theta_i = \frac{P_{\text{in}}}{w} \theta_i. \tag{3.4}$$

Here $P_{\text{in}} = (c\epsilon_0/2k)|\mathbf{c}|^2$ is the input power and $w = kc$ is the oscillation frequency of the field. As described previously in the last section, injecting the state corresponding to the minimal eigenvalue of Q_t leads to a maximal decrease of the systems kinetic energy.

Naturally we could also choose the highest eigenvalue for an optimal heating of the particles.

In general the GWS-operators $Q_{x_n^i}$, $Q_{\varphi_n^i}$ do not commute with each other, therefore their eigenvectors will be different. That means that the optimal many-body input state, we get from our eigenvalue-method (eigenvector of Q_t), is certainly not describable as superposition of optimal one particle states (eigenvectors of $Q_{x_n^i}$, $Q_{\varphi_n^i}$). The resulting field configuration is remarkable, as it does not maximize the force on each particle separately (which is in general not possible). Instead it takes the movement of all particles into account, leading to the best possible (stationary) energy decrease. Faster particles will be tackled more likely and so on, as we will see later.

3.2 GWS-light-cooling procedure

Based on equation (3.4) we are able to formulate a method for an effective cooling (or heating) of dielectric particles. The cooling procedure contains the following steps.

At the beginning the particles move freely in the waveguide (non-relativistic movement). We start by measuring the scattering matrix S at two following moments in time, in order to approximate the kinetic operator $Q_t \approx -iS^{-1}(t)[S(t) - S(t - \Delta t_{\mathrm{GWS}})]/\Delta t_{\mathrm{GWS}}$. We solve the eigenvalue-problem according to Q_t, and inject the eigenvector corresponding to the smallest (maximal negative) eigenvalue into the system, leading to an optimal energy reduction of our particle system.

This input state is only optimal at the time of the measurement, and loses its remarkable near field properties with time, due to the ongoing movement of the particles. Thus it should only be injected for a very short time (and one needs to work with pulsed input signals). After this short time step one repeats the procedure, starting over again with the measurement of S.

By this we gradually reduce the kinetic energy of the particles until the field forces are in range of the particle velocities, $mv_{\mathrm{fin}} \approx F\Delta t_{\mathrm{GWS}}$. A complete characterization of our cooling procedure is given alongside the simulation results, starting in chapter 5.

As the position and movement of the particles changes steadily, one needs to be able to measure S and accordingly shape the wavefront in a very short time, otherwise the mechanism will not work or loses much of its efficiency. This is the main difficulty to overcome in an experimental realisation.

Now we want to focus more on the conditions required for the simulation of our cooling method. In practice one only needs to compute the eigenvalue problem $Q_t\mathbf{u}_i = \theta_i\mathbf{u}_i$ and inject the eigenvector $\mathbf{u}_{\mathrm{min}}$, corresponding to the minimal eigenvalue θ_{min}, into the system. In our simulations we need to compute the inside of the system as well. Therefore, we have to calculate the field configuration and change the position and angular orientation of the particles according to the acting field forces and their velocities.

We evaluate the time evolution of the system with a straightforward Taylor series approach, discretising the basic equations of motion (1.30) and (1.31),

$$x^i_{n+1} = x^i_n + v^i_n \Delta t + \frac{1}{2m} F^i_n \Delta t^2 + O(\dot{F}^i_n \Delta t^3) \tag{3.5}$$

$$v^i_{n+1} = v^i_n + \frac{1}{m} F^i_n \Delta t + O(\dot{F}^i_n \Delta t^2). \tag{3.6}$$

Here explicitly done for the translation movement, the evolution of the angular orientation works analogously. It is now important to choose the length of the time step Δt small enough, such that we can neglect the change of the field force $\dot{F}$ during the time step (Δt should be taken as big as possible to avoid unnecessary computation costs). For our case this is not all that complicated. We work with pulsed input signals, besides that, the direction and magnitude of the force changes only due to the ongoing movement of the particles. Therefore a simple restriction might be

$$\Delta x \approx v \Delta t \ll \min(r, \lambda/3) \qquad \Rightarrow \qquad \Delta t \leq \frac{\min(r, \lambda/3)}{10v}, \tag{3.7}$$

with particle radius r and light wavelength λ. This makes sure, that the change of the particle position during one step is small in comparison to the wavelength (describing the field intensity peak width, the resolution limit of the field, here estimated as $\lambda/3$) and the size of the particles.

There are actually four different time scales of our system, besides the Taylor series time step, (ideally) following the schema

$$\Delta t_{\text{osc}} \ll \Delta t_{\text{puls}} \approx \Delta t_{\text{GWS}} < \Delta t_{\text{coll}}, \tag{3.8}$$

Here $\Delta t_{\text{osc}} = \tau = 2\pi/w$ is the oscillation period of the electromagnetic field, Δt_{GWS} is the time step for the GWS-operator approximation, Δt_{puls} is the period of the pulsed input signal and Δt_{coll} is the mean time between collisions of two particles.

Δt_{puls} equates to the time we inject an optimized field state $\mathbf{c}$ into the system. Thus it should also satisfy a relation similar to (3.7) for an optimal cooling, however this is not so strict as with Δt (obviously $\Delta t \leq \Delta t_{\text{puls}}$ is required). We want to keep in mind, that in the simulations we basically inject at each time step ($\Delta t_{\text{puls}} = \Delta t_{\text{GWS}}$) another optimized input state, without a continuous connection between these fields. This simplification of the pulsed operation has nearly no impact on the results. In real experiments one has to follow physics and connect two different input configurations via a continuous signal (i.e. a zero-crossing of the field amplitude). The periodic signal could be for example a sine ($\mathbf{c}(t) = \mathbf{c} \sin(2\pi t/\Delta t_{\text{puls}})$), a square-wave signal or of greater complexity.

3.3 Simulation in a waveguide

As already mentioned in section 1.2, the Helmholtz equation (1.14) holds only in a 2D-like system, where one of its dimensions is much smaller than the others. For the simulations we use a strictly two dimensional system, as defined in the following.

The dielectric particles shall be contained in a rectangular waveguide, with width W in x-direction and length L in y-direction. The field can be injected from asymptotic areas from both short sides (waveguide channels D), see figure 3.1, and satisfies Dirichlet boundary conditions along the waveguide boundaries.

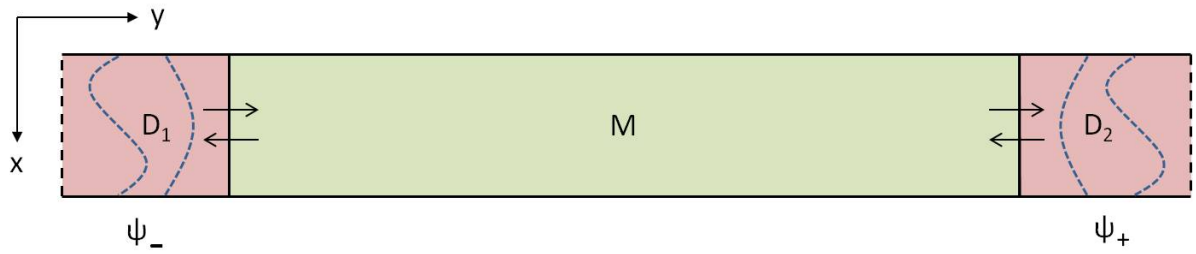

Figure 3.1: Schematic of the scattering problem in a rectangular multimode waveguide. The particles are contained in the scattering area M. In the distant channels D_i the field consists of plane waves (modes).

For this 2D-system the field in the channels D_i is given, according to section 2.1, by

$$\psi_\pm = (\psi_{\text{in}} + \psi_{\text{out}})_\pm = \sum_{n=1}^{N} c_{\text{in}}^n \sqrt{\frac{2}{W}} \sin(k_{x,n}x) \frac{e^{\mp i k_{y,n} y}}{\sqrt{k_{y,n}}} + c_{\text{out}}^n \sqrt{\frac{2}{W}} \sin(k_{x,n}x) \frac{e^{\pm i k_{y,n} y}}{\sqrt{k_{y,n}}}. \quad (3.9)$$

Here ψ_- is the field in the left channel and ψ_+ the one in the right. The different sines describes the cross-sectional field distribution at empty wave guide regions, far away from the particles, and are called the modes of the system. We regulate the number of possible input modes N, through the wavenumber k and the waveguide (channel) width W,

$$k_{x,n} = \frac{n\pi}{W}, \quad k_{y,\min} \approx \frac{\pi}{W}\sqrt{(N+0.5)^2 - N^2} \quad (3.10)$$

$$k = \sqrt{k_{x,n}^2 + k_{y,n}^2} \approx \frac{\pi}{W}(N+0.5). \quad (3.11)$$

The number of input modes is a very important quantity, since it basically controls the degrees of freedom in the field generation. For $N \to \infty$ one can inject any field configuration into the system one wants (that satisfies the boundary conditions), otherwise the basis is finite and the configurations are naturally restricted. (However in a 3D-system,

the wavenumber is anyway limited by the finite height of the waveguide, so that one gets the 2D-like scenario $k_z = 0$.) For our case of two semi-infinite waveguides as the asymptotic region the coefficient vector $\mathbf{c} = \mathbf{c}_{\text{in}}$ has length $2N$ (N modes per channel) and the scattering matrix S, as defined in eq. (2.5), has $2N \times 2N$ entries.

In the simulations we confine ourself usually to mode numbers between $N = 10 - 20$. The resulting field configuration ψ inside the waveguide, for a given input state $\mathbf{c}$, has been numerically calculated with an advanced finite element method (Helmholtz-equation (1.14) solved with the NGSolve software [16]). With ψ, we can calculate the force and the torque on the dielectric particles, following equations (1.28) and (1.29). For our 2D-scenario, the volume integrals reduces to area integrals and the surface integral becomes an integration over the circumference of the respective particle.

Our system is basically characterized by the ratio between particle radius r and waveguide width W (or wavelength $\lambda = 2\pi/k$), the number of input modes N and the number of scattering particles. The asymptotic field input is characterized by the input state $\mathbf{c}$. The field amplitude ψ scales with the absolute value $|\mathbf{c}|$ and the force on the particles is proportional to the input power P_{in}, as already presented in eq. (3.4). For the refractive index of the particles $n_s = \sqrt{\epsilon_s} = 1.44$ has been chosen, i.e. the particles change the field configuration decently.

In the upcoming chapters 4 to 6 we work in arbitrary units, therefore only relative values are important. For the characterization of the cooling procedure in chapter 5 and 6 we work (if not stated differently) with a wavelength smaller than (or similar to) the particle radius, so that the field can strongly focus upon the particles. Afterwards, in chapter 7, we will show some results for realistic values, under conditions that might be achieved in a possible first experimental realisation.

Chapter 4

Random field input and statistics

Before we get to the simulations of the cooling procedure, we want to take a look at the field statistics in a waveguide. The average field distribution for randomized input fields will be described theoretically and computed for an empty waveguide. Then we consider point particles and show their behaviour in such field distributions. Furthermore we will go over to circular particles and test their dynamics in field configurations of constant or randomized field inputs.

4.1 Empty waveguide statistics

We work with a pulsed input signal, each time step $\Delta t = \Delta t_{\text{puls}}$ a random field shall be injected into the empty waveguide. While the flux $|\mathbf{c}|^2$ (input power) into the system is constant, the coefficients (input state $\mathbf{c}$) of the respective wave train are created as random complex numbers,

$$c^j = C^j e^{i\varphi_j}, \quad |\mathbf{c}| = const., \tag{4.1}$$

$$C^j \text{ random} \in [0,1], \quad \varphi_j \text{ random} \in [0, 2\pi]. \tag{4.2}$$

We compare the statistics of such generated field configurations with the Gaussian distribution in a microwave-billiard-system (stadium billiard) [17]. This kind of probability distribution can be obtained through a random superposition of plane waves with a fixed wavenumber k at each point in the system.

$$\psi(\vec{r}) = \sum_i a_i \cos(\vec{k}\vec{r} + \varphi_i), \tag{4.3}$$

where a_i, the direction of $\vec{k}$ and the phase φ_i are (uniformly) randomized. In our case of a complex wavefunction this might be assumed for the real and imaginary part separately.

The amplitude distribution $P(\Psi)$ denotes the probability, that the wavefunction has the distinct value Ψ at a fixed location,

$$P(\Psi) = \langle \delta(\Psi - \sum_i a_i \cos(\vec{k}\vec{r} + \varphi_i)) \rangle = \sqrt{\frac{A}{\pi}} e^{-A\Psi^2}, \tag{4.4}$$

with $A \propto 1/\langle a_i^2 \rangle = \text{const}$. The expectation values of our system are therefore built as $\langle f(\Psi) \rangle = \int f(\Psi) P(\Psi) d\Psi$ for an arbitrary function $f(\Psi)$. Some mean values of a simple Gaussian distribution are stated below.

$$\langle \Re(\psi) \rangle = \langle \Im(\psi) \rangle = 0, \tag{4.5}$$
$$\langle |\psi| \rangle = \int |\Psi| P(\Psi) d\Psi = \tfrac{1}{2}\tfrac{\pi}{A}, \tag{4.6}$$
$$\langle |\psi|^2 \rangle = \int |\Psi|^2 P(\Psi) d\Psi = \tfrac{1}{A}. \tag{4.7}$$

Deviations of this distribution arise because of the finite size of our system through the applied boundary conditions and the finite number of input modes. The wavefunction is forced to $\psi = 0$ at the boundary of the waveguide. This leads for example to oscillations of the mean field density $\langle |\psi|^2 \rangle$ in dependence of the distance from the boundary, which might be described with a Bessel function J_0 [18].

$$\langle |\psi|^2 \rangle = \frac{1}{B}[1 - J_0(2k_\nu x')], \tag{4.8}$$

where x' measures the perpendicular distance from the boundary. Results are visualized in figure 4.1. While the frequency of the oscillations or rather the (mean) wave number k_ν increases with the number of included input modes, the amplitude decreases.

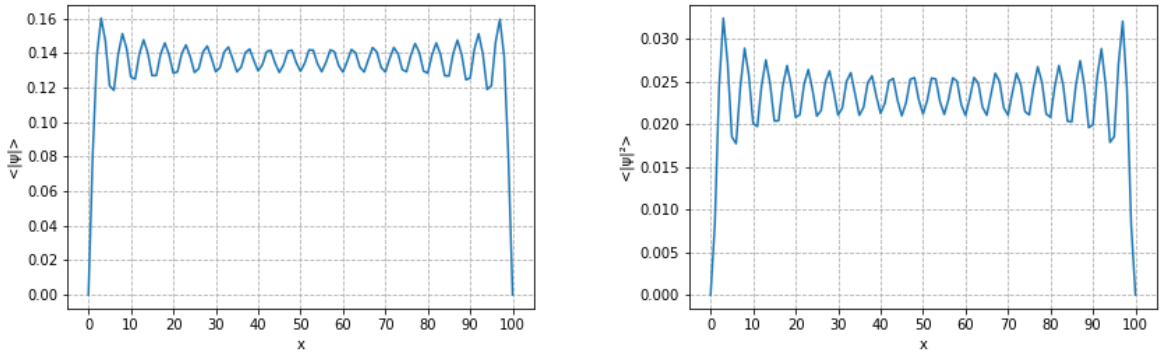

(a) $\langle |\psi| \rangle$ depending on location.

(b) $\langle |\psi|^2 \rangle$ depending on location.

Figure 4.1: Relevant mean values of the electrical field by irradiation of random fields, as a function of the position on the waveguide cross section, for $N = 20$ input modes. At the two margins $x = 0$ and 100 the field follows the Dirichlet boundary condition.

This position-dependent mean value of $\langle|\psi|^2\rangle$ is actually the most uniform intensity distribution one can achieve (for the used number of input modes). For instance, we could insert such a (cross-sectional) field configuration into the system by choosing $c^n \propto [1-(-1)^n]/k_{x,n}$ (Fourier series representation of a constant). However the field consists of different plane waves (each mode propagates with a different longitudinal wavenumber), resulting in a y-dependence (along the waveguide length) of the field intensity. That means a uniform distribution in a multimode waveguide can only be achieved by an averaging procedure.

The simulations follow our expectation, in the sense that the amplitude distribution has Gaussian form (4.4), as one can see in figure 4.2. The constant in the exponent $A = 1/\langle|\psi^2|\rangle$ is, as described in eq. (4.8), position dependent. Moreover the Gaussian distribution seems to be still valid at places near the boundary.

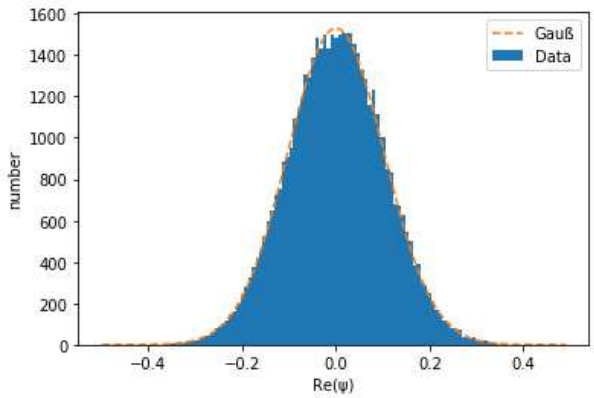

(a) Distribution of $\Re(\psi)$ in the middle of the waveguide.

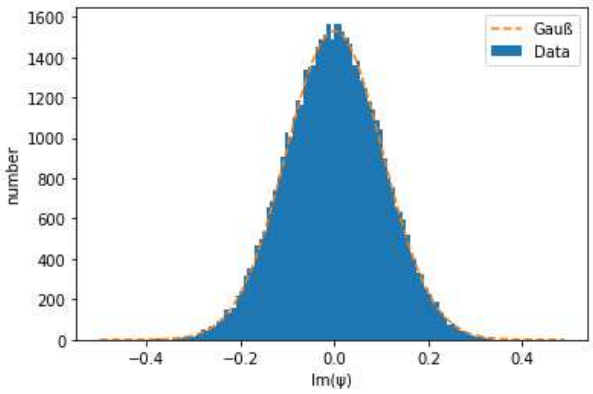

(b) Distribution of $\Im(\psi)$ in the middle of the waveguide.

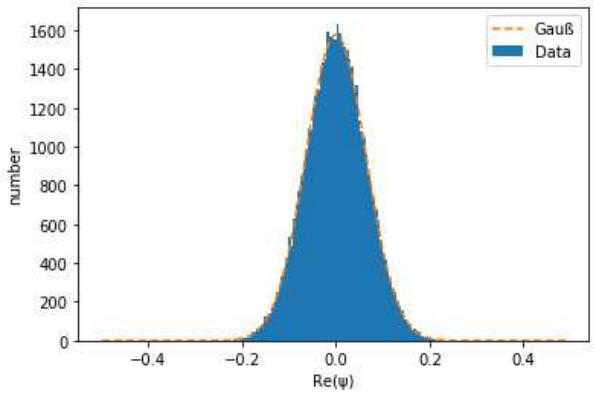

(c) Distribution of $\Re(\psi)$ near the boundary.

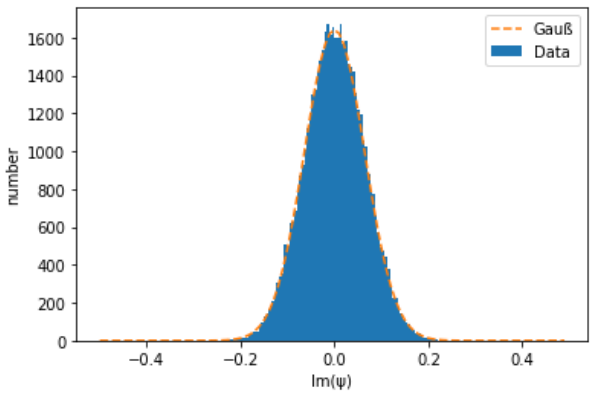

(d) Distribution of $\Im(\psi)$ near the boundary.

Figure 4.2: Amplitude distribution, histogram of the field configuration created with 50000 randomly generated field configurations.

The random behaviour of the wave functions can also be found in the auto-correlation function $\langle\psi(r'+r)\psi(r')\rangle$. We assume again a random superposition of plane waves, eq. (4.3), and get

$$\langle \psi(\vec{r}+\vec{s})\psi(\vec{r})\rangle = \frac{2}{A}\langle \cos(\vec{k_n}\vec{s})\rangle = \frac{2}{A}J_0(ks), \tag{4.9}$$

with the Bessel function J_0. This is of course only valid for the real and imaginary part of the wavefunctions separately. According data is plotted in figure 4.3.

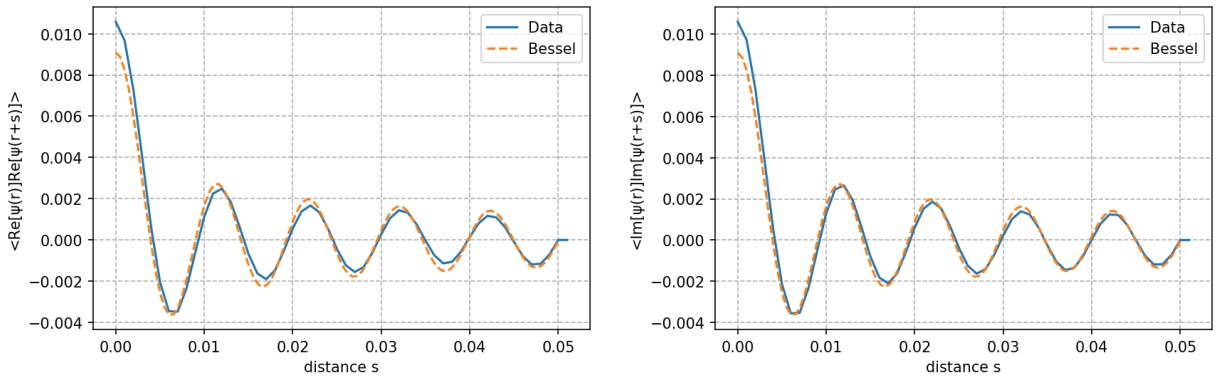

(a) Auto-correlation of $\Re(\psi)$ (b) Auto-correlation of $\Im(\psi)$

Figure 4.3: Auto-correlation function of the wavefunctions by injection of random fields into the system, starting point is the middle of the waveguide.

4.2 Forces on point-like dielectric particles

We look at the action of randomly generated fields on a scatterer placed in the waveguide. In order to simplify the system, we describe the dielectric scatterer as a point particle, which will be set in the middle of the waveguide with a defined initial velocity v_0.

The simulation time is divided in N equidistant and short time steps Δt. During each of the N time steps a different randomly generated field is directed into the system, following equation (4.1), such that short force pulses are acting on the particle.

According to equation (1.28), the field force, which acts on the point dielectrica (at a fix point in time), is

$$F^i = -\frac{1}{4}\epsilon_0 \int_M \partial_i \epsilon_R |\psi^2| d^3x = \frac{1}{4}\epsilon_0(\epsilon_s - 1)\int_M \delta(x^m - x_s^m)\partial_i|\psi^2|d^3x \tag{4.10}$$

$$= \frac{1}{4}\epsilon_0(\epsilon_s - 1)\left(\partial_i|\psi^2|\right)\big|_{x^m = x_s^m}, \tag{4.11}$$

with the constant dielectric function ϵ_s and the position x_s^m of the particle. The force results from the gradient of the field intensity $|\psi|^2$ at the particle position.

The point particle can be seen as a small perturbation, it hardly affects the field flow in the waveguide. Thus the results of the previous section are still valuable. As we have seen in figure 4.1, the mean field density $\langle|\psi|^2\rangle$ is location-dependent. Therefore the mean Lorentz force (at a given place) vanishes only at the extreme points of $\langle|\psi|^2\rangle$. At any other space point the force distribution is indeed not symmetric, as one can see in figure 4.4.

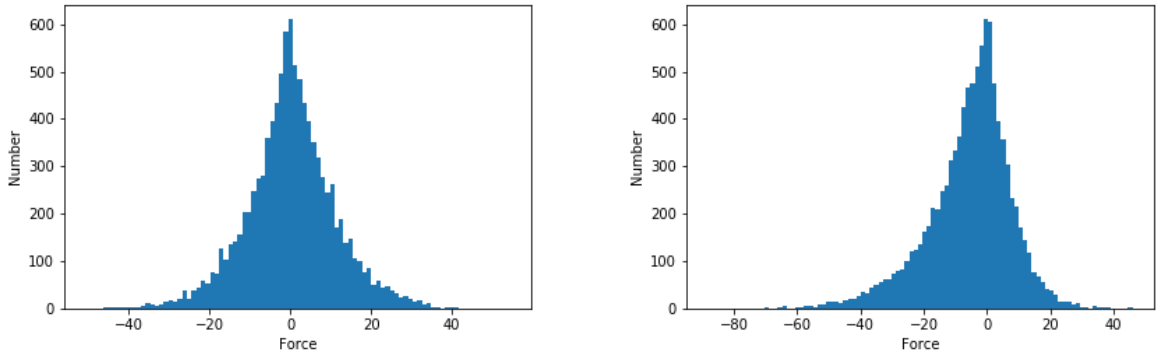

(a) At an extreme point $\partial_i\langle|\psi|^2\rangle = 0$.

(b) Between two extreme points.

Figure 4.4: Force distribution at two different positions in the waveguide, characterised by the gradient of $\langle|\psi|^2\rangle$. For the histogram 10000 randomly generated field distributions were used.

At first we are neglecting these oscillations, generated from boundary conditions and limitation of included wavemodes. For ideal conditions there is no space dependence of the force, we can emulate this partly by evaluating the force at each time step in the middle of the waveguide. No direction is distinguished and $\langle F^i\rangle = 0$ is valid. But the mean value of F^2 is surely non-zero.

A simple theoretical description can be done with a "delta force"-model, which describes the short force pulses with Delta functions, $F(t) = \sum_n A_n\delta(t - t_n)$.

$$v(t) = v_0 + \frac{1}{m}\int_0^t F(t')dt', \tag{4.12}$$

$$v^2(t) = v_0^2 + \frac{2}{m}v_0\int_0^t F(t')dt' + \frac{1}{m^2}\int_0^t\int_0^t F(t')F(t'')dt'dt'', \tag{4.13}$$

$$\langle E_{kin}\rangle = \frac{1}{2}m\langle v^2\rangle = \frac{1}{2}m\langle v_0^2\rangle + \int_0^t\langle v_0F(t')\rangle dt' + \frac{1}{2m}\int_0^t\int_0^t\langle F(t')F(t'')\rangle dt'dt'' \tag{4.14}$$

$$= \frac{1}{2}mv_0^2 + \frac{1}{2m}\int_0^t\int_0^t\langle F^2(t')\rangle\delta(t' - t'')dt'dt'' \tag{4.15}$$

$$= \frac{1}{2}mv_0^2 + \frac{1}{2m}\int_0^t\langle F^2(t')\rangle dt' \tag{4.16}$$

$$= \frac{1}{2}mv_0^2 + \frac{1}{2m}\sum_n\langle A_n^2\rangle H(t - t_n). \tag{4.17}$$

The force (4.11) is independent from the particle velocity (as $v \ll c$), therefore the energy of the particle increases systematically with time, indicated by the Heaviside function H in eq. (4.17). If we remove the gap between the pulses by injecting at each infinitesimal time step another randomly generated field into the system, then the kinetic energy will increase linearly with time,

$$\langle E_{kin} \rangle = \frac{1}{2} m v_0^2 + \frac{\langle A^2 \rangle}{2m} t. \tag{4.18}$$

Since we can not evaluate the force at infinite time points, we divide the simulation in N short time steps Δt as already mentioned. The behaviour of the kinetic energy during each time step will be approximated by a Taylor series, so that the force (and the field configuration) has to be evaluated only once per time step (or twice for measuring $\dot{F}$).

The velocity of the scatterer after the n-th time step is

$$v_{n+1} = v_n + \frac{1}{m} F_n \Delta t + \frac{1}{2m} \dot{F}_n \Delta t^2 + \mathrm{O}(\Delta t^3). \tag{4.19}$$

For the kinetic energy we get

$$\begin{aligned} E_{n+1} &= E_n + \dot{E}_n \Delta t + \frac{1}{2} \ddot{E}_n \Delta t^2 + \mathrm{O}(\Delta t^3) && (4.20) \\ &= \frac{1}{2} m v_n^2 + v_n F_n \Delta t + \frac{1}{2m} F_n^2 \Delta t^2 + \frac{1}{2} v_n \dot{F}_n \Delta t^2 + \mathrm{O}(\Delta t^3). && (4.21) \end{aligned}$$

Hence the force is independent of the particle velocity, $\langle v_n F_n \rangle = 0$ is valid. Regarding the term $\langle v \dot{F} \rangle$ things are not that easy anymore. Since we work with a point particle, we might not be able to neglect $\dot{F}$, as described around eq. (3.7). However, since the point particle does not change the field configuration, the field the particles senses depends only on the position in the waveguide. We obtain

$$\begin{aligned} \partial_t F^i &= \frac{1}{4} \epsilon_0 (\epsilon_s - 1) \int \partial_t \delta(x^m - x_s^m) \partial_i |\psi|^2 (x^m) d^3x && (4.22) \\ &= -\frac{1}{4} \epsilon_0 (\epsilon_s - 1) \frac{dx_s^j}{dt} \int \partial_j \delta(x^m - x_s^m) \partial_i |\psi|^2 (x^m) d^3x && (4.23) \\ &= \frac{1}{4} \epsilon_0 (\epsilon_s - 1) \frac{dx_s^j}{dt} \partial_j \partial_i |\psi|^2 \big|_{x^m = x_s^m}. && (4.24) \end{aligned}$$

leading to average terms like $\langle |\psi|^2 \rangle$ and $\langle |\partial_i \psi|^2 \rangle$. But still one could argue, that the direction of the force change $\partial_t F^i$ does not depend on the direction of the velocity. (At least if the mean field density is constant and if the field is not influenced by the particle, then the force change on the particle is as often positive as negative.). And therefore it results in

$$\langle v_n \dot{F}_n \rangle \propto \langle v_n^i v_n^j \rangle \langle \partial_i \partial_j |\psi|^2 \rangle = 0. \tag{4.25}$$

The relevant contribution to the energy change corresponds again to the quadratic force term,

$$\langle E_n \rangle = \frac{1}{2}mv_0^2 + \frac{1}{2m}\sum_{i=0}^{n-1}\langle F_i^2\rangle \Delta t^2 + \mathrm{O}(\Delta t^3) \tag{4.26}$$

$$= \frac{1}{2}mv_0^2 + \frac{1}{2m}\langle F^2\rangle \Delta t^2 n + \mathrm{O}(\Delta t^3). \tag{4.27}$$

The kinetic energy rises with the number of time steps n, as expected. However the increase is very small for sufficient short time steps $\Delta t \ll 1$, expanding the results of the delta force model. One should mention, that the result of the Taylor series is strictly speaking only valid for a small number of time steps n. For larger n the errors, caused by the higher orders in the series at each time step, might add up and be relevant (for example $\dot{F}^2$).

A different way to represent the behaviour is based on using the correlation between forces on the particle at different times. There are no such correlations between time steps, but indeed during each time step.

$$\langle E_{kin}\rangle = \frac{1}{2}m\langle v^2\rangle = \frac{1}{2}m\langle v_0^2\rangle + \int_0^t \langle v_0 F(t')\rangle dt' + \frac{1}{2m}\int_0^t\int_0^t \langle F(t')F(t'')\rangle dt'dt'' \tag{4.28}$$

$$\langle E_{n+1}\rangle = \frac{1}{2}m\langle v_n^2\rangle + \frac{1}{2m}\int_t^{t+\Delta t}\int_t^{t+\Delta t}\langle F_n(t')F_n(t'')\rangle dt'dt'' \tag{4.29}$$

$$= \frac{1}{2}mv_0^2 + \frac{1}{m}\sum_{i=0}^{n}\int_0^{\Delta t}\int_0^{t'} f_i(t'-t'')dt''dt', \tag{4.30}$$

with $\langle F_n(t')F_n(t'')\rangle = f_n(|t'-t''|)$. The behaviour depends therefore alone on the correlation function f during a time step. f includes how much the force changes during the time Δt and we can Taylor expand it. If we assume f to be well described by a constant $f \approx C + O(\Delta t)$, we get again the easy relation

$$\langle E_n\rangle \approx E_0 + \frac{C}{2m}n\Delta t^2. \tag{4.31}$$

Results confirming the linear increase of the energy with time are pictured in figure 4.5. The mean value of the kinetic energy of a particle, which is interacting with a pulsed randomized electric field (corresponding to a symmetric force distribution) is plotted.

A simple interpretation of the found behaviour can be given by a random walk of the velocity. While the mean particle velocity is always equal to the initial velocity, the mean square deviation $(\Delta v)^2$ from the initial velocity is increasing with time, i.e. with

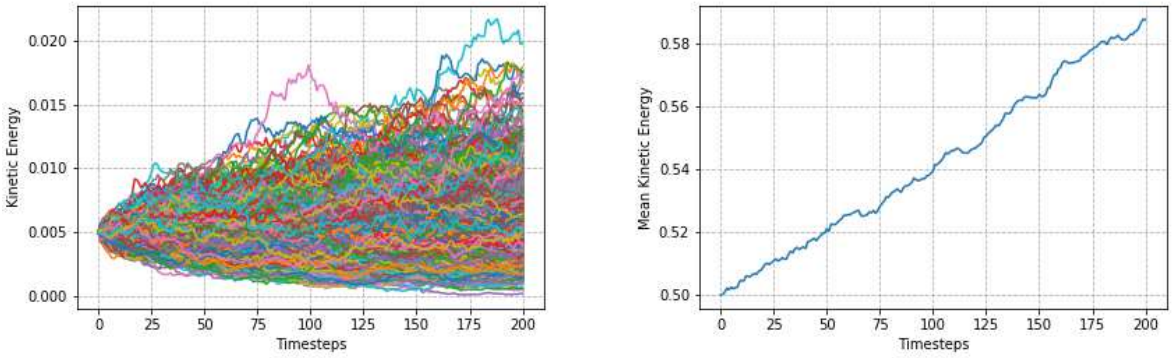

(a) Kinetic energy in dependence of time, all paths used for the mean value evaluation.

(b) Mean kinetic energy by irradiation of random fields.

Figure 4.5: Statistical evaluation of the kinetic energy of the particle, at each time step a randomly generated field is acting on the scatterer.

the number of time steps n.

$$\langle \vec{v} \rangle = \vec{v}_0, \tag{4.32}$$

$$\langle v^2 \rangle = v_0^2 + \frac{\langle F^2 \rangle \Delta t^2}{m^2} n, \tag{4.33}$$

$$\Delta v = \sqrt{\langle v^2 \rangle - \langle \vec{v} \rangle^2} = \frac{\sqrt{\langle F^2 \rangle} \Delta t}{m} \sqrt{n}. \tag{4.34}$$

If we are not considering the ideal conditions, deviations from this behaviour can appear, already illustrated by the asymmetric force distribution at the beginning of this section. The mean strength (and also the direction) of the force depends on the particle position. Since the particle is moving, the mean force changes with time. Some showcases are plotted in figures 4.6 and 4.7, where we have taken a relatively small initial velocity.

If the applied force is strong, one could expect, that a larger area of the waveguide will be visited by the scatterer in a given time. Therefore the asymmetric force distribution might not play a huge role, as one can see in figure 4.6. If the force is small, so that the particle will just slightly change its position, it is indeed possible, that the mean kinetic energy decreases, visualised in figure 4.7.

If we make the generalization from one to N particles (again assuming ideal behaviour), we would expect a linear rise of the mean kinetic energy, i.e. the temperature of the gas.

$$\langle E_n \rangle = E_0 + N \frac{\langle F^2 \rangle}{2m} \Delta t^2 n + \mathrm{O}(\Delta t^3). \tag{4.35}$$

The higher the velocity of the particles is, the more likely are collisions between them. In our case we work with elastic collisions, thus no kinetic energy is lost.

In addition, if we consider a Brownian motion (describing for example particles in a fluid), one usually defines a natural energy limit. The Brownian movement can be described by the Langevin equation, which includes a dissipative friction term. Therefore the kinetic energy will not increase linearly with rising velocity and converges at some time to a constant value. This behaviour is then analog to thermal diffusion. Instead of the velocity, it is then the particle position that can be characterized by a random walk.

We summarize, a randomized field input leads to a random movement of the particles. Since each input field acts a finite time ($\Delta t > 0$), the particles get heated, their kinetic energy raises proportional to F^2. This might also be the reason, why a cooling of a complex system is way harder than heating it. Deviations from this behaviour can occur, because of system restrictions, like a finite number of input modes.

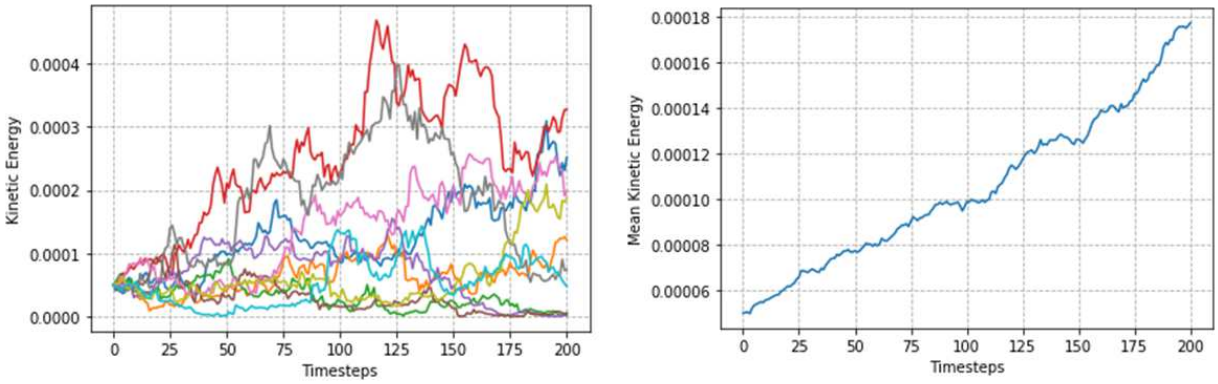

(a) Kinetic energy in dependance of time, selection of some paths.

(b) Mean kinetic energy by irradiation of random fields.

Figure 4.6: Statistical evaluation of the kinetic energy of the particle, for unideal conditions. At each time step a randomly generated field with a high input intensity is acting on the scatterer.

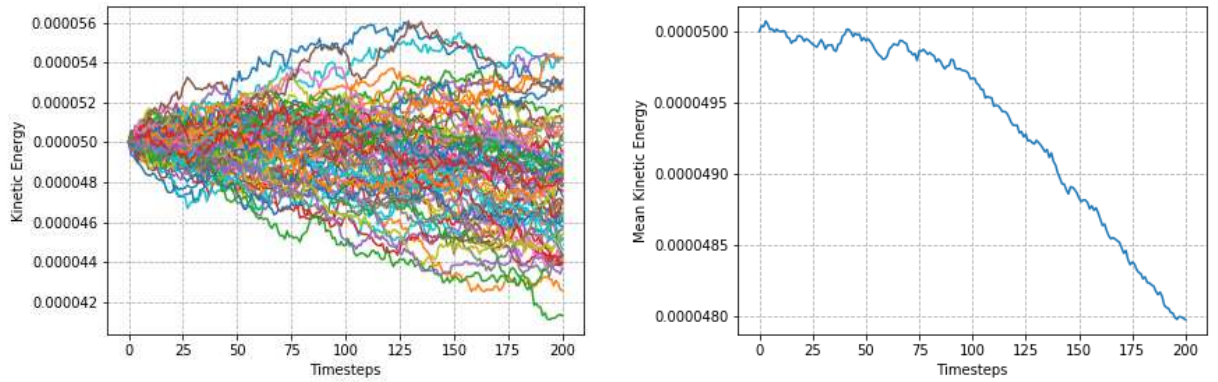

(a) Kinetic energy in dependence of time, all paths used for the mean value evaluation.

(b) Mean kinetic energy by irradiation of random fields.

Figure 4.7: Statistical evaluation of the kinetic energy of the particle, for unideal conditions. At each time step a randomly generated field with a low input intensity is acting on the scatterer, characterizable by $v_0 \gg F\Delta t$, $\langle F \rangle \neq 0$.

4.3 Test simulations with circular particles

We now consider particles with a finite radius, $rk \not\ll 1$. For this case, the interaction between field and particles is way more complicated. The scatterers certainly affect the field configuration in the waveguide and the forces on two (near) particles might be correlated. Instead of a theoretical description, we show here some simulation results and emphasize the similarities with the last section.

We consider a system, consisting of ten circular scatterers with random initial velocities. During the simulation we inject at each time step another randomized input field into the waveguide, as was done in the last sections. Here we will not take the average value over many tries, instead we only show results according to one example (time evolution). Some field configurations around the particles (with ongoing time) are visualised in figure 4.8. Regarding each particle, the white line indicates the velocity direction and the red line the direction of the field force.

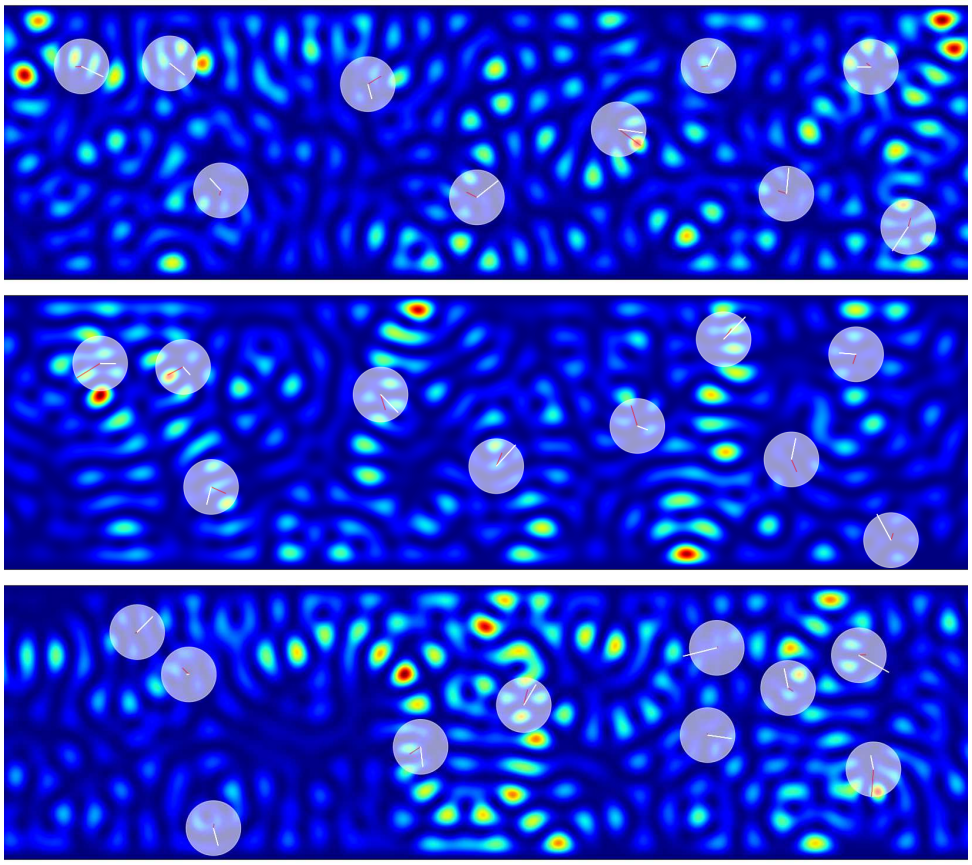

Figure 4.8: Example of field configurations $|\psi|^2$ for randomized field input states $\mathbf{c}$, Number of input modes $N = 10$.

The particle movement changes according to the acting field force (pulses), leading again to a small increase of the kinetic energy, see figure 4.10a. We expect, that the underlying increase is again caused by the absolute value of the field force, the F^2-term in the time evolution of the energy. For instance, if we assume, that the angle between velocity and

force of the different particles is random, the first order term in the energy evolution loses relevance, $\sum_{i=1}^{N} \vec{v}_i \vec{F}_i < \sum_{i=1}^{N} F_i^2 \Delta t/2m$. At least over few time steps the various randomized field configurations will likely lead to different force directions (an according video is linked in the appendix A.6), which also explains the small oscillations of the kinetic energy.

We also made a similar simulation with a constant input field. During the whole simulation only the first waveguide mode will be injected from both sides. The field configurations, which follow the ongoing time evolution, are visualised in figure 4.9. As the input is constant, the field around the particles changes steadily, corresponding to the current position (change) of the particles (see video link in the appendix A.6).

The corresponding kinetic energy of our particle system increases quite strongly with time, see figure 4.10b. Surprisingly the energy rises much more strongly than in the random field scenario. On the one hand the initial conditions might play a bigger role, as the field input is constant, the force direction changes smoothly with time. On the other hand this increase could be a sign for strong field (force) correlations between the different particles, reaching over long time periods. For example, if we think about the thermodynamics of a (ideal) gas, a uniform pushing (i.e. an increase in pressure) will increase the temperature until equilibrium is established (however a strict analogy might not be existing).

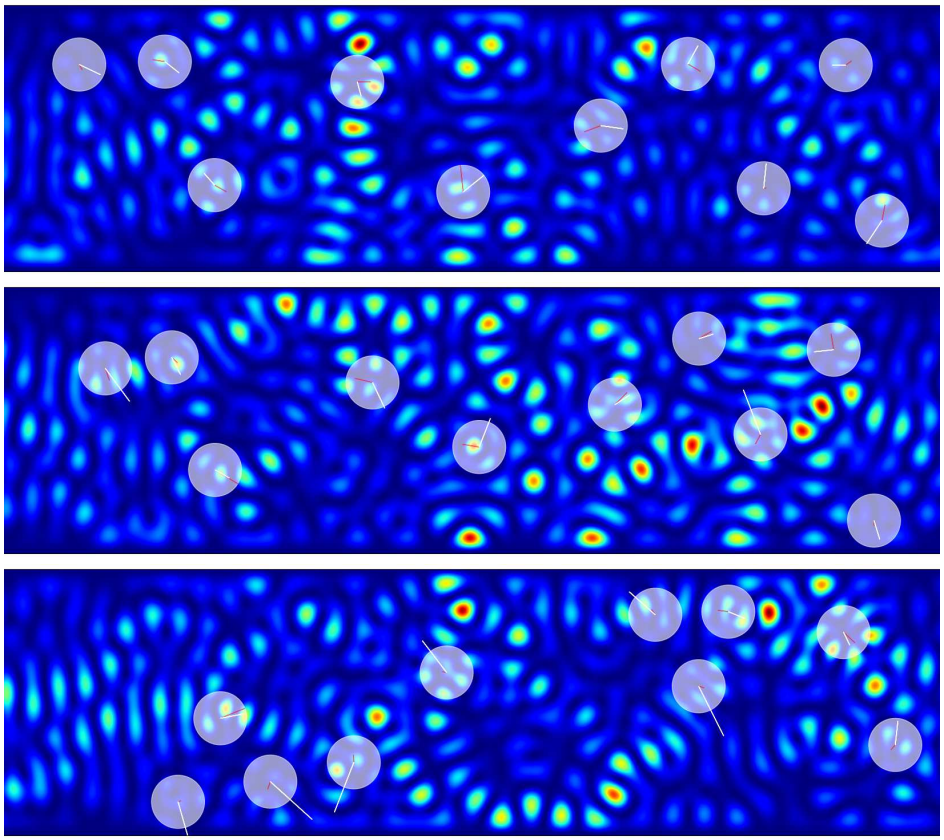

Figure 4.9: Example of field configurations $|\psi|^2$ for a constant plane wave input, Number of input modes $N = 10$.

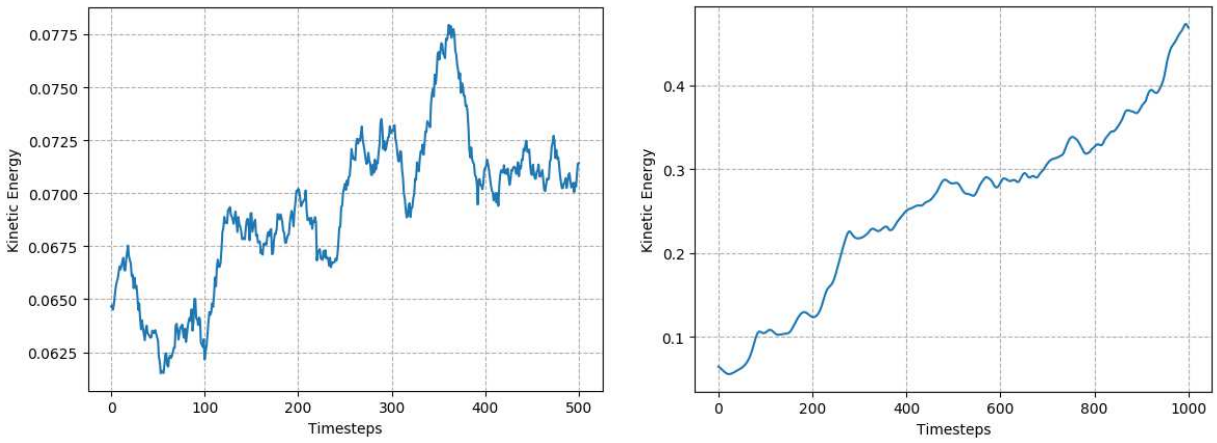

(a) Pulsed random field injection.

(b) Constant first mode injection.

Figure 4.10: Kinetic energy in dependence of time for random field and plane wave input states; same initial conditions (particle position and velocity).

We want to emphasize, during the simulations some collisions between particles occurred. As mentioned in section 1.4, we work with (elastic) hard-body collisions, and therefore they do not change the kinetic energy of the particle system directly. Furthermore in real systems there might be a small damping force present (internal friction), which will change the time evolution of the particles, see eq. (1.32). Friction will be included in chapter 7, however in most cases it's completely negligible. One only should keep in mind, that the particles can not be heated endlessly. On the one hand, the additional damping will lead to a friction limit and on the other hand our results are based on a non-relativistic regime (adiabatic conditions).

Chapter 5

Characterization of the cooling procedure

In this chapter we begin to characterize our cooling mechanism, especially by looking at the optimized field configurations around the scatterers. We start with one dielectric particle in the waveguide, show some simulation results of the cooling and heating procedure and analyse the field forces, which act on the particle. Then a second scatterer will be included and the optimal two particle field state will be discussed, in order to understand the cooling of a many particle system.

5.1 One particle cooling and heating

We consider a circular particle and show first simulation results. The wavelength has been chosen small enough, in order to get high resolution. That means the field can precisely focus upon the particle boundary. We follow the iterative procedure, documented in section 3.2, for an optimal (de-)acceleration of the particle. For now we work with constant input power P_{in} ($|\mathbf{c}|^2(t) = \text{const.}$) and pulse period Δt_{puls}.

Initially the dielectric scatterer has been set in the middle of the waveguide with an initial velocity v_0^i. We "follow its movement" by measuring the change in the scattering matrix $S(t)$ and are able to slow it down by injecting the best possible counteracting input field into the system. Figure 5.1 shows examples of the resulting field configuration (intensity $|\psi|^2$) around the particle. The field intensity peaks focus strongly upon the particle boundary areas on its backside (against the movement direction), so that the electric force (1.28) is (ideally) anti-parallel to the velocity.

By injecting at each time step $\Delta t = \Delta t_{\text{GWS}}$ the current eigenvector (corresponding to the smallest eigenvalue) of the kinetic operator Q_t into the system, we are able to slow down the particle iteratively. For the one particle case, the field configuration follows in principle the particle movement with time (see video link in the appendix A.6). The

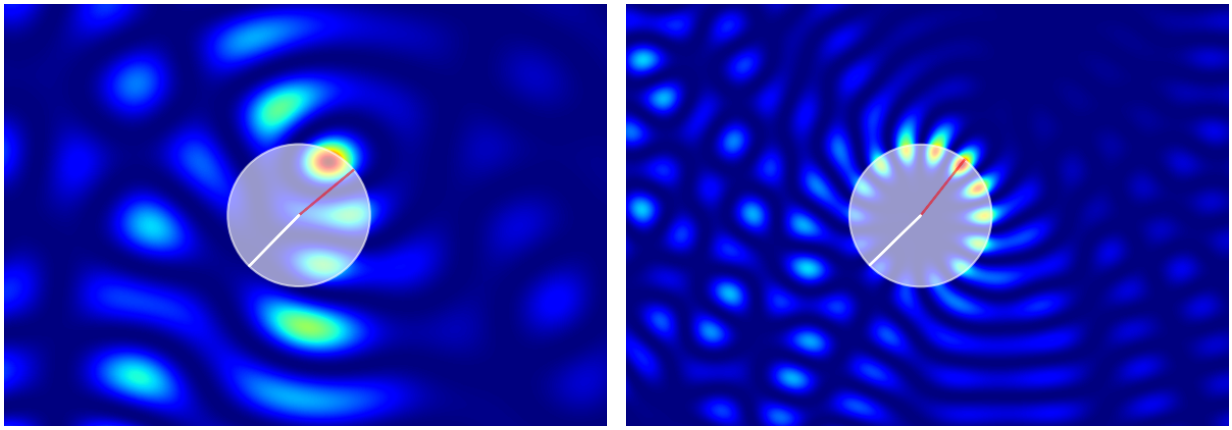

(a) $N = 10$. (b) $N = 20$.

Figure 5.1: Optimal field intensity configuration (colour) against particle movement, for two different numbers of input modes N. Achieved via an asymptotic injection of the eigenvector (input state) of the GWS-time-operator, corresponding to the smallest eigenvalue. The white line indicates the velocity direction, the red line the direction of the field force.

resulting time dependence of the kinetic energy of the scatterer is visualised in figure 5.2a. Likewise, injecting at each time step the eigenvector corresponding to the largest eigenvalue, leads to an optimal acceleration of the particle, see figure 5.2b.

The time dependence of both cases can be described theoretically with a Taylor-series. For ideal conditions the force F is anti-parallel (or parallel) to the velocity v and has a constant absolute value (at each time step Δt). The energy after the n-th time step is

$$E_{n+1} = \frac{1}{2}mv_n^2 \mp |v_n||F_n|\Delta t + \frac{1}{2m}F_n^2\Delta t^2 + \frac{1}{2m}v_n\dot{F}_n\Delta t^2 + O(\Delta t^3) \tag{5.1}$$

$$= \frac{1}{2}mv_0^2 \mp \sum_i^n |v_0||F_i|\Delta t + \sum_{i=1}^n \sum_j^{i-1} |F_i||F_j|\Delta t^2 + \frac{1}{2}\sum_i^n (F_i^2 + v_i\dot{F}_i)\Delta t^2 \tag{5.2}$$

$$= \frac{1}{2}mv_0^2 \mp |F| \sum_i^n |v_0|\Delta t + F^2 \sum_{i=1}^n \sum_j^{i-1} \Delta t^2 + \frac{1}{2}\sum_i^n (F^2 + v_i\dot{F}_i)\Delta t^2 \tag{5.3}$$

$$= \frac{1}{2}mv_0^2 \mp |v_0||F|n\Delta t - F^2\frac{n}{2}\Delta t^2 + F^2\frac{(n+1)n}{2}\Delta t^2 + \frac{1}{2}\sum_i^n v_i\dot{F}_i\Delta t^2 \tag{5.4}$$

$$= \frac{1}{2}mv_0^2 \mp |v_0||F|n\Delta t + F^2\frac{n^2\Delta t^2}{2} + \frac{1}{2}\sum_i^n v_i\dot{F}_i\Delta t^2. \tag{5.5}$$

For small enough time steps we can neglect $\dot{F}$, as described around eq. (3.7), resulting naturally in a quadratic decrease (or increase) of the kinetic energy for ideal conditions. The clearly visible deviations from the ideal quadratic curves, in figure 5.2, are due to

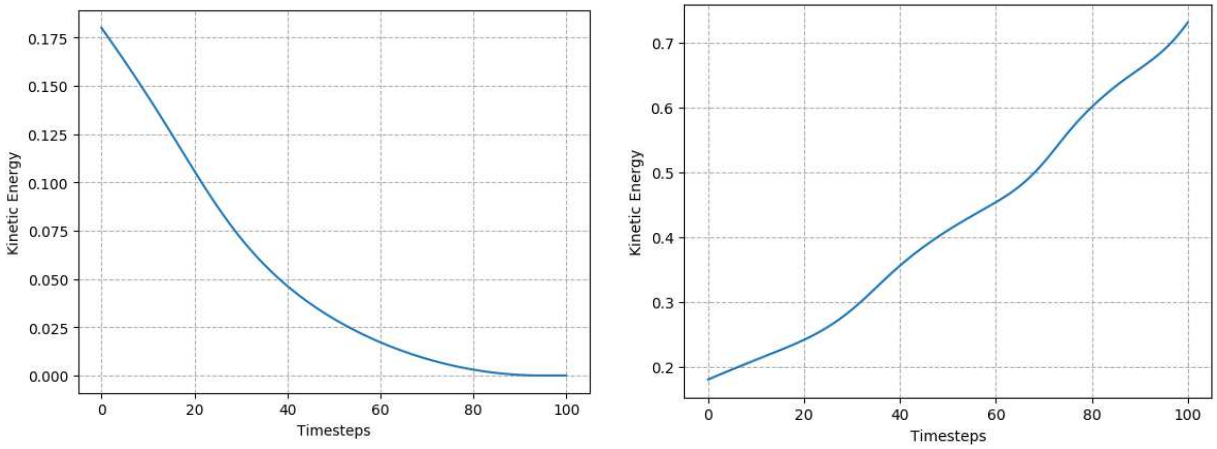

(a) One particle cooling.

(b) One particle heating.

Figure 5.2: Kinetic energy in dependence of time during the cooling procedure (in arbitrary units), for $N = 10$ (number of input modes). At each time step the optimized input state gets injected into the system.

geometric aspects (in our finite system) and will be discussed in the upcoming sections 5.2 and 5.3.

Regarding the cooling procedure, at some point the force $F\Delta t$ will be larger than the particle velocity. Then the minimum energy is reached and a further field input beyond this time, leads to an oscillation of the velocity (and the energy) around $|v_{\text{fin}}| \approx |F|\Delta t/2m$. If we want to reach lower values one can naturally decrease the input power P_{in} ($|F| \propto P_{\text{in}}$) or the length of the time step Δt. A cooling procedure, where the input power of the field gets reduced, according to the velocity, will be presented in section 5.4.

In addition, one can also represent this quadratic behaviour by looking at the corresponding differential equation, where the field force shows against (or in) direction of the velocity e_v^i,

$$m\frac{dv^i}{dt} = F^i(t) \approx \mp|F|e_v^i. \tag{5.6}$$

Furthermore we want to shortly compare the results with those of a randomized field input, described in section 4.2. While by random input states on average the first order term $v_n F_n \Delta t$ in the energy evolution vanishes, the optimal cooling/heating input states just maximize the absolute value of the first order term, see also eq. (5.1). A heating with the GWS-states, figure 5.2b, is surely faster than the small linear increase in figure 4.6.

5.2 State correlation and force oscillation

We check how similar the different optimal input states are to each other, by looking at their correlation between different points in time. Moreover we provide insight into the absolute value of the field force during the cooling and heating procedure.

We consider the test example, which we already used in the last section. The according absolute force $|F|$ acting on the scatterer is plotted in figure 5.3. For both cases (cooling and heating) $|F|$ changes decently with time, which explains the visible deviation from the ideal quadratic curves in the kinetic energy evolution, figure 5.2.

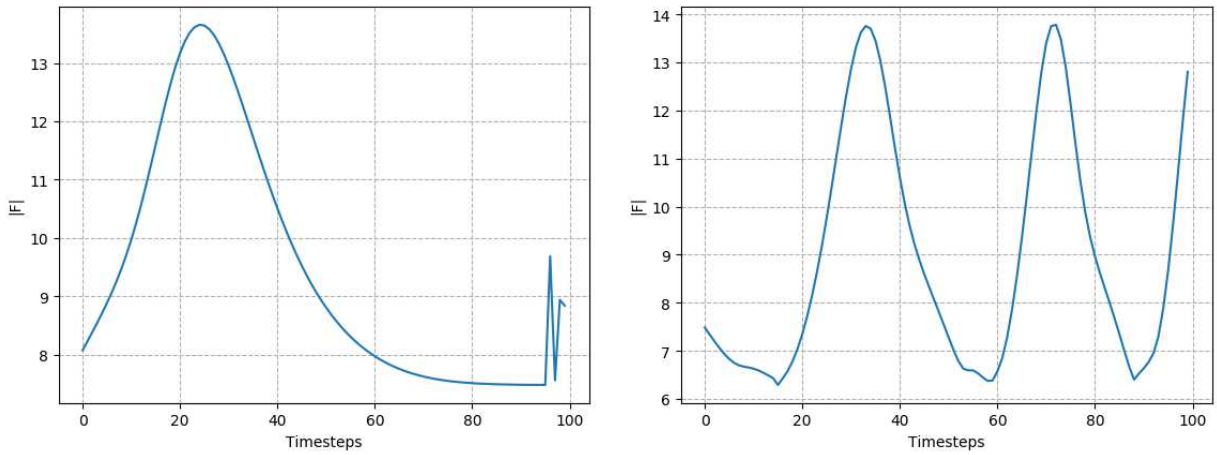

(a) One particle cooling.

(b) One particle heating.

Figure 5.3: Force absolute value in dependence of time during the GWS-time-method, Number of input modes $N = 10$.

These changes occur, because the generated field around the particle is not equally efficient for different moments in time, i.e. for different positions (and also velocity directions) of the particle in the waveguide. For the heating fields the absolute force $|F|$ clearly oscillates, and the "oscillation frequency" increases with the particle velocity. We would see a similar oscillation for the cooling case, if we start with a larger velocity. (The particle was during the whole simulation far away from the waveguide boundaries, the oscillations are seemingly only caused by the finite mode number N.) At the end of the cooling procedure the particle position does not really change much. However the force $F\Delta t/m$ gets larger than the velocity v, thus the velocity direction (and the optimal field configuration) changes rapidly (particle gets pushed too strong), which explains the last few time steps.

A further quantity, which gives insight is the correlation between the different input states. We have chosen the Pearson-correlation-coefficient for the evaluation. In principle it shows how similar the states are on a scale from 1.0 to -1.0 (from identical to completely different or inverted). In figure 5.4 a colormap of the correlation $\langle \Psi_{\text{in}}(t)\Psi_{\text{in}}(t')\rangle_P$ for all moments in time t, t' is presented. (In the diagonal $t = t'$ the coefficient is obviously 1.)

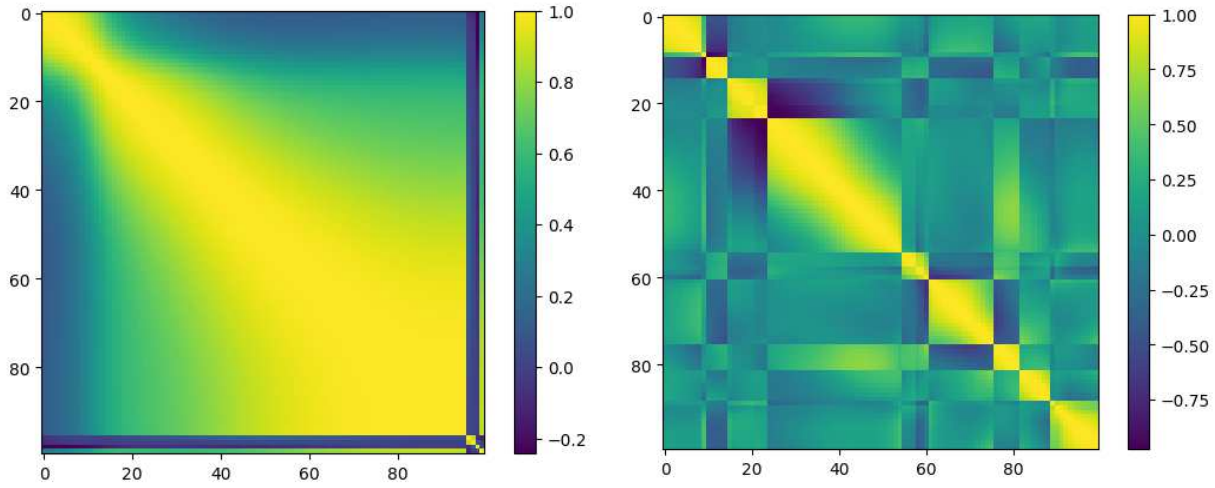

(a) One particle cooling.

(b) One particle heating.

Figure 5.4: Colormap of the Pearson correlation between the field input states for all moments in time t, t' during the GWS-time-method (mean value of the correlation from real and imaginary part of ψ_{in} from both input channels), for $N = 10$. (Yellow means high correlation and blue small too no correlation at all.)

During the cooling procedure the input states can be correlated over long times (depends on the velocity). We see especially, that the correlation broadens with ongoing time (yellow colour), since the particle velocity decreases. For such a case we could imagine, that there might even be a possible continuous transition between the input states (over many time steps). At the end of the cooling the velocity direction starts to oscillate, as described before, leading also to an oscillation of the input states.

During the heating the field input seems to change more rapidly. This might be mainly because of the higher velocities (faster position change) and probably be connected with the limited degree of freedom in the field generation and geometric restrictions, as the according absolute force plot 5.3 suggests. For instance, if we take $N = 20$ modes, instead of $N = 10$, the scattering matrix contains more information (and the wavelength is half as long). Therefore the field might be shaped better around the particle and the force does not oscillate that much in time. On the contrary the state correlation between different time steps might shrink, as there are more degrees of freedom.

5.3 Force direction and geometry influences

For an optimal energy reduction, the generated force should act precisely in the opposite direction of the particle velocity. We discuss the deviations from this ideal behaviour, on the basis of some examples. We will see, that geometric aspects play a relevant role.

In figures 5.5 and 5.6 the angle between force and velocity and the corresponding kinetic energy change $\partial_t E_{\text{kin}}$ are visualised in dependence of the number of input modes N. These

quantities are presented for two different particle sizes and positions, for each number of input modes the optimal cooling state has been injected into the system.

As a reminder on section 3.3, changing the mode number N includes fundamentally two important aspects. With rising N the input field can be adjusted more precisely and also the operation wavelength λ decreases (for fix waveguide dimensions). Thus we will see a combination of two effects in the figures. On the one hand a large number of input modes certainly allows us to adjust the near field around particles better, on the other hand a reduced wavelength leads to smaller field intensity peaks. This also means, the distance between field areas of large and small intensity $|\psi|^2$ shrinks, see for instance figure 5.1.

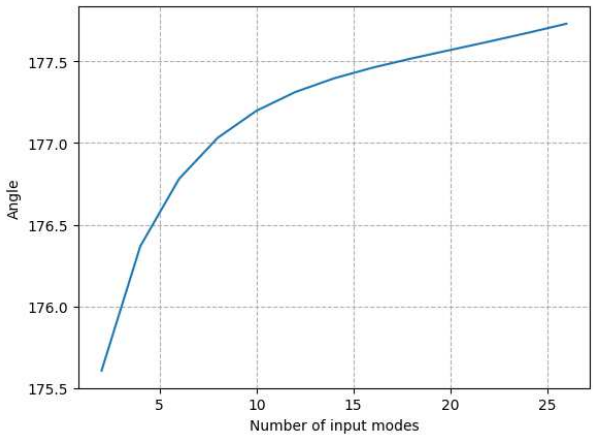

(a) Angle between force and velocity. Particle at the center of the waveguide.

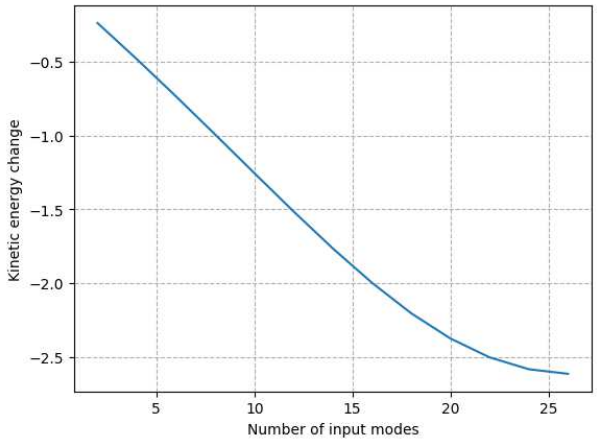

(b) Kinetic energy change. Particle at the center of the waveguide.

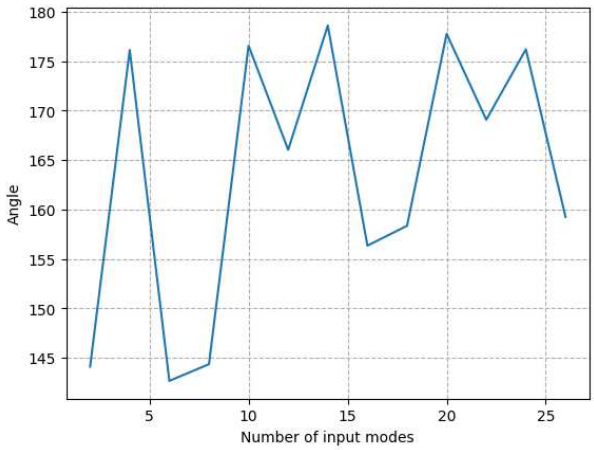

(c) Angle between force and velocity. Particle positioned offcenter.

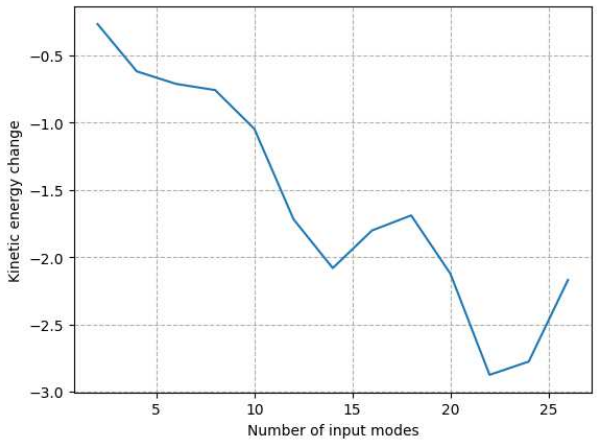

(d) Kinetic energy change. Particle positioned offcenter.

Figure 5.5: Example of force direction and energy transfer for a small particle in dependence of the mode number N, with $r/\lambda < 1$ for all N.

For a small particle, with regards to figure 5.5ab, the size of the field intensity peaks is greater than the particle diameter $2r$ (the force on the particle results primary from one intensity peak) and the angle between field force and velocity as well as the kinetic energy change get optimized with increasing N, as expected. If the particle is not positioned in

the middle of the waveguide, but rather close to the boundary, geometric influences lead to some deviations, see figure 5.5cd.

If the size of the field intensity peaks is smaller than the particle diameter, it is indeed possible, that the kinetic energy change gets worse with increasing N (even when the angle rises), see figure 5.6. The smaller the wavelength is, the more the energy gets distributed in the waveguide.

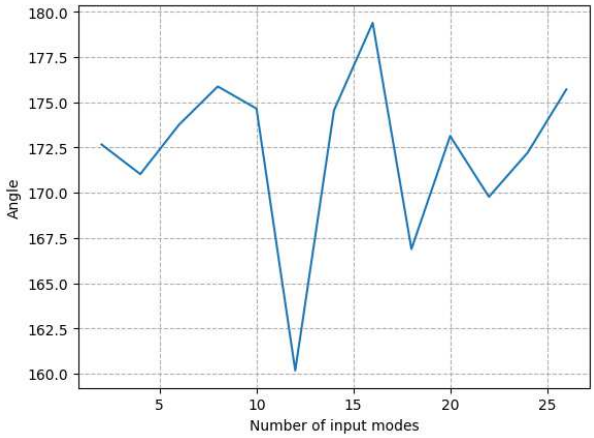

(a) Angle between force and velocity. Particle at the center of the waveguide.

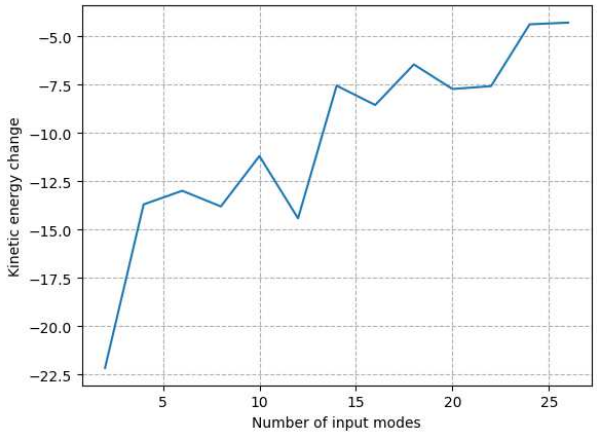

(b) Kinetic energy change. Particle at the center of the waveguide.

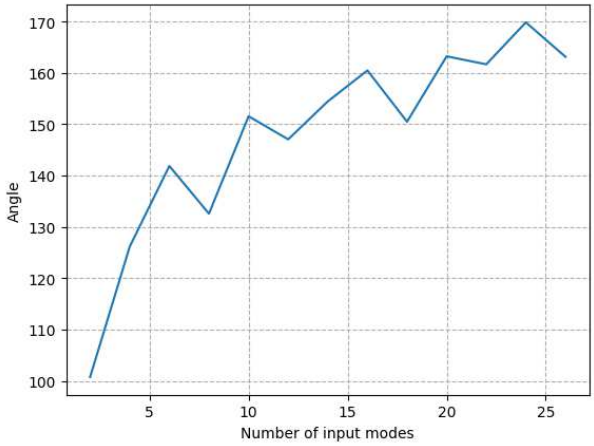

(c) Angle between force and velocity. Particle positioned offcenter.

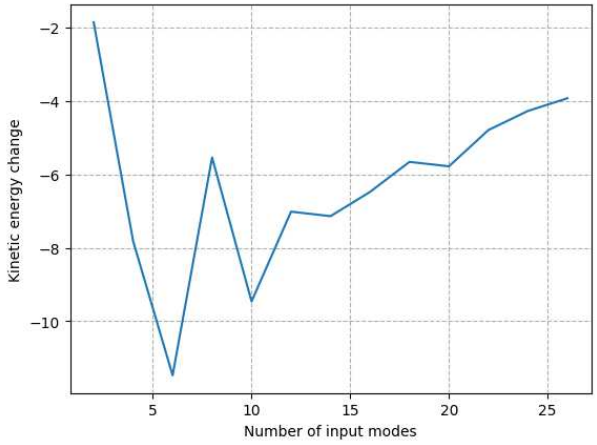

(d) Kinetic energy change. Particle positioned offcenter.

Figure 5.6: Example of force direction and energy transfer for a large particle in dependence of the mode number N, with $r/\lambda > 1$ for all N.

We summarize, there is a relative big impact from the geometry of the system or rather the particle position in our finite system. At least, if a small particle is positioned in the middle of the waveguide, the behaviour is according to expectations. That means the angle between force and velocity, and the kinetic energy change are getting more optimal with a rising number of input modes. The ratio between wavelength and particle radius (for a circular particle) is a relevant quantity for the cooling, as it in principle characterizes how strong the electric field interacts with the particle.

5.4 Input flux regulation

We modify our cooling procedure in order to achieve the best possible conditions. We develop an algorithm, which reduces the power of the input field according to the velocity of the particle, so that the acting force is (ideally) proportional to the velocity. This is of interest, if one wants to achieve a very fast cooling over many orders of magnitude (especially later in many particle systems).

As described in eq. (5.5), the F^2-term reduces the efficiency of the cooling naturally. If we reach velocities in range of the applied force $F\Delta t$, we cannot slow down the particle further. Thus the logical solution is, to scale down the force according to the velocity, which is partly possible with the knowledge of our system, we access via $S(t_n)$. The only additional information we need is the initial particle energy E_0.

We estimate the optimal input power $P = P_{\text{in}}$, via a prediction of the kinetic energy curve $E(t)$ during the cooling. The GWS-Time-relation enables us to estimate the energy change, which the optimal input state $\mathbf{c}$ causes, see also eq. (3.4),

$$E_{n+1} \approx E_n + \frac{P_n}{w}\theta_n^{\min}\Delta t + \frac{1}{2m}|F|^2\Delta t^2, \tag{5.7}$$

where $\theta^{\min} < 0$ is the minimal eigenvalue of Q_t ($Q_t\mathbf{c} = \theta^{\min}\mathbf{c}$). In order to find a condition for the input power, we assume again $Fv = -|F||v|$ and claim $|F|\Delta t = am|v|$, where $a < 1$ is a tunable constant,

$$|F_n||v_n| = \frac{P_n}{w}(-\theta_n^{\min}) \stackrel{!}{=} \frac{a}{\Delta t}m|v_n^2| = \frac{2a}{\Delta t}E_n, \tag{5.8}$$

$$E_{n+1} \approx E_n - 2aE_n + a^2E_n = (1-a)^2E_n = (1-a)^{2(n+1)}E_0. \tag{5.9}$$

Therefore the input power should be regulated like the following,

$$P_n \approx \frac{2aw}{\Delta t}\frac{E_n}{(-\theta_n^{\min})} = \frac{2a}{\Delta t}wE_0\frac{(1-a)^{2n}}{(-\theta_n^{\min})}. \tag{5.10}$$

At each time step the input power gets modulated in accordance to the current particle energy E_n and its upcoming change $\theta_n^{\min}$, in order to achieve $F_n\Delta t/m \approx av_n$.

The corresponding relation for the absolute value of the input state (input flux $|\mathbf{c}|^2$) is

$$|\mathbf{c}|_n = \sqrt{\frac{2k}{c\epsilon_0}P_n} \approx \sqrt{\frac{aE_0}{\epsilon_0\Delta t}}2k\frac{(1-a)^n}{\sqrt{-\theta_n^{\min}}}. \tag{5.11}$$

In figure 5.7 a comparison of the the cooling with and without the flux regulation is given, the kinetic energy in dependence of time is visualised (logarithmic plot).

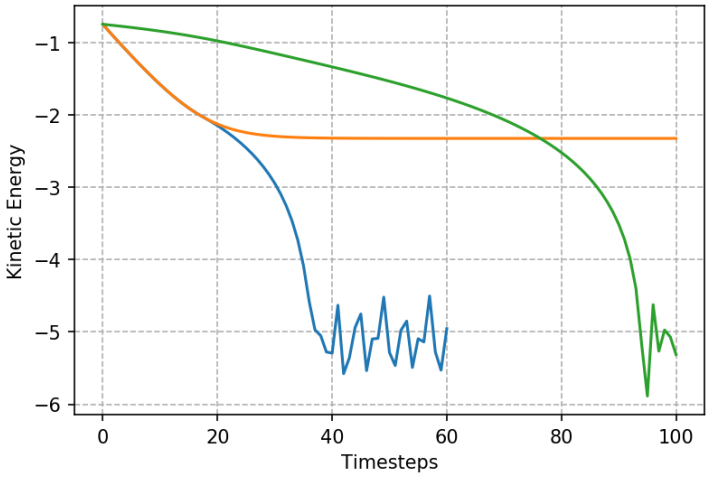

Figure 5.7: Comparison of the energy during the cooling (logarithmic plot). Input flux regulation with (blue curve) and without (orange curve) a minimal flux value; $a = 1/10$. The constant flux (green curve), corresponds to the minimal flux of the blue curve.

As the method is based on predicting E_n, it looses on accuracy for large n, and will stop working, see orange curve in figure 5.7. In this example the kinetic energy decreases only in the first fifteen time steps exponentially. In general the kinetic energy reduction gets slightly overestimated, since the angle between force and velocity is not perfectly 180 degrees (and $\dot{F}$ reduces the cooling efficiency slightly).

Thus we are able to control and modulate the strength of the field force only for a limited time. Since the error increases with the number of time steps, one might change the input power until a fixed minimal value is reached. Thereby we achieve a faster de-acceleration of the particle, reaching a known (magnitude of the) final velocity, as the blue curve in figure 5.7 shows. The green curve corresponds to a constant input power.

The ideal exponential decrease of the kinetic energy can also be described by the according differential equation,

$$\frac{dv^i}{dt} = \frac{F^i}{m} \approx -a\frac{v^i}{\Delta t}, \tag{5.12}$$

and equation (5.9) might be evolved for small parameter a,

$$E_n \approx (1-a)^{2n} E_0 = e^{2n\ln(1-a)} E_0 \approx e^{-2na} E_0. \tag{5.13}$$

For the one particle case, the regulated force acts ideally like a frictional force. If we compare eq. (5.12) with the friction term in eq. (1.32), one might denote a field friction constant $\gamma_a = a/\Delta t$. Moreover, instead of changing the input power one could also regulate the length of the time step Δt in equation (5.10).

It is noteworthy, if we want to appropriately reduce the force for a long time, we could also measure $|F|$ during the cooling. This requires further test measurements (test input fields), in order to estimate the second derivative of the kinetic energy $\partial_t^2 E_{\text{kin}}$ [15].

Therefore we can achieve quite a good control over the cooling, if needed. However, in most cases a straight-forward approach with a constant input power and time step length leads to convenient results. It turns out, that a small modification in the presented flux regulation leads to an effective and more stable energy reduction in the many body scenario, see section 6.4.

5.5 Two particles: Translation and Rotation

We consider a second moving particle and show the optimal cooling field configuration. Here the second particle shall have a more complex shape and perform a rotation movement around its center of mass. The two particle behaviour gives already many indications, how many-body cooling will work out.

In figure 5.8 an example for an optimal field configuration, reached via our GWS-time-method, is given. The light field tackles both particles efficiently. The translation of the circular particle as well as the rotation of the other one (S-shape) gets counteracted.

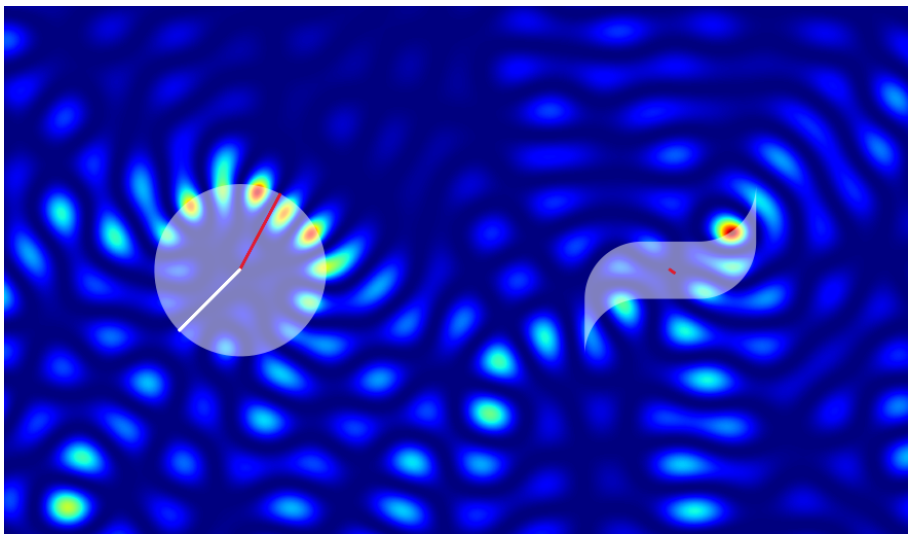

Figure 5.8: Field configuration around the particles, for an optimal reduction of their kinetic energy. Number of input modes $N = 20$.

If we make the comparison with the single particle case, figure 5.1b, one notices, that the field tackles now each particle slightly less efficiently. The field has not enough degrees of freedom to reduce the velocity of each particle on its own perfectly, instead the collective movement (the kinetic energy of the particle system) will be reduced optimally.

For example, if one particle is way faster than the other, it is very likely, that only this particle gets focused by the light field, until both particles have comparable energy (or rather velocities). Therefore such optimal field configurations are non-trivial, to the point, where one can hardly see their efficiency with the naked eye, in many particle systems.

It is worth mentioning, that particles with complex shapes can only be tackled well by the light field, if the size of the field intensity peaks (limited by the wavelength) is in range or smaller than the particle area to resolve. For instance, for the used S-shape structure, the field needs to be able to focus upon particle boundary areas with a large lever, in order to de-accelerate the rotation. That means a small enough wavelength is important and a decent number of input modes is of advantage.

Furthermore we can also enhance the particle movement, for this case the field intensity peaks will be on the other side of the scatterers. However, if one particle gets tackled slightly better than the other, at some point only the faster particle will be accelerated even more. Such velocity differences between the scatterers might only be cured through collisions between them.

5.6 Perturbation approach for $\epsilon_s \approx 1$

This section shall make clear, that the optimal many-body states, which we construct from the change of the scattering matrix, are indeed special. We try to reproduce an optimal two particle state as a superposition of optimal one particle states. We will see, that this hardly works, even in special conditions.

We consider a symmetrical system of two identical, circular scatterers. The particles shall not change the field flow significantly, i.e. their relative permittivity needs to be near to one, $n_s = \sqrt{\epsilon_s} = 1.01$. Under these conditions we try to recreate the optimal cooling field configuration, visualised in figure 5.9b. The optimal one particle configuration for the left scatterer is plotted in figure 5.9a, the one for the right scatterer is the mirror-inverted.

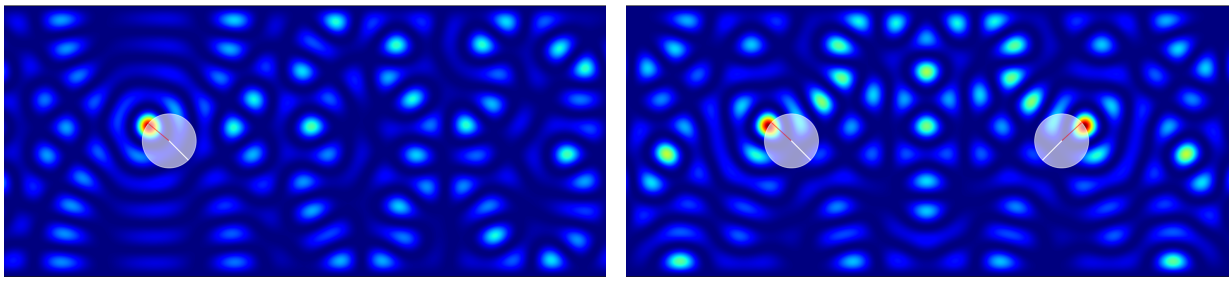

(a) One particle optimization. (b) Two particle optimization.

Figure 5.9: Field intensity configurations for $N = 10$ and $n_s = 1.01$, reached via an injection of the optimal cooling state. The white line indicates the velocity direction, the red line the force direction.

This special symmetry is not needed, but it makes things simpler (same input from both channels). It is clear, that both particles get tackled equally strong by the field. For a reconstruction attempt the equally weighted superposition of the optimal one particle states $\mathbf{c}_1$ and $\mathbf{c}_2$ is the reasonable choice, $\mathbf{c}_\mathrm{m} \propto \mathbf{c}_1 + \mathbf{c}_2$. With this input state we indeed achieve a very similar field configuration as in figure 5.9b (one can hardly see the difference

in the field intensity). However, this input field is quite different from the optimal one, input state $\mathbf{c}_{\mathrm{id}}$, see figure 5.10.

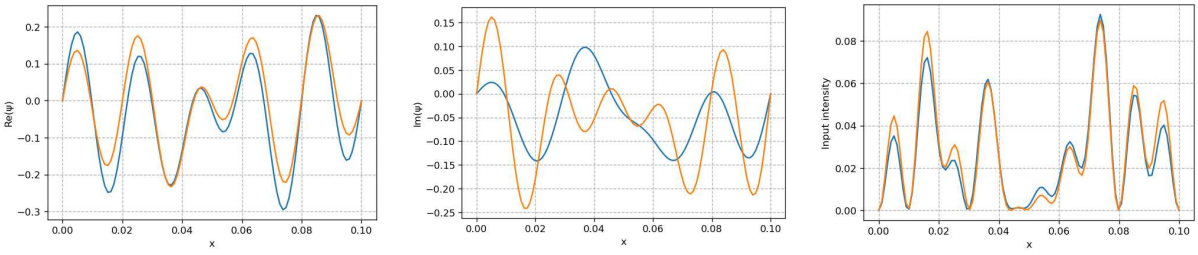

(a) Real part of ψ_{in}. (b) Imaginary part of ψ_{in}. (c) Input intensity $|\psi_{\mathrm{in}}|^2$.

Figure 5.10: Cross-sectional distributions of the input field ψ_{in}. The blue curves corresponds to the optimal state $\mathbf{c}_{\mathrm{id}}$, the orange curves to the mixed state $\mathbf{c}_{\mathrm{m}}$.

The imaginary part of the field inputs differs strongly. Only the input intensity of both states is very alike, that seems to be enough in order to get a similar intensity configuration inside the whole waveguide. The according change of the particle energy is only a little smaller, $\partial_t E(\mathbf{c}_{\mathrm{m}})/\partial_t E(\mathbf{c}_{\mathrm{id}}) \approx 0.96$.

In accordance to quantum mechanics the mean field intensity is invariant under a phase transformation $e^{i\varphi}$ of the field ψ. However a global phase transformation will not make $\mathbf{c}_{\mathrm{m}}$ similar to $\mathbf{c}_{\mathrm{id}}$. One also might think, that a relative phase in the superposition, like $\mathbf{c}_{\mathrm{m}} = \mathbf{c}_1 + e^{i\varphi}\mathbf{c}_2$, leads to convenient results. But this is not the case, the even superposition is the best approach. (At least in the simulations when the phase is fixed.)

It is noteworthy, if we consider a system with different particle velocities $|v_1| > |v_2|$, the appropriate one particle superposition is not simply $\theta_1\mathbf{c}_1 + \theta_2\mathbf{c}_2$, where θ_i are the corresponding eigenvalues to $\mathbf{c}_i$. The optimal two particle field focuses even stronger on the faster particle, i.e. $\mathbf{c}_1$ need to be weighted more strongly.

To sum up, we are not able to recreate the optimal input state via superposition, however one can achieve similar intensity configurations, leading to a slightly smaller kinetic energy change of the two particle system. If the dielectric function differs strongly from vacuum, a superposition approach results in very different intensity configurations. Even with more knowledge of such a system, there might be no easy way to reconstruct the optimal many-particle state, as the forces on the different scatterers are correlated (one needs to examine the system in its entirety).

Chapter 6

Many-body light cooling

In this section we finally consider the cooling of a many particle system. We begin with ten moving particles in the waveguide, then we compare the cooling results with the outcomes of randomized field configurations and a constant plane wave input. Furthermore, we test the robustness of the cooling procedure in the cases of restricted mode access, absorption and complex shaped particles. Afterwards we showcase a regulation of the input power, for appropriate magnitudes of the field forces, and discuss the cooling for large particle numbers.

6.1 Ten particle cooling

We show some results of the cooling procedure for a system, which contains ten identical circular dielectric particles. Regarding the electric field input into the waveguide, we work again with constant input power P_{in} and pulse period $\Delta t = \Delta t_{\text{puls}}$.

Initially the scatterers are placed at random positions in the middle section of the waveguide with randomized velocities (with a defined maximal absolute value). As documented in section 3.2, we are able to slow down the particles through injections of optimal input fields, based on the changes of the system's scattering matrix $S(t)$.

Figure 6.1 shows examples of the optimal field configuration (intensity $|\psi|^2$) around the particles, during the cooling procedure. The corresponding time dependence of the kinetic energy is visualised in figure 6.2.

During each time step Δt only few particles get tackled strongly by the field. The (stationary) field can not de-accelerate all particles at the same moment. Out of all possible configurations, the one, which decreases the kinetic energy of the particle system the most, will be chosen. That means faster particles will get focused more likely. However, there is always the possibility, that each scatterer in a set of particles get slowed down partially and only their collective motion is reduced optimally.

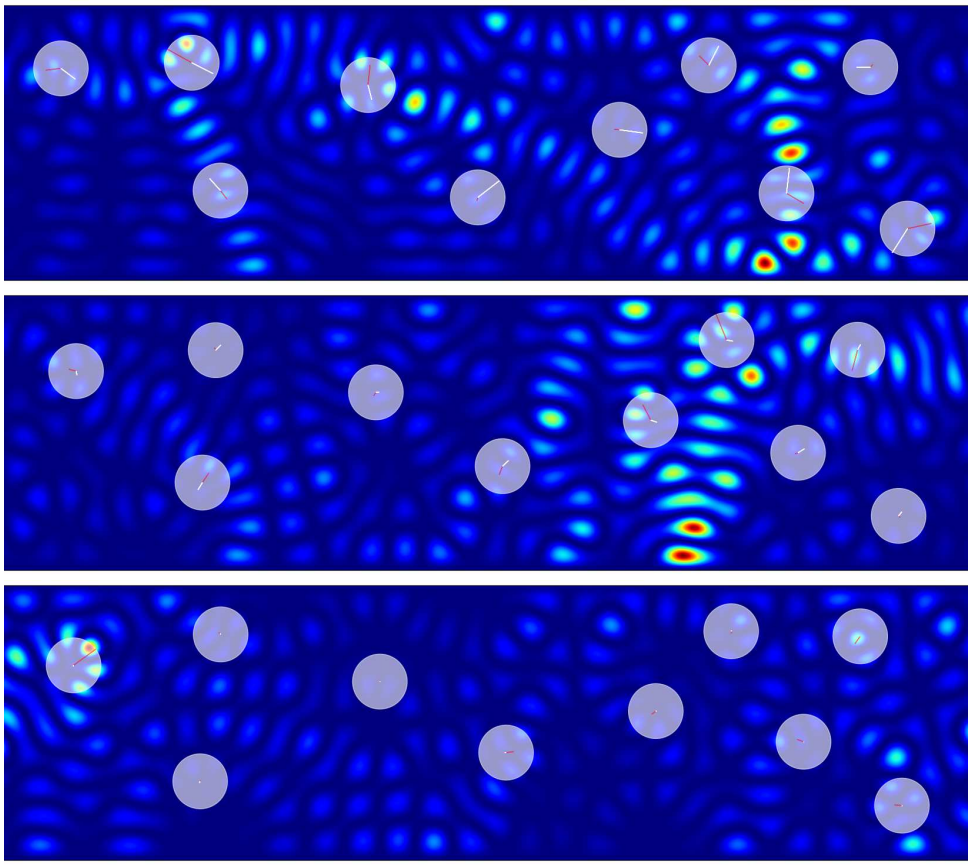

Figure 6.1: Examples of the field configuration $|\psi|^2$ during the cooling, created via injection of the respective optimal input state $\mathbf{c}$, for $N = 10$ input modes. The white lines indicate the velocity directions, the red lines the directions of the field force.

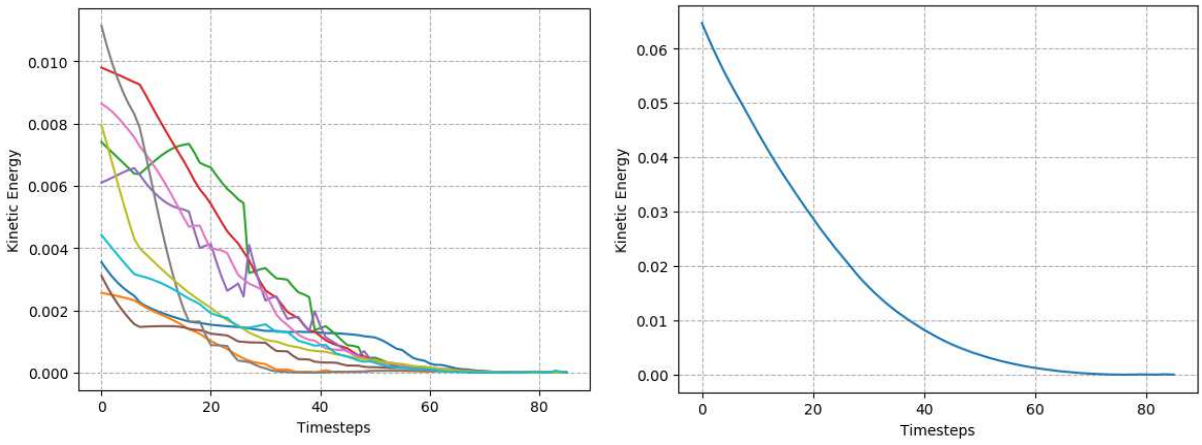

(a) Kinetic energy of each particle.

(b) Sum of the particle Energies.

Figure 6.2: Kinetic energy in dependence of time during the cooling procedure (in arbitrary units), for a system of ten particles. Number of input modes $N = 10$.

The time dependence of the system's kinetic energy, plotted in figure 6.2b, is very similar to the single particle case, see figure 5.2a. The energy decreases steadily until the particle velocities have reached the magnitude of the field force, $mv_{\text{fin}} \approx |F|\Delta t$. However, the behaviour of the kinetic energy of each of the ten particles is not necessarily monotonic. For instance, during some time steps a particle gets heated, so that other particles can be cooled down better, as visualised in figure 6.2a.

The kinetic energy of an N_p particle system, during the cooling, can be described by a recursive Taylor series. The energy after the n-th time step is

$$E_{n+1} \approx \sum_{i=1}^{N_p} \frac{1}{2} m_i v_{n,i}^2 + v_{n,i} F_{n,i} \Delta t + \frac{1}{2m_i} F_{n,i}^2 \Delta t^2 \tag{6.1}$$

$$= E_n + \frac{P_{\text{in}}}{w} \theta_{\min,n} \Delta t + \sum_{i=1}^{N_p} \frac{1}{2m_i} F_i^2(\mathbf{c}_n) \Delta t^2. \tag{6.2}$$

As a reminder, here P_{in} is the input power and w is the oscillation frequency of the input field. $F_{n,i}$ is the field force, acting on the i-th particle with velocity $v_{n,i}$. At each time step Δt the current eigenvector $\mathbf{c}_n$, corresponding to the minimal (maximal negative) eigenvalue $\theta_{\min,n}$ of the kinetic operator Q_t gets injected into the system.

The correlation between the different input fields $\psi_{\text{in}}(\mathbf{c}_n)$ might give a further insight in the cooling procedure. In figure 6.3 a colormap of the Pearson-correlation-coefficient $\langle \Psi_{\text{in}}(t) \Psi_{\text{in}}(t') \rangle_P$ for all moments in time t, t' is presented (in the diagonal $t = t'$ the coefficient is obviously 1, see also section 5.2 for the one-particle case).

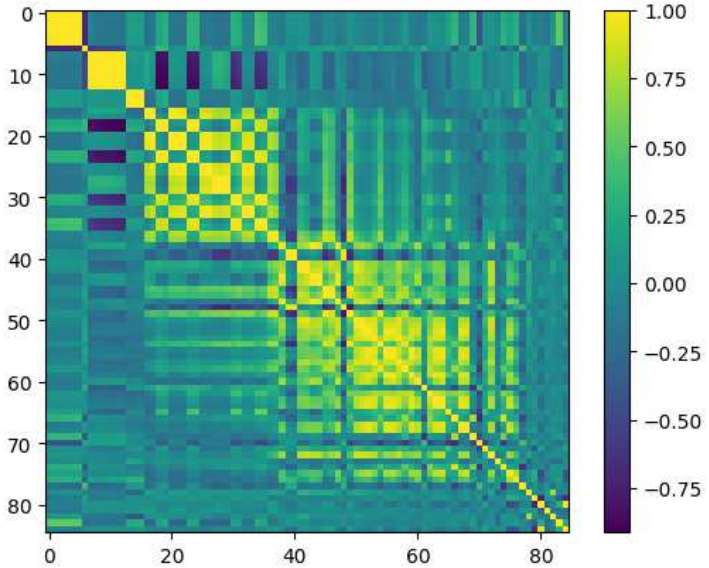

Figure 6.3: Colormap of the Pearson correlation between the field input states for all moments in time t, t' (mean value of the correlation from the real and imaginary part of ψ_{in} for both channels), $N = 10$.

At the beginning the states are correlated for some time steps, since the particles have different initial velocities $|v|$. That means the one or two fastest particles might be tackled at first, until a tackling of other particles leads to a similar energy reduction. After some time many particles have a similar absolute velocity, and it gets very likely that the optimal state focuses on another set of particles at each time step. Sometimes input states might even oscillate between different sets of particles, which would explain the large oscillation in their correlation (repeated change between yellow and blue areas). Therefore (at least) our static optimization makes a pulsed operation unavoidable.

Note, during the shown example no collisions between particles occurred, however they can influence the cooling efficiency (especially for greater particle numbers) and will be discussed in section 6.5. Lastly we want to compare the results of our cooling procedure with the one of a randomized or a constant input field, as described in section 4.3. If we compare the field configurations (figures 6.1, 4.8 and 4.9), one sees with the naked eye, that the field intensities are way more focused during the cooling procedure (with fewer, but spatially resolved peaks). An arbitrary random or constant input leads to a more chaotic field configuration, the field (energy) gets distributed more strongly in the waveguide. While such chaotic fields lead usually to a small increase in the particle energy (figure 4.10), the optimal cooling states enable us to reduce the kinetic energy over many magnitudes (see figure 6.2 and also section 6.4). In chapter 7 a (short) second comparison based on a further example will be given.

6.2 Robustness of the cooling

Here we test the cooling procedure for different restrictions, that might be present in realistic or reachable scenarios. The initial particle positions and velocities shall, however, be the same, as in the last section.

At first we look on the cooling efficiency in dependence of the number of input modes N. Figure 6.4 shows the time dependence of the kinetic energy for different mode numbers. The logarithmic plot makes the different curves more visible. For all curves, the input flux $|\mathbf{c}|^2$ has been held constant. Additionally the reached final energy after the cooling and the required time duration are plotted.

One sees, that the efficiency of the cooling does not depend strongly on the mode number. There is naturally a minimal value of N, for our example 4 input modes might be insufficient (blue curve), however $N = 6$ leads already to convenient results (orange curve). As we work here with relatively big particles (in comparison to the wavelength of the input field), higher mode numbers lead actually to longer cooling times (and a smaller final energy). That is the case, since the operation wavelength decreases with N, as already discussed for the single particle scenario in section 5.3. On the one hand the field needs enough degrees of freedom, on the other hand a small wavelength leads to a stronger distribution of the field energy in the waveguide (which can result in smaller field forces).

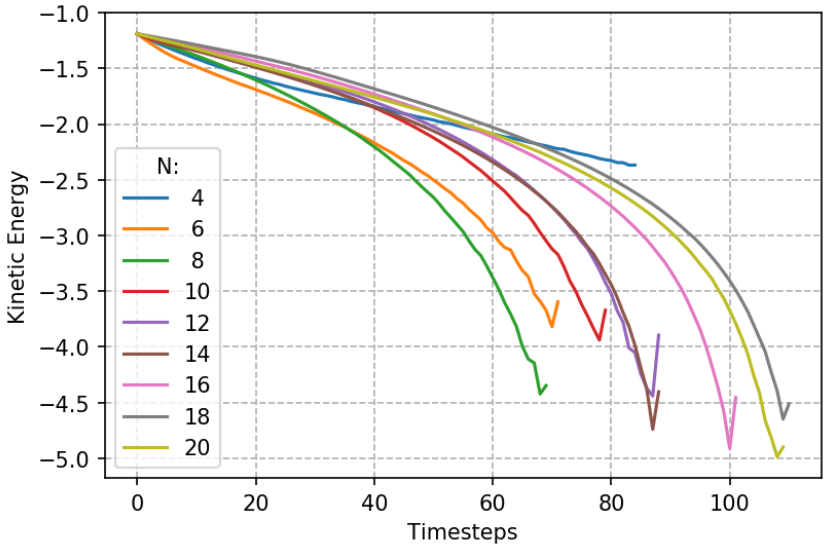

(a) Kinetic energy (logarithmic plot). Each curve corresponds to another mode number.

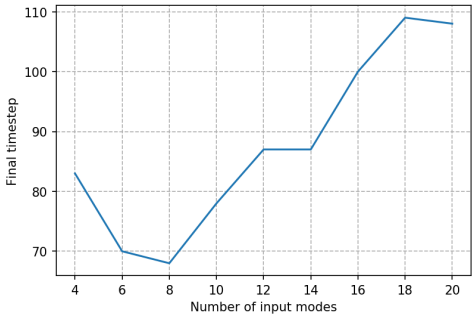

(b) Duration of the cooling.

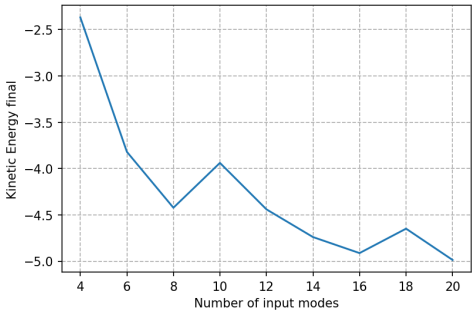

(c) Reached final kinetic energy.

Figure 6.4: Behaviour for the different number of input modes N. Cooling procedure for a ten particle system.

We now consider a scenario, where we have incomplete access to the scattering matrix S. We assume, that we are not able to measure (or control) all possible N modes in the channel. Instead we have only access to the first M modes, i.e. we are only able to use the information in S regarding these modes. From the changes in this sub-matrix S_{sub} of S, we approximate an incomplete GWS-time-operator $-iS_{\text{sub}}^{-1}\partial_t S_{\text{sub}}$ and inject the eigenvector, corresponding to the eigenvalue with the most negative real part, into the system. The results for a different number of used modes M out of $N = 20$ are visualised in figure 6.5.

The smaller M is, the longer the cooling takes (until the minimal energy is reached, further cooling durations lead only to oscillations in E_{kin} for constant input flux and time step length). At some point, there is too little information for a consistent cooling of the particles. In our example, this is the case for $M = 10$ (green curve), as the minimal energy value is not stable (i.e. the cooling depends too strongly on the particle positions).

Thus, at least in this example, our cooling method seems to work well, even if we are not able to evaluate few transitions from input to output modes (entries of S) correctly.

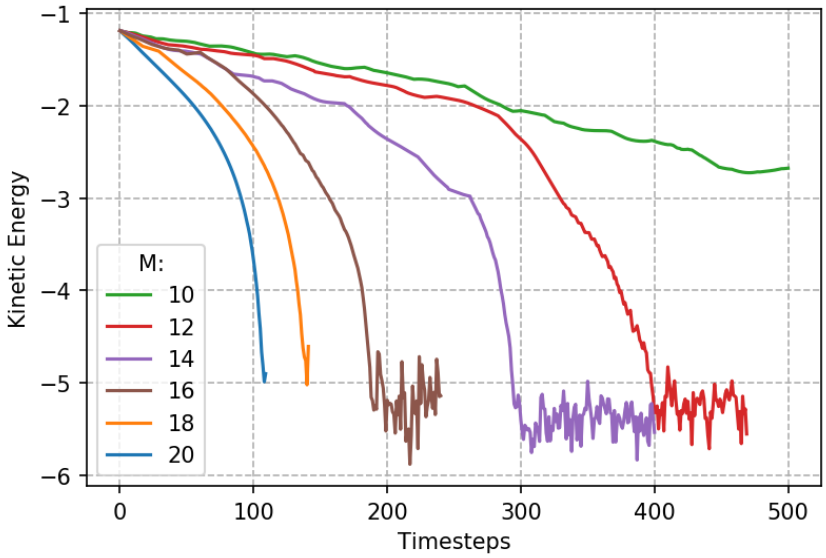

(a) Kinetic energy (logarithmic plot). Each curve corresponds to another number of used modes.

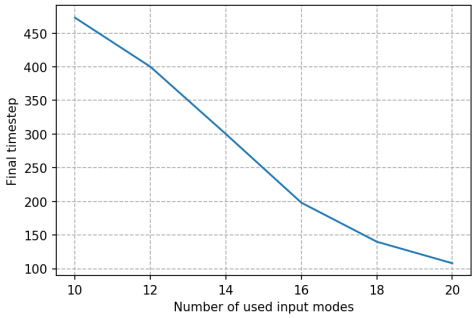

(b) Duration of the cooling.

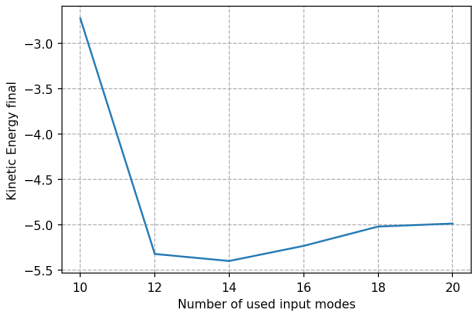

(c) Reached final kinetic energy.

Figure 6.5: Behaviour for the different numbers of used modes M out of $N = 20$ input modes. Cooling procedure for a ten particle system.

The next test we consider is small absorption of the field inside the dielectric matter. The absorption in the particles might be described through a complex refractive index $n_s = n_1 + in_2$. The stronger the field gets absorbed, the weaker is the resulting optical force. The remaining field force on the respective particle can be written as

$$F^i = \frac{\epsilon_0}{4}(\Re(n_s^2) - 1) \int_{\partial V} |\psi|^2 dA^i = \frac{\epsilon_0}{4}(n_1^2 - n_2^2 - 1) \int_{\partial V} |\psi|^2 dA^i. \tag{6.3}$$

The non-vanishing imaginary part n_2 of the refractive index reduces F^i and leads furthermore to a non-unitary scattering matrix $S^{-1} \neq S^\dagger$, since a part of the field input (flux) gets absorbed in matter. The GWS-time-relation (2.25) changes, and the GWS-time-operator Q_t is non-hermitian (complex eigenvalues). The results of the cooling procedure in dependence of n_2 are visualised in figure 6.6. Each time step we injected the eigenvector of Q_t, corresponding to the eigenvalue with the smallest (most negative) real part, into the system.

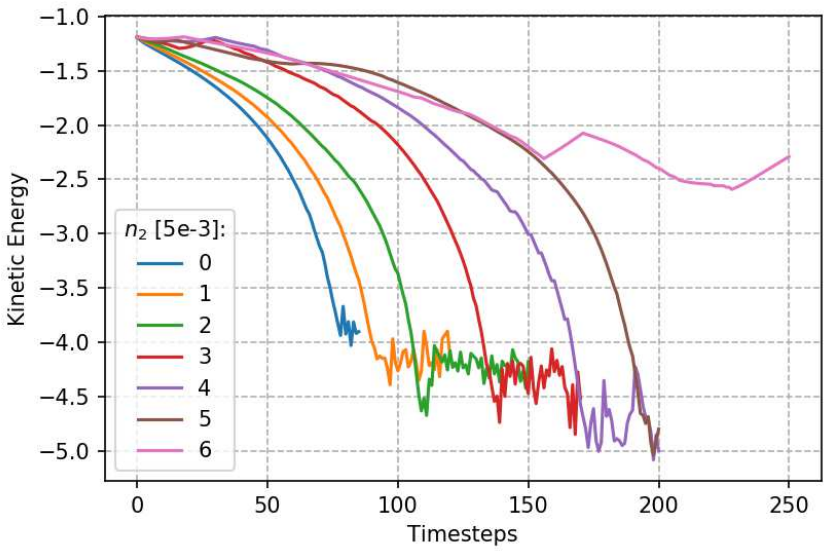

(a) Kinetic energy (logarithmic plot). Each curve corresponds to another imaginary part of n_s.

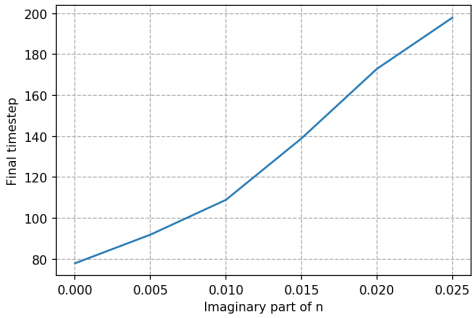

(b) Duration of the cooling.

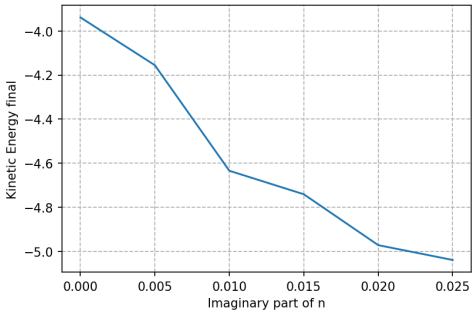

(c) Reached final kinetic energy.

Figure 6.6: Impacts of absorption in the particles, modelled through the imaginary part of the refractive index. Cooling procedure for a ten particle system and $N = 10$ modes.

For $n_1 = 1.44$, with increasing n_2 (from zero in steps of $5 \cdot 10^{-3}$) the cooling takes longer, and accordingly smaller energy values are reached, since the force on the particles decreases. The cooling fails at $n_2 = 0.03$ (pink curve), as the kinetic energy seems not to converge to a stable value. At this point too much information is lost, due to the damping of the electric field in matter.

It is worth mentioning, that the absorption losses depend on the size of our particles as well as on the wavelength of the electric field. For instance, for a plane wave the field amplitude declines exponentially in matter $\psi_{\text{test}} = Ae^{in_s k^j r^j} = Ae^{in_1 k^j r^j} e^{-n_2 k^j r^j}$. Thus we are able to reach higher imaginary parts of the refractive index, if the ratio between wavelength and particle radius is smaller. We present such a regime in chapter 7, where we evaluate (amongst other things) the robustness of our cooling procedure analogously on another example.

6.3 Complex shaped scatterers

Until now we worked with identical circular particles. In this section we want to show, that our cooling procedure still gives good results, if the scatterers have complex shapes and inherit a more complex movement. In a gas of arbitrarily shaped particles, the kinetic energy of the particles is distributed in translation and rotational motion (energy).

In order to test our cooling method for complex particle shapes, we consider a test example of ten particles, with three different shapes (circle, square and "S"-shape) in different particle sizes. We compare the cooling outcomes for different forms of motion and simpler shaped particles, see figure 6.7.

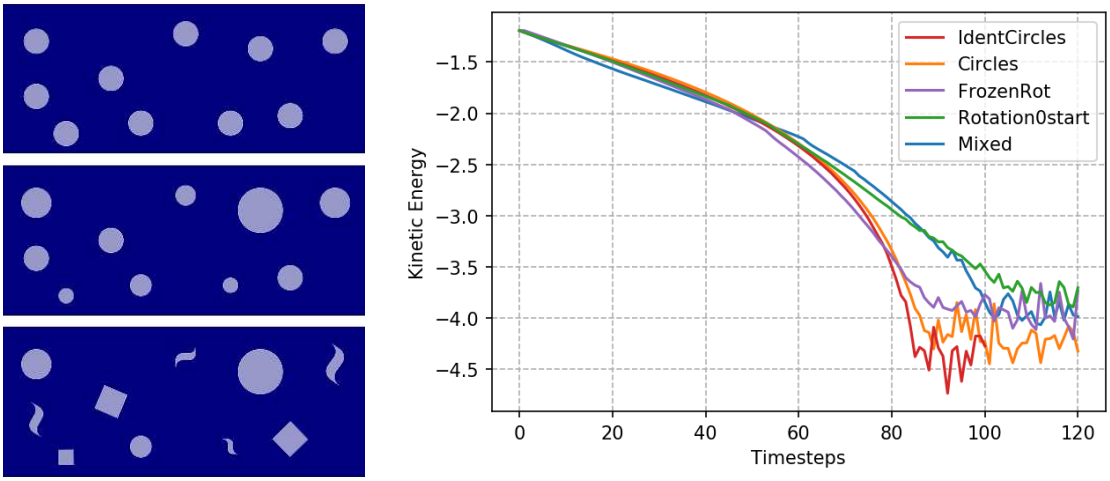

(a) Comparison between the different used shapes.

(b) Kinetic energy (logarithmic plot). Each curve corresponds to another scenario.

Figure 6.7: Behaviour for different particle shapes and movement. Cooling procedure for a ten particle system and $N = 10$ modes, $n_s = 1.44$. The different curves in b) correspond to identical circles (red), different sized circles (yellow) and complex shapes with frozen rotation (purple), no initial rotation (green) and mixed initial motion (blue).

In figure 6.7a the different particles are shown in the waveguide (initial particle positions). We consider the cases of identical circles, different sized circles and complex shapes. The corresponding behaviour of the kinetic energy during the cooling procedure is visualised in figure 6.7b, where some scenarios are compared (starting with the same initial energy). While the cooling of identical and different sized circles takes the least amount of time (red and yellow curve), the complex shaped scatterers only take a little longer to cool down (blue curve).

Here, also additional curves are shown for other velocity distributions. The green curve corresponds to no initial rotation movement and the purple curve shows the outcome, if the rotation degree of freedom is frozen during the whole procedure. This is not physical, as the field forces will certainly act a small torque on the squares and the S-shapes. Nevertheless, it makes clear, that the cooling duration increases, if there are more degrees of freedom in motion. Usually the field can't focus on the particle motion precisely, i.e. a

reduction of translation is sometimes connected with a slight increase in rotation motion. Lastly, for the blue curve the corresponding energy distribution is plotted in figure 6.8.

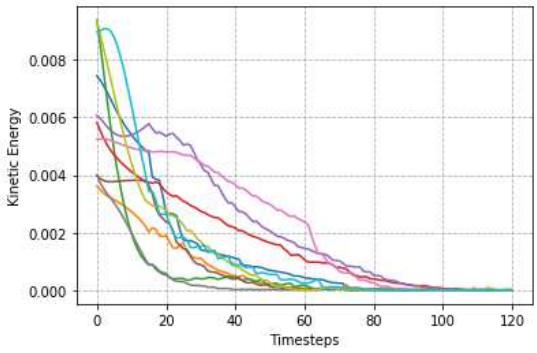

(a) Kinetic energy of each particle. Each colour corresponds to a different particle.

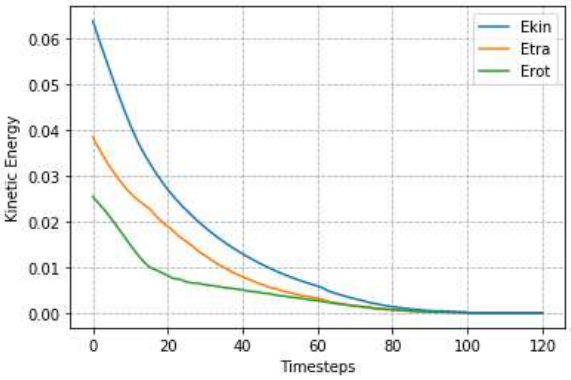

(b) Translation and rotation energy.

Figure 6.8: Cooling procedure for a ten particle system and $N = 10$ modes. Example for complex shaped particles and movement.

It should be mentioned, that we worked, for simplicity, with particles of identical mass (otherwise heavier particles would take longer to cool down, however they would also have smaller velocities in thermal equilibrium). Thus in this section we primarily emphasized, that the different shaped particles can be tackled efficiently by the electric field, while the physical duration of the cooling procedure might vary a bit. Furthermore, as discussed in section 5.5, for an efficient cooling of complex shaped scatterers, the wavelength of the field must be small enough, to resolve certain parts of the particle boundary.

Regarding the implementation for correct simulations, in order to compute the time evolution of the angular orientation (1.31), we naturally need to know the moment of inertia I of the respective particle. For the used shapes (square and S-shape), with a constant mass distribution, I can be calculated analytically.

6.4 Including flux regulation

We now want to discuss one way to get a better control of the cooling. While one might be able to estimate the curvature $\partial_t^2 E_{\text{kin}}$ or rather $|F|^2$ with additional test measurements [15], we make predictions from the initial system energy and its changes $\partial_t E_{\text{kin}}$. In this section we try to reach an exponential decrease of the energy with time, based on the results of the one particle case, see section 5.4.

For the many particle cooling things get much more complicated, as it is basically impossible that all particles get slowed down during the same time step. Instead it is likely, that each optimized input state focuses upon some particles partly. Although we never know the angle between force and velocity (of each particle), we are still able to reach convenient results through a simple modification of eq. (5.10).

We reduce the exponent, until the energy converges to slower values, with an additional tunable constant b. The input power at the n-th time step shall be regulated as

$$P_n = \frac{2a}{\Delta t} w E_0 \frac{(1-a)^{2bn}}{(-\theta_n^{\min})}, \tag{6.4}$$

where $a, b < 1$. As this input flux regulation is quite empirically, there might possibly be a better algorithm, based on clear theoretical assumptions. However, for the right adjustment of b, one achieves indeed an exponential decrease of the kinetic energy, visualised in figure 6.9. Since the time dependence of P_n is not ideal, the energy oscillates a little.

For $b = 1$ the kinetic energy change gets overestimated (red curve), i.e. the input power gets underestimated each step, which leads to an inefficient cooling. A smaller value of b compensates this partly, to the point, where $P_n(b)$ is slightly too big (orange curve). In this case at some point the particles get pushed too strong, this short heating process makes P_n again more appropriate (i.e. we more or less force an exponential decrease of the energy). Thus a correct value of b enables a cooling over many magnitudes, which can hardly be reached with a constant input power.

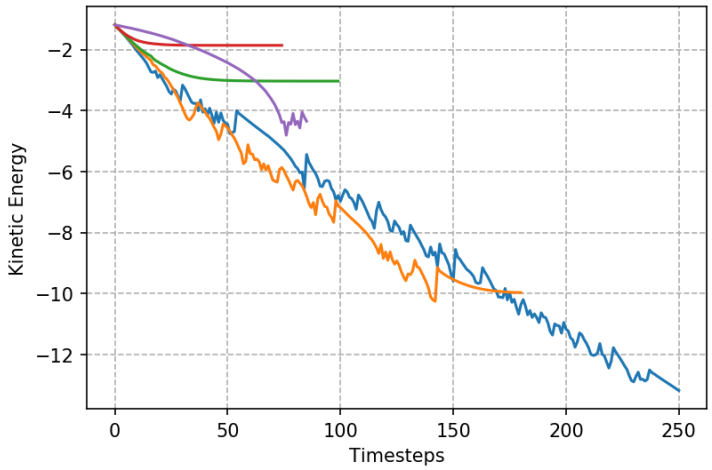

Figure 6.9: Kinetic energy with and without a reduction of the input power during the cooling procedure (logarithmic plot). Ten circular particles and $N = 10$ modes. For a constant value (purple) and regulation with $a = 1/10$ and $b = 1$ (red), $b = 2/3$ (green), $b = 3/5$ (orange), $b = 1/2$ (blue) of the input power.

It is noteworthy, that in general the cooling takes longer, the more particles are contained in the system. The appropriate value of b depends likely on the particle number, but should work for many different particle configurations (positions and velocities) in the waveguide. Moreover, instead of changing the input power (input flux, force), one could change the length of the time step Δt, the optimal input states get injected. However, this should be only done, if one wants to overcompensate other present forces. The smaller Δt is, the less achievable is the procedure in real experiments. Furthermore, at some point n one would need to estimate the GWS-time-operator over a time step $\Delta t_{\text{GWS}} > \Delta t_n$, in order to measure a difference in the scattering matrix S (this is not ideal).

6.5 Cooling efficiency for greater particle numbers

So far we have shown cooling results on a set of ten scatterers. In this section we want to emphasize the efficiency of our cooling procedure in dependence of the number of particles. An example of a system of fourty particles will be shown and a possible particle number limit will be discussed.

The larger the particle number N_p is, the more particles will be tackled only partly and some will even be accelerated by the field during one time step. The amount of particles, that can be tackled precisely (against their velocity direction) is usually very small (one or two). It is clear, that the more complex our system is, the longer the cooling procedure takes. We make general arguments on the basis of the energy evolution during the cooling, see also section 6.1,

$$E_{n+1} \approx \sum_{i=1}^{N_p} \frac{1}{2} m_i v_{n,i}^2 + v_{n,i} F_{n,i} \Delta t + \frac{1}{2m_i} F_{n,i}^2 \Delta t^2 \tag{6.5}$$

$$= E_n + \frac{P_{\text{in}}}{w} \theta_{\min,n} \Delta t + \sum_{i=1}^{N_p} \frac{1}{2m_i} F_i^2(\mathbf{c}_n) \Delta t^2. \tag{6.6}$$

For instance, if we compare the minimal eigenvalues of the GWS-operator (kinetic energy change) of an one- and a two particle system, they often do not differ much. Even though a two particle system has the double kinetic energy, the kinetic energy change $\partial_t E_{\text{kin}}$ is usually only slightly higher than for one particle. That means the (absolute value of the) first order term in the energy evolution increases hardly with N_p. However, if we take a look at the second order term, it increases basically linearly with the particle number N_p.

Thus, the more particles are in the system, the less efficient our cooling procedure becomes. This is only normal, as the field has limited degrees of freedom, the sources of the field (asymptotic input) are far away from the particles. However, if the energy would increase at one time step, one could always decrease the length of the step Δt or the input power, so that the first order term is again dominant.

We now make a simple assumption. We consider a very dense system, high particle number and small system volume. In order to cool down the system, the field only needs to be able to cool one particle decently at every time step, while all other particles get chaotically tackled by the field. The corresponding energy evolution would be

$$E_{n+1} \approx E_n - |v_{1,n}||F_{1_n}|\Delta t + \sum_{i=1}^{N_p} \frac{1}{2m_i} F_i^2(c_n) \Delta t^2. \tag{6.7}$$

That means, a cooling is possible as long the kinetic operator Q_t has a negative eigenvalue (which might be likely for any particle number). However, its efficiency decreases with

N_p, leading to much longer cooling times (and one needs to work with smaller input power or time step length).

Furthermore, between two measurements of the scattering matrix, for the approximation of Q_t, no (or only few) collisions between particles are allowed. Since collisions change the movement of the particles abruptly, they can lead to an inappropriate Q_t. The average time between collisions decreases with N_p, however the duration, an optimized input field gets injected into the system, is often anyway smaller.

Lastly we want to show an example for $N_p = 40$ particles. A cooling field configuration is visualised in figure 6.10, the behaviour of the kinetic energy during the cooling procedure is plotted in figure 6.11. The used time step was taken one magnitude smaller as in the last sections.

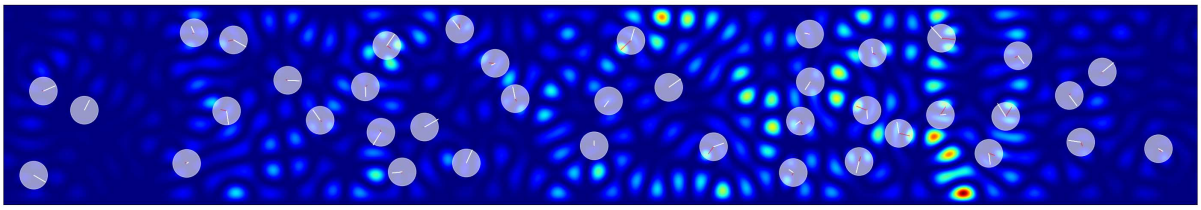

Figure 6.10: Example of an optimal cooling field configuration for a 40 particle system. Number of input modes $N = 10$.

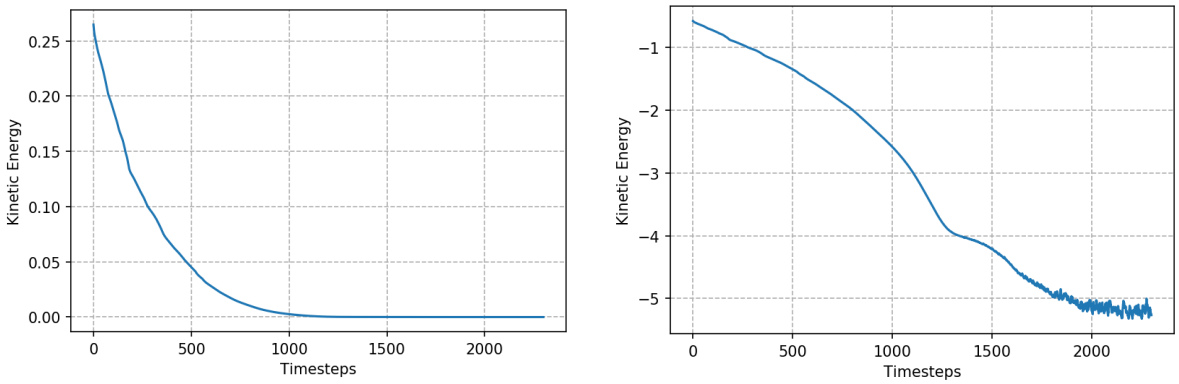

(a) Kinetic energy

(b) Logarithmic plot

Figure 6.11: Kinetic energy during the cooling procedure for a 40 particle system. Number of input modes $N = 10$.

In the appendix A.6 videos of the cooling regarding two different scenarios (of different input power, with and without some collisions) are linked. Few collisions between particles do not really influence the cooling efficiency. We expect, that collisions are mainly relevant, if the optimal field focuses strongly on one of the (in the collision) involved particle, leading in the worst-case scenario to an energy increase at this time step. This should be no big deal, as long as the average time between collisions is larger than the field injection time, see eq. (3.8).

Chapter 7

Simulations with realistic values

In this chapter we want to present some results for realistic values, working in SI units. That means not, that the simulations in the last chapters are unrealistic. We rather work here with a smaller ratio between wavelength and particle radius, with values that are close to those used in experiments. Moreover, we give some possible orders of magnitude for the particle velocities, the duration of the time steps and discuss some error sources of our approach.

7.1 Unit scaling and system values

We discuss and define here the initial values and conditions of our particle system, that we have chosen for the upcoming simulations. Moreover the needed rescaling for the numerical computations will be emphasized.

The higher the mean particle velocity is, the smaller is the feasible injection time Δt_{puls} of the respective optimal cooling state (see section 3.2). Therefore a small initial velocity v_0 is crucial for a first experimental realisation, we consider already pre-cooled particles with velocities around the magnitude $10^{-3} m/s$. Furthermore, as the scattering forces are usually small, it makes sense to work with mesoscopic particles with a small mass m and radius r, in order to reach significant accelerations.

In addition, to make things more realistic, we include an internal damping of the particles (friction force), see eq. (1.32). Since we work in vacuum the friction constant γ is very small and does not really influence our cooling procedure, it only becomes relevant for larger velocities (for instance during heating processes).

In such cases there exist some other cooling approaches (feedback cooling [1][3]), however they are normally restricted to one particle, as the measurement of particle position and motion is required. Thus our cooling procedure might find its place in these conditions. A short introduction to other cooling methods will be given in the next chapter.

We choose the following values for the computation:

$$\begin{aligned} &r = 150\text{nm}, \quad m = 3 \cdot 10^{-17}\text{kg}, \quad \gamma = 6\text{Hz}, \quad \langle v_0 \rangle = 4 \cdot 10^{-3}\text{m/s}, \\ &\lambda = 1064\text{nm}, \quad P_{\text{in}} = 2\mu\text{W}, \quad \Delta t_{\text{puls}} = \Delta t_{\text{GWS}} = 1\mu\text{s}. \end{aligned} \tag{7.1}$$

We selected these values, as they should be reachable (or are already used) in experiments [1][19]. The input power P_{in} has been adjusted so, that the field forces F^i on the particles are about one magnitude higher than gravity.

$$|F| \leq 4 \cdot 10^{-15}\text{N} \quad \Rightarrow \quad |a| \approx 100\text{m/s}^2 \approx 10g. \tag{7.2}$$

Therefore the terrestrial acceleration $g = 9,81\text{m/s}^2$ might be neglected (although we work only in a 2D-scenario and not all particles will sense the forces simultaneously). For these field forces the time step $\Delta t = \Delta t_{\text{puls}}$ was chosen small enough, in order to cool down the systems kinetic energy over some magnitudes. That means the cooling procedure would also work for slightly higher Δt_{puls}, especially for smaller P_{in}.

For $N = 10$ input modes the wavelength λ is defined as above. However if we change the number of input modes (later during the robustness tests), the operation wavelength changes accordingly, see eq. (3.10). That means we decided to let the waveguide (channel) width $W \approx 5,6\mu\text{m} \approx 37r$ constant in all simulations for this chapter. (In contrast the results in chapter 6 are based on a smaller ratio $W/r \approx 10$.)

We are working again with $N_p = 10$ dielectric, circular particles with refractive index $n_s = 1.44$ (similar to silica), initially they are placed (close to each other) in the middle of the waveguide with random velocity directions and absolute values taken as

$$|v_{0,i}| \quad \text{random out of} \quad \left(1 \pm \frac{1}{2\sqrt{N_p}}\right) \cdot \langle v_0 \rangle, \tag{7.3}$$

$$E_0 \approx \frac{N}{2} m \langle v_0 \rangle^2 \widehat{=} N k_B T_0 \quad \Rightarrow \quad T_0 \approx 17.4\text{K}. \tag{7.4}$$

This initial velocity (temperature T_0) might be reached for example through Helium-cooling. Using our cooling procedure, we are then able to cool down the system even further, in principle up to quantum-mechanical limits.

Now we want to talk more about the implementation, for an accurate simulation a rescaling of the system is needed. In particular during the numerical solving of the Helmholtz-equation (1.14), an appropriate reference length scale is indispensable. For a correct rescaling one needs to scale all system values according to their unit dependence with characteristic reference scales (this reduces numeric rounding errors), therefore one speaks often of dimensionless system parameters.

Here it is sufficient to rescale the length (space) of the system, we define our length scale as $R = W/W_s = 5,6 \cdot 10^{-5}\text{m}$, where $W_s = 0.1$ shall be the waveguide width in the

simulation. With R we "erase" the length units of all system values, besides that we work additionally with input fluxes in units of ϵ_0 (i.e. $\epsilon_{0,s} = 1$). From now on the index s denotes the values used in the simulation, while the symbol without the index denotes the unit-dependent realistic value.

$$v^i = v_s^i R, \quad \epsilon_{0,s}|\mathbf{c}|_s^2 = 1, \quad \epsilon_0|\mathbf{c}|^2 = \frac{2k}{c}P_{\text{in}}, \quad F_s^i = \frac{1}{4}(n^2-1)\int |\psi|^2 r_s e_r^i d\varphi, \tag{7.5}$$

$$F^i = \epsilon_0|\mathbf{c}|^2 F_s^i R, \quad v_s^i(t+\Delta t) = v_s^i(t) + \epsilon_0|\mathbf{c}|^2\frac{F_s^i}{m}\Delta t - \gamma v_s^i(t)\Delta t. \tag{7.6}$$

Since $[\epsilon_0|\mathbf{c}|^2/m] = 1/\text{s}^2$, the simulated force F_s^i should be unit-less and can easily be rescaled with R, so that $[F^i/m] = 1\text{m/s}^2$ denotes the correct acceleration. As the input power is given, we might not need to worry about the difference between the 3D-scenario and the 2D-simulations.

7.2 Results

We show the most important results, where we compare the cooling with the injection of a constant input field and test the robustness of our cooling procedure on different scenarios, as in the last chapter.

We shortly re-emphasize our cooling procedure. Each microsecond the scattering matrix S gets measured, for an estimation of the kinetic operator Q_t. The eigenvector corresponding to the most negative eigenvalue of Q_t will be calculated and injected into the system, the same duration $\Delta t = 1\mu\text{s}$ (here again with a constant absolute value $|\mathbf{c}|$). We repeat this procedure until (or beyond) the time, the kinetic energy of the particle system reaches its minimal value.

In figure 7.1 we compare some field configurations during the cooling procedure with the one of a constant plane wave injection (first mode, $c_{i\neq 0,N} = 0$, $c_0 = c_N = |\mathbf{c}|/\sqrt{2}$). The respective behaviour of the particle energy is plotted in figure 7.2. While the intensity peaks of the optimal cooling field configurations are located in such a way, that the silica beads get slowed down the best, the field configuration of the plane wave input changes only because of the movement of the particles (the signatures of the long stretched intensity maxima's of the first mode are visible).

The plane wave input changes the kinetic energy of the system only slightly and apparently chaotically, as visualised in figure 7.2b. With ongoing time the particles get distributed quite strongly in the waveguide, i.e they dissipate from their chosen initial positions (in the middle of the waveguide) in all directions.

During the cooling the particles get slowed down iteratively until their velocities are in range of the field forces, $|v_{\text{fin}}| \approx |F|\Delta t/m$. In our example this takes only two hundred

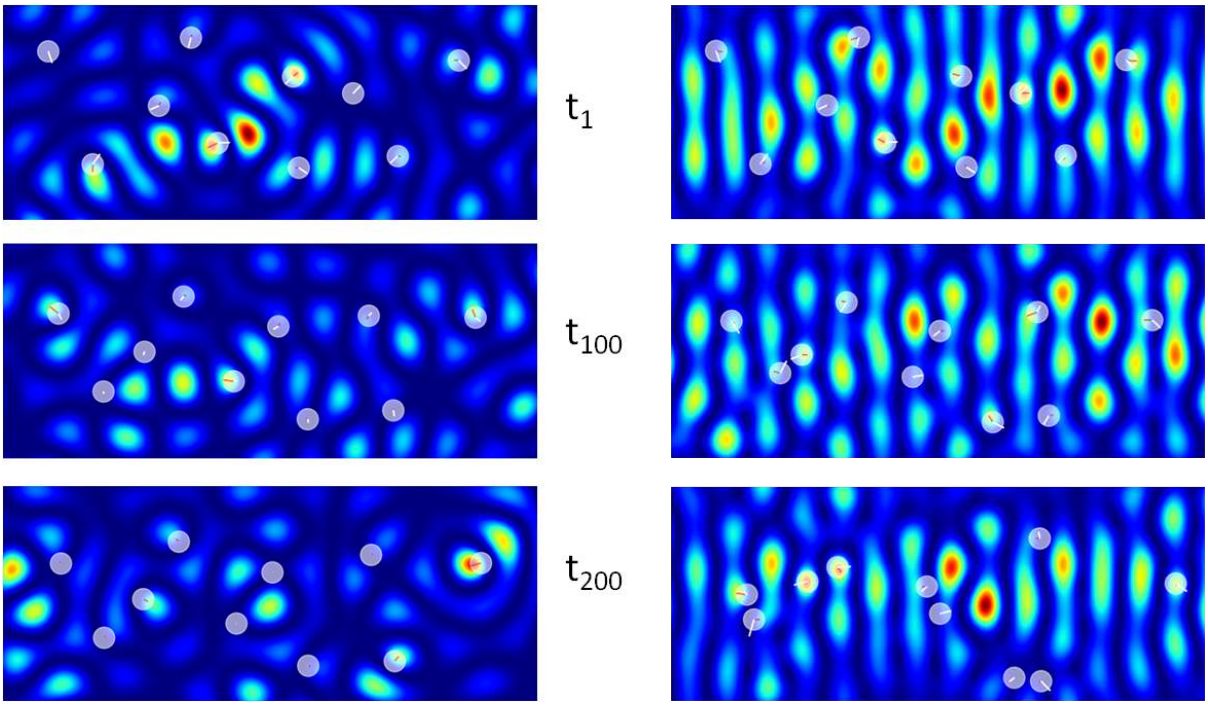

(a) Optimal cooling state injection. (b) Constant first mode injection.

Figure 7.1: Comparison between field intensity configurations $|\psi|^2$ during the time evolution for a ten particle system and $N = 10$ modes.

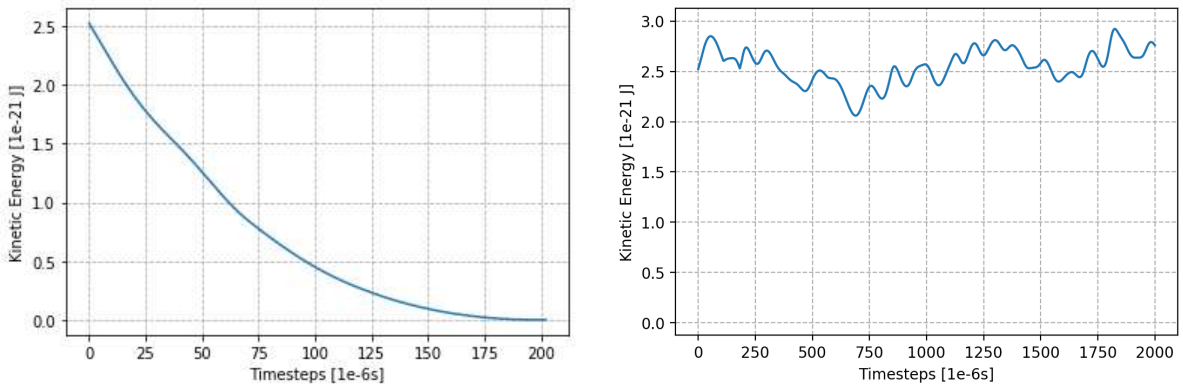

(a) Optimal cooling state injection. (b) Constant first mode injection.

Figure 7.2: Comparison between the kinetic energy evolution for a ten particle system and $N = 10$ modes.

iterations, that means around $2 \cdot 10^{-1}$ms. The field forces are so large, that the particles do not move much in the waveguide. We were able to reduce the kinetic energy from $E_0 \approx 2.5 \cdot 10^{-21}\text{J} \,\widehat{\approx}\, 18\text{K}$ to $E_{\text{fin}} \approx 2.3 \cdot 10^{-25}\text{J} \,\widehat{\approx}\, 1,7\text{mK}$.

The included frictional force is too small in order to play a relevant role, its influence in the reduction of the kinetic energy of the system is beyond one permille, see figure 7.3a. Only for long times during the plane wave insertion there might be a friction limit reachable, as plotted in figure 7.3b. The particles get heated until the damping, due to friction, is of the same magnitude. It must be mentioned, that this required a long simulation time, thus the relative error in the time evolution might be high (some percentages). Furthermore, we had to increase the input power and (most importantly) the friction constant to $\gamma = 100\text{Hz}$.

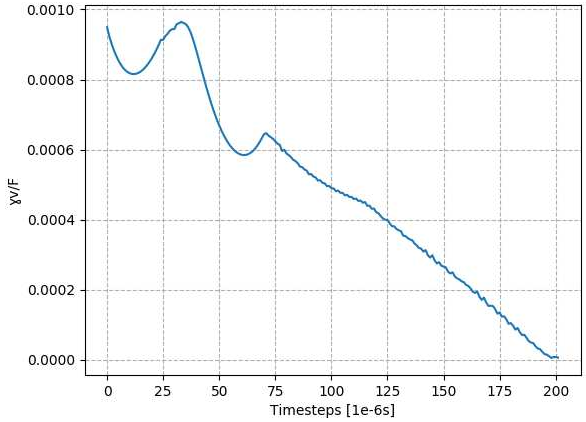

(a) Ratio between frictional and field energy reduction $-\sum_{i=1}^{N_p} \gamma v_i^2 / \sum_{i=1}^{N_p} \vec{v}_i \vec{F}_i$ during the cooling, for $\gamma = 6\text{Hz}$.

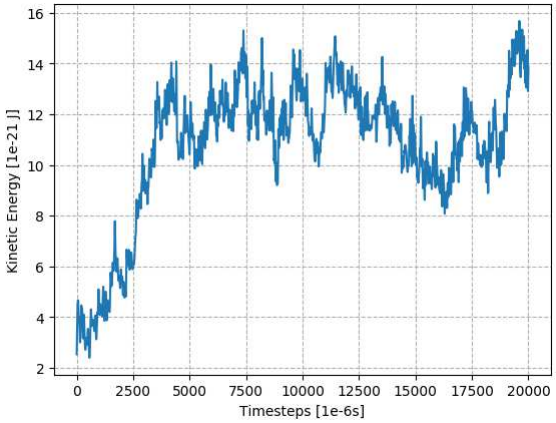

(b) Kinetic energy during the constant plane wave injection, possible friction limit for $\gamma = 100\text{Hz}$.

Figure 7.3: Influence of friction during the kinetic energy evolution for a $N_p = 10$ particle system and $N = 10$ modes.

Now we want to check the robustness of the cooling procedure, in accordance to sections 6.2 and 6.3, where several scenarios (tests) are explained in detail. We also suggest to compare the upcoming results with those of these two sections.

We start by testing our cooling method for a different number of input modes N. Figure 6.4 shows the time dependence of the kinetic energy for different mode numbers. For all curves, the input flux $|\mathbf{c}|^2$ has been held constant. Additionally the reached final energy after the cooling and the required time duration are plotted.

The cooling works for all mode numbers between $N = 4 - 20$ decently. For $N = 2$ the field (input generation) has too little degrees of freedom for a stable cooling (blue curve), the kinetic energy increases at later times again (not shown). The minimal duration of the cooling procedure varies from 200 to 450µs and the reached final energy values are around 10^{-25} Joule. For $N = 10$ the intensity peaks have comparable size as the particles, see figure 7.1a, this might be the reason, why the cooling takes the least amount of time around this value.

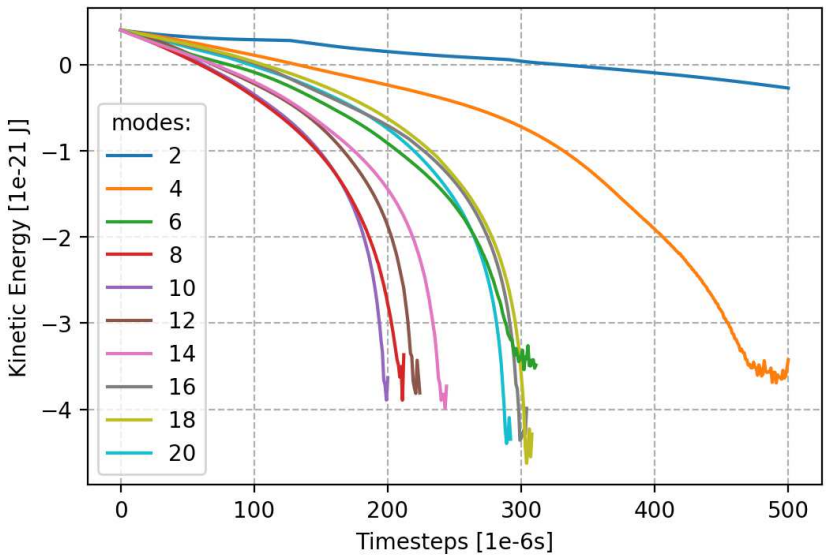

(a) Kinetic energy (logarithmic plot). Each curve corresponds to another mode number.

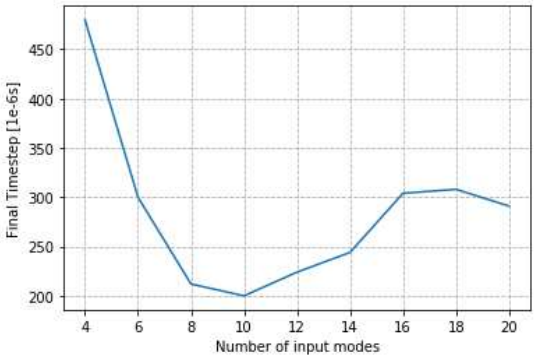

(b) Duration of the cooling.

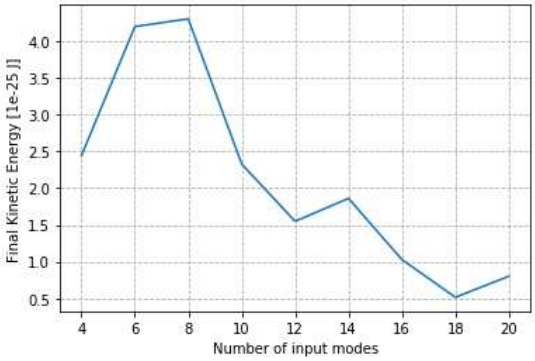

(c) Reached final kinetic energy.

Figure 7.4: Behaviour for the different number of input modes N. Cooling procedure for a ten particle system.

Next we consider a scenario, where we have incomplete access to the scattering matrix S. We assume, that we can only resolve transitions (from input to output field) between the first M modes. From the changes in this sub-matrix of S, we approximate an incomplete GWS-Time-operator and inject the eigenvector corresponding to the smallest eigenvalue into the system. The corresponding results for a different number of used modes M out of $N = 20$ are visualised in figure 7.5.

The smaller M is, the longer the cooling takes, from 280 to 1400µs. At some point, there is too little information for a consistent cooling of the particles. In our example, this is the case for $M = 8$ (blue curve), as the minimal energy value is not stable (i.e. the cooling depends too strong on the particle positions).

Therefore an incomplete scattering matrix might not be problematic in experiments, as long as only few transitions between input and output modes are missing (and the measurement errors are small).

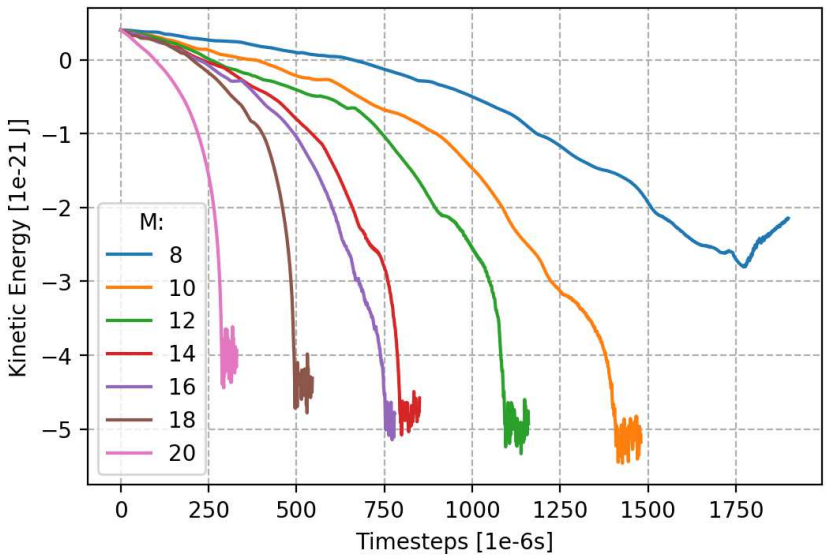

(a) Kinetic energy (logarithmic plot). Each curve corresponds to another number of used modes.

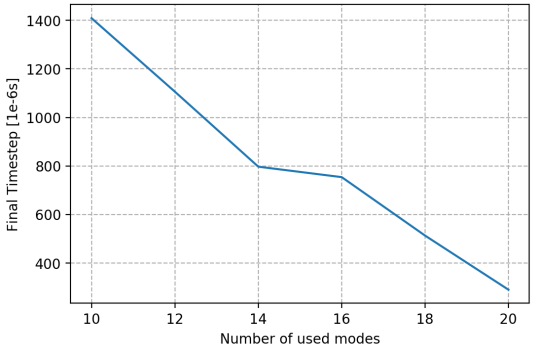

(b) Duration of the cooling.

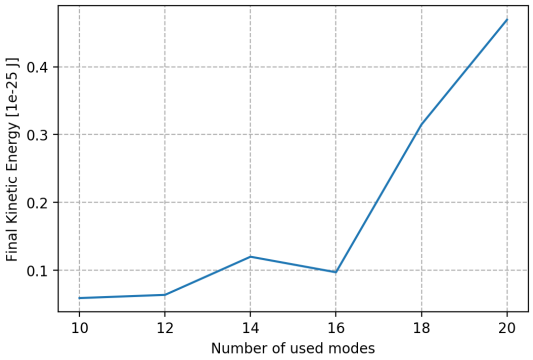

(c) Reached final kinetic energy.

Figure 7.5: Behaviour for a different number of used modes M out of $N = 20$ input modes. Cooling procedure for a ten particle system.

Usually the electric field gets absorbed partly in matter, this essentially results in an information loss and a non-hermitian GWS-operator. In order to test the impact of absorption, we gradually increase the imaginary part of the refractive index $n_s = n_1 + in_2$ of the silica beads. The respective results are illustrated in figure 7.6.

For $n_1 = 1.44$, with increasing n_2 (from zero in steps of $6 \cdot 10^{-2}$) the cooling takes longer, and accordingly smaller energy values are reached, since the force on the particles decreases. Until the cooling fails at $n_2 = 0.36$ (pink curve), as the kinetic energy does not converge to a stable value. At this point too much information is lost, due to the damping of the electric field in matter.

While for the ideal behaviour (no absorption, blue curve) only two hundred iterations of our procedure are needed, the successful case with the highest absorption $n_2 = 0.3$ (brown curve) takes five times longer (thousand estimations of Q_t within 1ms). At this point we want to remember, that the absorption losses depend highly on the ratio between particle radius and wavelength.

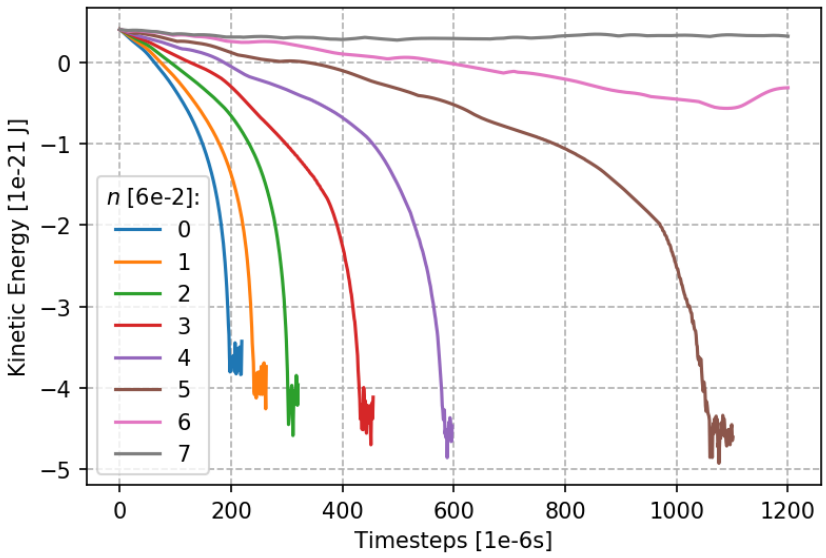

(a) Kinetic energy (logarithmic plot). Each curve corresponds to another imaginary part of n_s.

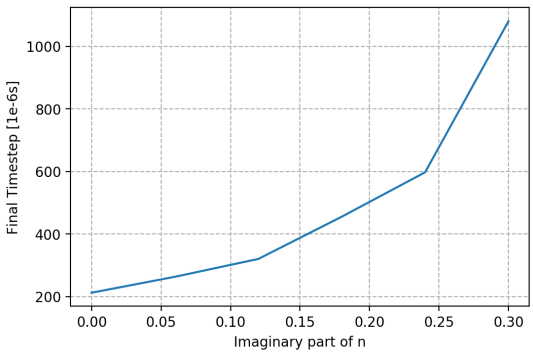

(b) Duration of the cooling.

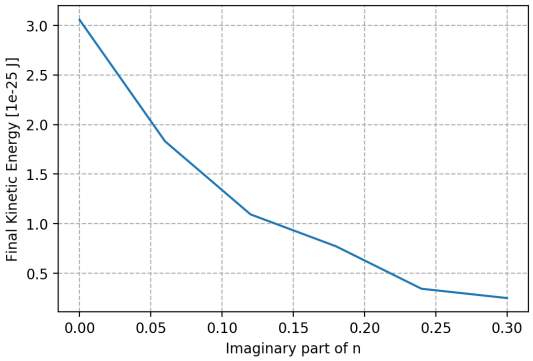

(c) Reached final kinetic energy.

Figure 7.6: Impacts of absorption in the particles, modelled through the imaginary part of the refractive index. Cooling procedure for a ten particle system and $N = 10$ modes.

The last robustness test, we want to show, is the scenario of different particle shapes and an included rotational movement of scatterers. As friction plays anyway no role during the cooling, we spare us to formulate a frictional damping of the angular momenta.

Like in section 6.3, we compare cases of identical circles, different sized circles and mixed shapes (circle, square, S-shape), that are presented in figure 7.7a. For each of these cases the results of the cooling procedure are compared in figure 7.7b. The cooling of identical circles (yellow curve) and different sized circles (red curve) takes nearly the same time. For the case of mixed particle shapes we have done two different scenarios, one, where all particles only translate initially (green curve) and one, where the initial translation and rotation energy is the same.

We decided to work with $N = 20$ modes, so that the wavelength $\lambda \approx 1064/2 = 532$nm is small enough to tackle the rotation movement well. Otherwise it would take a long time to reduce the rotation of the square-shaped particles. (This mainly depends on the wavelength and not on N. A cooling would also work with $N = 10$, if λ is small enough.)

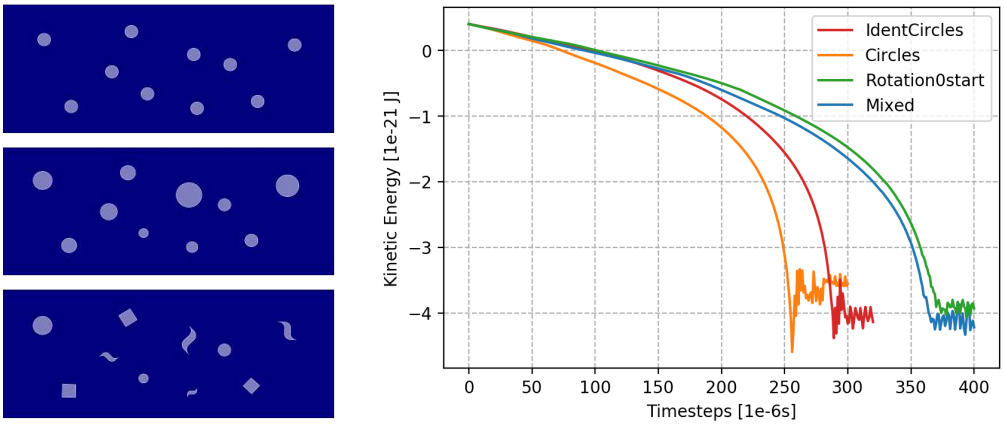

(a) Comparison between the different used shapes.

(b) Kinetic energy (logarithmic plot). Each curve corresponds to another scenario.

Figure 7.7: Behaviour for different particle shapes and movements. Cooling procedure for a ten particle system and $N = 20$ modes. The different curves in b) correspond to identical circles (red), different sized circles (yellow) and complex shapes with no initial rotation (green) and mixed initial motion (blue).

For all the different scenarios we reach essentially the same final energy of the particles. The behaviour of the mixed scenario (blue curve) is presented in figure 7.8 with more detail. The time dependence of translation and rotation energy as well as the kinetic energy of each particle on its own, during the cooling procedure, are visualised.

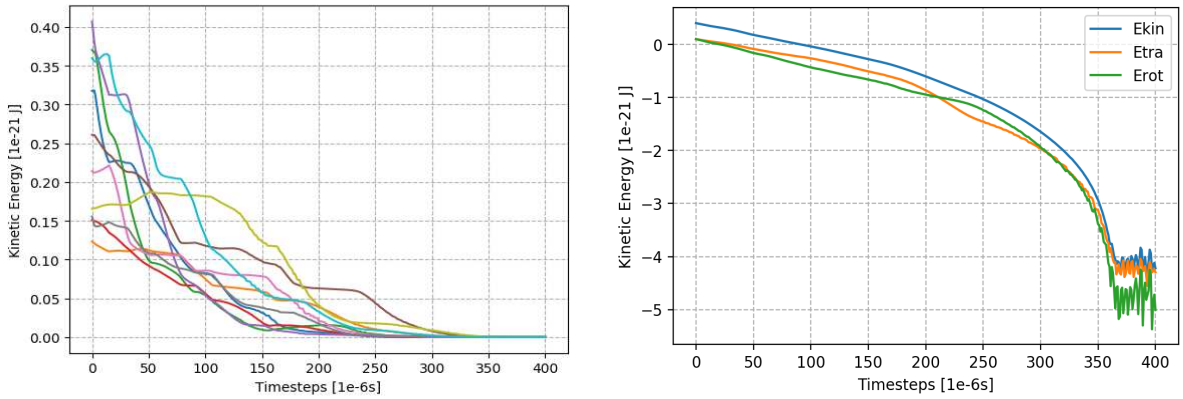

(a) Kinetic energy of each particle. Each colour corresponds to another particle.

(b) Translation and rotation energy of the particle system (logarithmic plot).

Figure 7.8: Cooling procedure for a ten particle system and $N = 10$ modes. Example for complex shaped particles and movement.

So far in this chapter we worked with a constant input flux and time step length. The input power $P_{\text{in}} = 2\mu\text{W}$ and the step length $\Delta t = 1\mu\text{s}$ has been chosen so, that the system gets cooled down around four magnitudes of the kinetic energy and that gravitation might be negligible. Thus one could reach smaller energy values, if one of these two quantities gets reduced (adjusted) during the cooling. The results of an input power regulation, according to section 6.4, are plotted in figure 7.9.

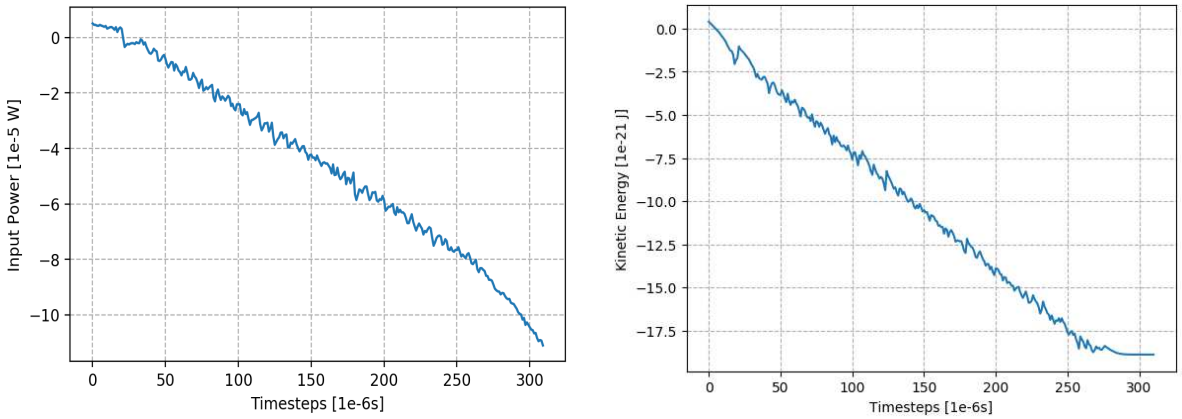

(a) Input power (logarithmic plot). (b) Kinetic energy (logarithmic plot).

Figure 7.9: Cooling procedure for a ten particle system and $N = 10$ modes with flux regulation in absence of other forces (gravitation etc.), $a = 1/10$, $b = 1/2$.

Here the input power is initially $P_{\text{in}} \approx 30\mu\text{W}$ and follows essentially the exponential decrease down to pico-watt. The small oscillations of P_{in} with time comes from the oscillations in the kinetic energy and might be flattened. We reduced the system energy to temperatures far smaller than 1mK (here theoretically down to femto-kelvin, values that will not be reached in realistic scenarios).

7.3 Time scale and errors

Based on the chosen realistic values, we now address the validity of the simulations as well as some different unconsidered aspects, which can lower the cooling efficiency.

At first we want to share some results of the cooling for different time step lengths of the internal time evolution Δt and of the estimation of Q_t, Δt_{GWS}. As mentioned in section 3.2, after every $\Delta t_{\text{puls}} = \Delta t_{\text{GWS}}$ long time step another optimized state gets injected into the system.

Thereby we spare us to work with a continuous input and we also estimate the kinetic operator Q_t, while field forces act on the particles. As Q_t includes the movement of all particles, it is clear, that velocity changes during the measurements are not ideal. However, for appropriate values, our cooling fields mainly reduce the velocity absolute values and do not change the direction. A comparison between our usual approach and a cooling with pauses (field-free durations, where Q_t can be measured during a free movement of the scatterers) is presented in figure 7.10.

We used smaller initial velocities and larger time steps, even with these values a (nearly) force-less estimation of Q_t is hardly better. It is only beneficial, if the forces are in range of the velocities $F\Delta t_{\text{GWS}}/m \approx v$. The cooling without pauses is twice as fast.

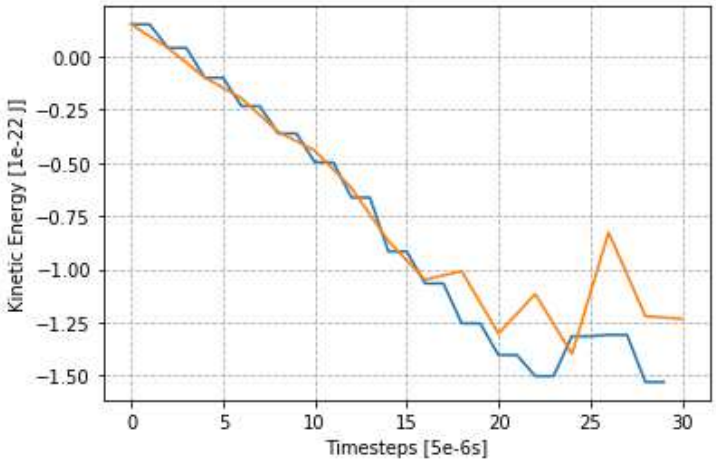

Figure 7.10: Cooling procedure for a ten particle system and $N = 10$ modes with (blue) and without (orange) pauses (durations of $\psi = 0$). The orange curve is stretched by a factor of two ($t \to t/2$).

Next we want to shortly address the error in the simulations. Since the used time evolution is a simple Taylor series expansion of the particle velocities and positions (in principle only up to the first order in Δt), the simulation time step Δt needs to be small. In figure 7.11a the kinetic energy during the cooling procedure for different values of Δt is plotted. There are only minor differences at the end, i.e. the so far used step length (blue curve) is fine.

Also relevant is the duration between two measurements of S. Figure 7.11b shows the cooling results for different sizes of Δt_{GWS}, varied from $0,5\mu$s to 32μs (blue to pink curve) in factors of two. The estimation of the GWS-time-operator seems to work fine up to and including $\Delta t_{\mathrm{GWS}} = 16\mu$s. The different values of the reached final energy occur mainly, due to the increased injection time of the optimal cooling states. For longer injection times, the particles get pushed more strongly, $F\Delta t_{\mathrm{puls}}/m \approx v_{\mathrm{fin}}$.

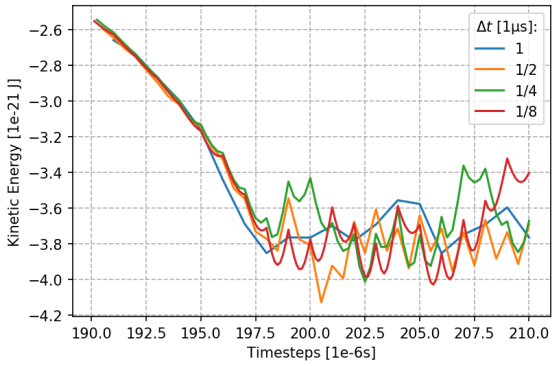

(a) Different simulation steps Δt (section of the final steps).

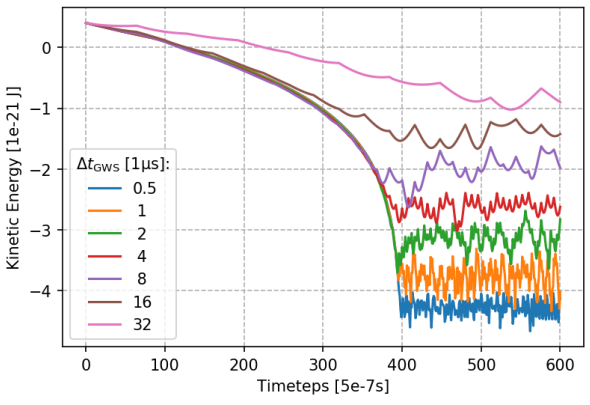

(b) Different size of $\Delta t_{\mathrm{GWS}} = \Delta t_{\mathrm{puls}}$.

Figure 7.11: Kinetic energy (logarithmic plot) during the cooling procedure for different time scales, for a ten particle system and $N = 10$ modes.

Furthermore, some issues, which decrease the cooling efficiency, are not included in the simulations. Here we have mainly the finite measuring times of the scattering matrix S and the finite computation times of the GWS-operator Q_t and its eigenvectors (or only the eigenvector corresponding to the smallest eigenvalue) in mind. The duration of an input field injection should be only a few micro seconds, therefore the estimation of S and Q_t, as well as the shaping of the input field according to the optimal eigenvector needs to be achieved in even smaller times (otherwise the particles have moved too much and the input states are already wrong or less efficient).

Some other non-ideal conditions, like incomplete mode access or absorption, have been tested in the previous section. It is also hard to say, how well the cooling procedure will work in a real three dimensional scenario, where the interaction between field and particles leads to changes in the direction of the electric field. These changes of the field polarisation are not included in our (scalar field) model.

Lastly, we want to check the accuracy of the underlying adiabatic approach. It is based on (see also section 1.2)

$$\partial_t^2 D^i = \partial_t^2[\epsilon_R \psi e^{-iwt} e_z^i] \approx -w^2 \epsilon_R \psi e^{-iwt} e_z^i = -w^2 D^i. \tag{7.7}$$

Therefore one might evaluate some basic restrictions over a finite area (a volume, where one particle is contained)

$$w\epsilon_R|\psi| \gg \partial_t \epsilon_R|\psi|,\ \epsilon_R|\partial_t\psi|, \tag{7.8}$$

$$\int w\epsilon_R|\psi|dV \gg \int \partial_t\epsilon_R|\psi|dV,\ \int \epsilon_R|\partial_t\psi|dV, \tag{7.9}$$

$$\epsilon_s \int_V w|\psi|dV \gg v^i(\epsilon_s - 1)\int_{\partial V}|\psi|dA^i,\ \epsilon_s\int_V|\partial_t\psi|dV. \tag{7.10}$$

The remaining integrals reach over the volume V or the surface ∂V of one scatterer. We estimate them (their magnitude) through working with constant integrands and circular particles,

$$w\frac{4}{3}\pi r^3 \gg |v|\frac{\epsilon_s - 1}{\epsilon_s}4\pi r^2,\ |\partial_t\psi|/|\psi|\frac{4}{3}\pi r^3 \tag{7.11}$$

$$w \gg 3\frac{\epsilon_s - 1}{\epsilon_s}\frac{|v|}{r},\ |\partial_t\psi|/|\psi|. \tag{7.12}$$

The time derivative of ψ is mainly caused by the pulsed operation of the input field (besides the movement of the particles). Thus we might estimate it simply as $|\partial_t\psi| \approx 2\pi|\psi|/\Delta t_{\text{puls}}$ (the prefactor depends on the time dependence). Neglecting some constants leads to

$$w \gg \frac{|v|}{r},\ \frac{2\pi}{\Delta t_{\text{puls}}}. \tag{7.13}$$

In other words, we obtain for the time scales, with $\tau = 2\pi/w$, and for the velocities,

$$\tau \ll \Delta t_{\text{puls}}, \tag{7.14}$$

$$\frac{|v|}{c} \ll kr. \tag{7.15}$$

For an optimal cooling we usually assume, that Δt_{puls} is restricted by the particle velocities, similar to eq. (3.7). Then the restrictions above essentially equate to each other. For the realistic values in section 7.1 we get $1,5 \cdot 10^{-11} \ll 1$, thus the adiabatic approach is likely valid. Another simple (but less accurate) way to check the validity could be based on the considered field energy conservation (flux conservation),

$$P_{\text{out}} = (1 - \frac{\theta_{\text{min}}}{w})P_{\text{in}} \approx P_{\text{in}} \quad \Rightarrow \quad |\theta_{\text{min}}| \ll w. \tag{7.16}$$

Chapter 8

Comparison with existing cooling methods

In this chapter a short review of existing cooling methods will be provided, in order to place our cooling procedure in the right context. Thus we primarily focus on methods in optomechanics, which consider neutral dielectric particles in the mesoscopic regime. However we will see, that the existing techniques are quite different from our approach, as they are usually based on trapping a single particle in an electric potential in order to measure and counteract its movement.

8.1 Levitation and feedback cooling

The base of optical feedback cooling is essentially the precise knowledge of the particle position and movement. With so-called optical tweezers one can trap a nano-sized dielectric particle purely with light. As source for this and the next section and as further reading serve the reviews "Levitated Nanoparticles for Microscopic Thermodynamics"[3] and "Optomechanics with levitated particles"[1].

A tightly focused laser beam enables a 3D-trapping of the nanoparticle. In order to treat the particle as a single dipole (point-like behaviour), the particle radius has to be considerably smaller than the wavelength of the laser light, $r < \lambda/5$. Then the conservative gradient force (1.25) or rather (4.11) pulls the particle towards the region of maximum field intensity $|\psi|^2$, i.e. towards the focal point of the laser light.

The force can be described by (the gradient of) a potential, which traps the particle, leading to a mechanic oscillation of its center of mass. The potential is strong enough, so that gravitation and stochastic forces (due to the interaction of the particle with its environment) are compensated. For low enough oscillation amplitudes (near the bottom of the potential) the particle sees approximately a harmonic potential, giving rise to the equation of motion,

$$\partial_t^2 x + \Gamma \partial_t x + \Omega_0^2 x = \eta(t) \tag{8.1}$$

This equation describes the movement of a laser trapped particle under interaction with its environment (Brownian motion) for each of the three coordinates $x = x_1, x_2, x_3$ (nearly decoupled motion). Here Ω_0 is the frequency of the trap (harmonic oscillation frequency), Γ is the total damping rate (friction constant), consisting out of different damping rates (gas damping, photon shot noise). The right side specifies the Langevin force (white noise), with vanishing average value and $\langle \eta(t)\eta(t') \rangle \propto \delta(t - t')$.

In feedback cooling one now changes the form of the potential, according to the movement of the particle, in order to reach an artificial damping, or one includes an external damping mechanism. This requires a precise detection of the particle movement, leading to additional problems (calibration of the detectors, etc.).

An additional damping term proportional to the particle velocity (linear feedback cooling) seems hard to achieve for nano-sized dielectric particles. Existing methods work for particles bigger than 1µm, using radiation pressure up to $T \approx 1mK$, and for nano-sized charged particles in a 1D-regime (single degree of freedom), using the coulomb force.

Instead, non-linear feedback cooling leads to convenient results, using a parametric modulation of the trapping potential ($\partial_t x^2 \propto x \partial_t x$). The feedback signal (generated by the trapping light or by a probe beam) is tuned so, that the potential is stiffened (larger laser power P, $\Omega_0 \propto \sqrt{P}$), if the particle moves away from the center, and its relaxed, if it moves towards the center. Thus parametric feedback cooling can be used to reduce a dielectric nanoparticles centre-of-mass temperature to few millikelvin, this works for all three motional degrees of freedom simultaneously as the optical gradient force points always to the trap center.

A combination of feedback with passive cavity cooling can reach even smaller temperatures, up to the mechanical ground-state of the oscillating particle and is presented at the end of the next section. The major motivations for such optomechanical experiments are to study (the transition to) quantum mechanics of macroscopic objects, non-equilibrium thermodynamics and general force sensing applications.

8.2 Cavity cooling

A Fabry-Perot cavity in combination with a levitation mechanism enables great cooling options for the contained particle (levitated cavity optomechanics). In contrary to the levitation in an optical tweezer, the light field is naturally an active participant in the dynamics of the system. The simplified Hamiltonian of the light-matter system might be written as

$$\hat{H} = \frac{\hbar w_{\text{opt}}}{2} \left(\hat{p}_{\text{opt}}^2 + \hat{q}_{\text{opt}}^2 \right) + \frac{\hbar w_q}{2} \left(\hat{p}^2 + \hat{q}^2 \right) + U_{\text{int}}(\hat{q}_{\text{opt}}, \hat{q}), \tag{8.2}$$

Here U_{int} describes the interaction between the two quantum harmonic oscillators, with the space and momentum operators of the particle $\hat{q}$, $\hat{p}$ and the light field $\hat{q}_{\text{opt}}$, $\hat{p}_{\text{opt}}$. Besides this conservative part, there are again stochastic forces present, due to a coupling with the environment (Langevin equations for each of the two oscillators).

Now under special conditions the red-sideband cooling mechanism enables a 1D-ground-state cooling of the particle. It occurs in near resonance $w_{opt} \approx -w_q$, between the effective optical frequency $w_{\text{opt}} = \Delta = w_{\text{cav}} - w_L$ (detuning between cavity resonance frequency and laser frequency) and the mechanical frequency of the levitated particle w_q.

The trapping of the particle in the cavity can either be done with the cavity modes (one mode for trapping and one for cooling) or by an additional trapping field, as done with an optical tweezer. In both scenarios the particle has to be smaller than the light wavelength, so that the modelled point-dipole does not change the trapping field drastically.

A combination of feedback cooling, which enables stable trapping and position sensing, and the strong cavity sideband cooling is pictured as the optimal scenario. We now want to shortly review a recent publication in this field [19], where the cavity is not driven, but populated by the scattered tweezer light field. This enables ground-state cooling in a room-temperature environment using the following set-up.

A spherical silica particle with a diameter of 140nm is trapped inside a vacuum chamber using an optical tweezer (with wavelength $\lambda_{\text{tw}} = 1064\text{nm}$ and power in the focus $P \approx 400\text{mW}$ of the laser beam, leading to an oscillation frequency $w_x/2\pi = 505\text{kHz}$). The particle gets positioned in an optical cavity, where the cavity frequency satisfies $w_{\text{cav}} = w_{\text{tw}} + \Delta$. Driven by the optical tweezer the particle coherently scatters dipole radiation, this scattered light gets partly collected by the cavity (the polarization of the laser light defines the dominant radiation direction towards the cavity mirrors).

Now the particle needs to be positioned at an intensity minimum of the cavity standing wave field. Here the particle essentially does not sense the field and accordingly all dipole scattering into this cavity mode is inhibited, due to destructive interference. Thus only inelastically scattered Stokes- and anti-Stokes photons at sideband frequencies $w_{\text{tw}} \pm w_x$ can propagate in the cavity. While anti-Stokes scattering processes along the cavity reduce the particle energy (mechanical oscillation) by $-\hbar w_x$ per photon, Stokes processes increase it. At the optimal detuning $\Delta \approx w_x$ the anti-Stokes sideband is in resonance with the cavity and therefore largely enhanced, leading to the desired cooling towards the ground-state.

Since anti-Stokes scattering is inhibited near the ground state (particle can't be cooled further), one can estimate the temperature of the particle motion directly through a measurement of the sideband asymmetry. By this approach the particle movement along the cavity axes has been reduced to the ground state, $T \approx 12\mu\text{K}$, even though working at an environment pressure of 10^{-6}mbar.

8.3 Comparison with our method

The standard laser cooling of atoms is based on the Doppler shift, requiring an internal level structure. Since in dielectric solids such an internal structure is not accessible, one needs other techniques. The existing cooling approaches, presented in the last sections, change and control the movement of one particle by trapping it in a potential. Ideally the considered point dipole's center of mass is forced on a harmonic oscillation, with deviations due to environment contact. Collisions with the gas or photon noises apply natural damping and heating rates.

In non-linear feedback cooling an additional damping gets applied due to modulation of the trapping potential, therefore the accurate position and velocity of the particle is needed. It enables 3D-cooling of the dipole's center of mass from room-temperature 300K up to few mK. Cavity cooling works the best again with an trapped particle using an optical tweezer. Here the light field acts actively and the resonance sideband cooling mechanism allows even ground-state cooling (usually μK). However the particle needs again to be positioned precisely and the ground state energy is completely defined by the trapping potential.

In contrary, our method works completely differently and for more than one dielectric particle. The particle(s) move more or less free in the system. Instead of trapping the particle(s), we modulate the field according to the macroscopic system changes. The resulting field configurations ideally lead to a damped linear movement of the particles (without oscillations). As we only access far-field information of the system, encoded in (the changes) of the systems scattering matrix, we neither need to control nor measure the precise position of the particles.

As our method is only defined semi-classically (and it is not based on a fundamental photon exchange), we don't expect to reach ground state cooling. Possible extensions of our approach to the quantum regime are, however, envisionable. Anyway our formalism allows to freely scale the magnitude of the forces, through the input power, up to quantum mechanical or other limitations. Thus in our 2D-approach reaching temperatures in range of millikelvin for a set of arbitrarily shaped particles seems realistic, including translation as well as rotational degrees of freedom in motion. The big drawbacks are, on the one hand the requirement of a nearly complete access to the far-field information and on the other hand the limitation to small starting velocities, some mm/s, in order to evaluate and generate the optimal field states fast enough (within few μs).

Other advantages/disadvantages of the introduced cooling techniques are the following. The optical tweezer trapping of a particle inhibits additional complication, it is only stable for pressures $p > 10^{-6}$mbar. Thus feedback and cavity cooling of levitated particles are either done in a "bad" vacuum or even in environment conditions. Even though the great cooling rates overshadows other interaction processes, once the cooling mechanism is stopped, there is not much time to test physics with the cooled particle due to heating processes through its environment. Our cooling procedure could be done in ultra-high-vacuum, furthermore it works also for larger particles. The particles are allowed to

change the field configuration drastically and we are not restricted to the single dipole approximation.

Considering all aspects one might classify our technique as linear many-body feedback cooling. A successful implementation of our method would enable a cooling or heating of arbitrarily shaped particles (nearly) independently of their location in the system. It gives much more freedom in the energy manipulation of dielectric particles.

Chapter 9

Conclusion

In summary, we considered a system of moving dielectric particles, usually in a mesoscopic regime. In terms of scattering theory, the piecewise dielectric function ϵ_R of the particle system modulates the scattering landscape the light field senses. The non-relativistic particle motion is included through its changes $\partial_t \epsilon_R$ with time, and suggests an adiabatic approach, where the electromagnetic field adjusts itself nearly instantaneously to the particle movement. On the one hand the field amplitude, in monochromatic scalar field approximation, is given by the Helmholtz equation, a simple wave equation, where only the different propagation speeds of light in vacuum or matter plays a role. On the other hand the field applies gradient forces on the particles in direction of higher field intensity.

Macroscopic relations of the field-matter interaction (scattering problem) are provided by continuity equations. These are the flux conservation (energy conservation) and by a differential view the GWS-intensity-relations, connecting changes of the outgoing field (encoded in the scattering matrix) with internal system changes. Here the so-called GWS-time-operator contains the differential macroscopic energy change, caused by interaction between particles and field, for any possible input field. Its eigenvalues are linearly proportional to the energy change, the eigenvectors equate to the corresponding field input state. Thus an injection of a field proportional to the eigenvector with the smallest (most negative) eigenvalue, leads to a maximal energy decrease of the particle system.

In order to test different aspects of the field-matter interaction, we used a 2D-multimode waveguide system. For an empty waveguide, randomized input fields lead to a Gaussian distribution of the field amplitude at any point in the system. Averaging over all field configurations results in a uniform field intensity distribution inside the waveguide. Deviations occur due to boundary conditions and a finite number of input modes. Moreover, randomized field configurations heat contained particles, because each field input is injected for a finite time. While the mean velocity stays the same, the root mean square deviation rises, resulting in a small linear increase of the temperature with time. Only a connection with the environment (gas, vacuum fluctuations) leads to a damping, which counteracts this heating process.

If we consider constant input fields, then the energy of the particle ensemble can increase even more strongly, a behaviour probably caused by strong field force correlations between different particles (as in a gas under pressure). In contrast, the optimal cooling states reduce the particle motion significantly. Here, each state needs to get injected a short time, since the ongoing (damped) movement of the particles changes these ideal field configurations strongly. For instance, for particle velocities around mm/s, a cooling state should be injected no longer than few µs, until the next optimal field input has its turn (iterative cooling).

If only one dielectric particle is in the waveguide, the force generated by the optimal cooling states acts in principle as a pure damping. The absolute velocity will be reduced, while the movement direction stays nearly the same. On the contrary, optimal heating fields generate field intensity peak(s) on the other side of the particle, and thereby heat the particle efficiently. The force, the particle senses, depends quite strongly on geometric aspects, like particle shapes, the position in the waveguide as well as the ratio between wavelength and particle radius, but in any case, our method yields the optimal field states (for cooling or heating).

Most importantly, our cooling procedure provides also convenient results for many-particle systems. The optimal fields enable the best possible energy transfer, reachable from far-field modulation. Either many particles get slowed down a bit or few get focused strongly. Faster scatterers are cooled more likely, until many particles have comparable energy. Then the optimal field configurations switch between different sets of particles.

As tested on a ten particle system, our approach proves robust to missing far-field information, absorption in the particles and works also well for complex particle geometries. In minor extent, an incomplete access to scattering matrix entries or absorption, primarily lead to longer cooling times, i.e. a reduction of the efficiency. The amount of field absorption allowed in the particle depends again on the ratio between wavelength and particle size. The smaller the particle, the higher can be the imaginary part of the refractive index. More degrees of freedom in motion result also in longer cooling durations. In any case, for a small enough wavelength the particle boundary can be resolved by the field and translation as well as rotation motion get reduced equally.

In general, the reached final energy is defined by the strength of the field force. Thus one is able to reach smaller values, in principle up to quantum mechanical limits, by a reduction of the input power or the injection time of the field input. With knowledge of the starting temperature one might even make predictions and reduce the input power according to the energy change, in order to reach an exponential decrease of the macroscopic system energy.

With rising particle number the cooling procedure loses on efficiency, since the field comes from the asymptotic region (it has finite degrees of freedom) and collisions between particles can lead to errors in the GWS-operator estimation. Therefore the field injection time should be reduced accordingly, a strict limit of particles (per volume) is not imagined. The general efficiency of our approach depends strongly on how fast the scattering matrix, the GWS-time-operator and its relevant eigenvector can be estimated. And above all how

fast the wavefront can be shaped according to the current optimal cooling state. In our example we showed a cooling of ten particles from 18K to a few mK, which required already a pulsed operation at μs time scales. Advances in light modulation will enable higher initial velocities.

Currently there exists no comparable cooling technique in the mesoscopic regime. The existing approaches are usually limited to one point-like particle, as they focus upon trapping the dielectric particle for example with an optical tweezer [1][3]. In feedback cooling the position of the trapped particle is constantly monitored and optical forces against its motion are generated. Cavity cooling requires an exact positioning of the particle in the cavity, in order to cool it down using resonance conditions. Here the latest approach [19] realises even cooling to the mechanical ground state, from room temperature to some μK. In contrast, our procedure enables cooling of multiple particles and degrees of freedom in motion, without local information. Thus it offers perspectives in non-equilibrium thermodynamics and preparation of macroscopic many-body quantum states.

Bibliography

[1] Millen et al: *Optomechanics with levitated particles*, Reports on Progress in Physics 83, 026401, 2020.

[2] Urvoy et al: *Direct Laser Cooling to Bose-Einstein Condensation in a Dipole Trap*, Physical review letters 122, 203202, 2019.

[3] Gieseler, Millen: *Levitated Nanoparticles for Microscopic Thermodynamics—A Review*, Entropy 2018, 20, 326, 2018.

[4] Yoshihiko et al: *Optical binding of two cooled micro-gyroscopes levitated in vacuum*, Optica 5, 910-917, 2018.

[5] Dholakia, Zemanek: *Colloqium: Gripped by light: Optical binding*, Reviews of modern physics 82, 1767, 2010.

[6] Ambichl et al: *Focusing inside Disordered Media with the Generalized Wigner-Smith Operator*, Physical review letters 119, 033903, 2017.

[7] Horodynski et al: *Optimal Wave Fields for Micro-manipulation in Complex Scattering Environments*, Nature Photonics 14, 149-153(2020), 2019.

[8] Rotter, Gigan: *Light fields in complex media: Mesoscopic scattering meets wave control*, Reviews of modern physics 89, 015005, 2017.

[9] Bartelmann et al: *Theoretische Physik*, Springer-Verlag, p.400-403 & 538-542, 2015.

[10] Novotny, Hecht: *Principles of Nano-Optics, Forces in confined fields*, Cambridge University Press, p.419-428, 2012.

[11] Jones: *Electromechanics of Particles*, Cambridge University Press, p.1-43 (1995), 2005.

[12] Hüpfl: *The Generalised Wigner-Smith Operator*, Bachelorarbeit, TU Wien, 2019.

[13] Wigner: *Lower limit for the energy derivative of the scattering phase shift*, Physical Review 98, 145–147, 1955.

[14] Smith: *Lifetime matrix in collision theory*, Physical Review 118, 349–356, 1960.

[15] Hüpfl: *Light cooling with the Generalised Wigner-Smith Operator*, Manuscript in preparation, TU Wien, 2019.

[16] Netgen/NGSolve: NGSolve open source Finite Element Library at https://ngsolve.org/ (latest visit 7.20.20).

[17] Stöckmann: *Qantum Chaos: Scattering System*, Cambridge University Press, p.230-233, 2006.

[18] Bäcker et al: *Friedel oscillations in microwave billiards*, Physical review E 80, 066210, 2009.

[19] Delic et al: *Cooling of a levitated nanoparticle to the motional quantum ground state*, Science 367, 892–895, 2020.

Appendix

A.1 Magnetic particles

Here we want to shortly formulate the GWS-intensity relations and the acting field forces for magnetic particles, by analogy to chapter 1 and 2. Our starting point are Maxwell's equations for magnets and no free moving charges (only magnetization forces).

$$\partial_i E^i = 0, \tag{1}$$
$$\partial_i B^i = 0, \tag{2}$$
$$\epsilon_{ijk}\partial_j E^k + \partial_t B^i = 0, \tag{3}$$
$$\epsilon_{ijk}\partial_j H^k - \epsilon_0 \partial_t E^i = 0, \tag{4}$$

for linear matter with

$$D^i = \epsilon E^i = \epsilon_0 E^i, \quad H^i = \frac{1}{\mu} B^i = \frac{1}{\mu_0 \mu_R} B^i. \tag{5}$$

Instead of the electric field E^i, the magnetic field B^i or rather H^i is the important quantity. We restrict ourself on magnetic particles, with constant relative permeability μ_s, leading to a piecewise constant permeability of the system μ_R (one in vacuum and constant in matter). We derive the Helmholtz equation for H^i with following steps.

We build the rotor of eq. (4) and insert the time derivative of eq. (3) to get

$$\delta_{ij}^{lm}\partial_j\partial_l H^m + \epsilon_0 \partial_t \partial_t B^i = 0, \tag{6}$$
$$\partial_j\partial_i H^j - \partial_j\partial_j H^i + \epsilon_0 \partial_t^2 B^i = 0. \tag{7}$$

An expression for the divergence of the H-field is included in eq. (2),

$$\partial_j H^j = -\partial_j \ln(\mu) H^j. \tag{8}$$

Equation (7) is therefore writeable as

$$\left[-\partial_i\partial_j \ln(\mu_R) - \partial_i \ln(\mu_R)\partial_j - \partial_m\partial_m\delta_{ij} + \frac{1}{c^2}\left(\partial_t^2 \frac{1}{\mu_R} + 2\partial_t \frac{1}{\mu_R}\partial_t + \frac{1}{\mu_R}\partial_t^2\right)\delta_{ij}\right] H^j = 0. \tag{9}$$

This is the equation for the magnetic field, we want to simplify it strongly, making the following assumptions. We consider again a 2D-like system, where now only the transverse H-field shall be relevant. Our system shall be well described by a harmonic oscillation in time, leading to

$$H^i = \psi e^{-iwt} e_z^i, \tag{10}$$

in complex notation. Where w is the oscillation frequency in radiant and e_z^i is the unit-vector in z-direction.

The dielectric function shall not change in H-field direction (i.e. $\partial_i H^i = 0$),

$$\partial_j \ln(\mu) H^j = \partial_z \ln(\mu(x,y))\psi = 0, \tag{11}$$

thus the H-field is parallel to all boundaries and ψ is a continuous function. The resulting modified Helmholtz-equation is

$$\left[\Delta + \frac{1}{\mu_R} k^2\right] \psi = \left(\frac{1}{c^2}\partial_t^2 \frac{1}{\mu_R} - 2i\partial_t \frac{1}{\mu_R}\frac{k}{c}\right)\psi, \tag{12}$$

with $w = kc$, the vacuum wavenumber k, speed of light c and the Laplace-operator Δ.

The right side of eq. (12) can be neglected, if the movement of the magnetic particles is small. The particle velocities have to be much smaller than the speed of light, this shall be our last assumption. Since the permeability is non-continuous, such a description might be only reasonable for a finite area. The stationary, scalar Helmholtz equation describes the field amplitude and reads

$$\left[\Delta + \frac{1}{\mu_R} k^2\right] \psi = 0. \tag{13}$$

The E-field can be calculated easily from the H-field using eq. (4) and its harmonic oscillation in time,

$$E^i = \frac{i}{w} \epsilon_{ijk} \partial_j H^k. \tag{14}$$

We evaluate a term for the field force density, acting on a magnetic scatterer, starting from the Lorentz-force formula,

$$f_b^i = \rho_b^j E^i + \epsilon_{ijk} j_b^j B^k = \delta_{ki}^{lm} \partial_l M^m B^l = \mu \left[\partial_k(\chi H^i) H^k - \partial_i(\chi H^k) H^k\right] \tag{15}$$

$$= \mu \left[\partial_k(\chi) H^m H^k + \chi \partial_k H^m H^k - \partial_i \chi H^k H^k - \frac{\chi}{2}\partial_i (H^k H^k)\right] \tag{16}$$

$$= -\frac{1}{2}\partial_i \chi H^k B^k = \frac{\chi}{2}\partial_i (H^k B^k) = \mu_0 \mu_s \frac{\chi}{2}\partial_i (H^k H^k) \tag{17}$$

Here, $M^i = \chi H^i = (\mu_R - 1)H^i$ is the magnetization (magnetic dipole density). Since the magnetic susceptibility χ is piecewise-constant (Heaviside function), we were able to shift the derivative to the fields and vice-versa (product rule/partial integration as in section 1.3).

We evaluate the mean value over an oscillation period of the field $\tau = 2\pi/w$ and obtain the mean force density

$$\langle f^i \rangle_\tau = \frac{\mu_0}{4}\mu_R(\mu_R - 1)\partial_i|\psi|^2 = \frac{\mu_0}{4}\mu_R\frac{\partial \mu_R}{\partial x_s^i}|\psi|^2, \tag{18}$$

where x_s^i describe the position of the particles. This force will lead to a change of the kinetic energy of the system E_{kin} (sum of the kinetic energy of all particles). The logical value for the local change in the field energy (energy density e_{kin}) is for adiabatic conditions

$$e_{\text{kin}} = f^i dx_s^i = f^i v^i dt, \tag{19}$$

$$\left\langle \frac{de_{\text{kin}}}{dt} \right\rangle_\tau = \frac{\mu_0}{4}\mu_R\frac{\partial \mu_R}{\partial x_s^i}|\psi|^2\frac{dx_s^i}{dt} = \frac{\mu_0}{4}\mu_R\frac{\partial \mu_R}{\partial t}|\psi|^2. \tag{20}$$

Here $v^i = dx_s^i/dt$ denotes the local velocity of any part of the material (i.e. in general it consists translation and rotation speed).

The GWS-intensity-relations for magnetic particles can be derived as in section 2.3, one only need to work with the correct wave equation (13) for the magnetic case. Thus the GWS-relations read

$$\mathbf{c}^\dagger Q_\alpha \mathbf{c} = \frac{1}{2}\int_M \frac{d}{d\alpha}\left(\frac{k^2}{\mu_R}\right)|\psi|^2 d^3x. \tag{21}$$

We want to remember, that ψ describes now the amplitude of the H-field, as noted in eq. (10). (The two scenarios are different, because we specified the field directions different, so that the respective Helmholtz equation holds. For the dielectric case the E-field shows in transverse direction, for the magnetic case its the B-field.)

For time as parameter, $\alpha = t$, we can again connect the GWS-time-operator Q_t with the kinetic energy change of the system, caused by the interaction between magnetic field and particles.

$$\mathbf{c}^\dagger Q_t \mathbf{c} = \frac{k^2}{2}\int_M \frac{d}{dt}\left(\frac{1}{\mu_R}\right)|\psi|^2 d^3x \tag{22}$$

$$= -\frac{k^2}{2}\int_M \frac{1}{\mu_R^2}\frac{d\mu_R}{dt}|\psi|^2 d^3x = -\frac{2k^2}{\mu_0\mu_s^3}\frac{dE_{\text{kin}}}{dt}. \tag{23}$$

Thus our cooling procedure works surely in the (two-dimensional) electrostatic and magnetostatic cases. However, for metallic particles things are more complicated, since there is an induced current $j^i = \sigma E^i$ in the particles, which essentially leads to a further term in the wave equation. For this case our cooling approach should be tested separately.

A.2 GWS-relation in the non-stationary case

We want to show, how the GWS-relations will change in a non-adiabatic case. We differentiate the modified Helmholtz equation (1.13) with respect to a system parameter α, multiply with ψ^* and integrate over the volume of the scattering area M. We obtain after partial integration

$$\int_M \vec{\nabla}\psi^*\vec{\nabla}\psi_\alpha d^3x = \int_{\partial M} \psi^*\vec{\nabla}\psi_\alpha d\vec{A} + \int_M \psi^* \left(k^2\epsilon_R + \frac{2ik}{c}\partial_t\epsilon_R + \frac{1}{c^2}\partial_t^2\epsilon_R\right)\psi_\alpha d^3x \tag{24}$$

$$+ \int_M \psi^* \left(k^2\partial_\alpha\epsilon_R + \frac{2ik}{c}\partial_\alpha\partial_t\epsilon_R + \frac{1}{c^2}\partial_\alpha\partial_t^2\epsilon_R\right)\psi d^3x. \tag{25}$$

Then again, we can multiply eq. (1.13) with ψ_α^*, complex conjugate and integrate over the volume of M. Leading to

$$\int_M \vec{\nabla}\psi^*\vec{\nabla}\psi_\alpha d^3x = \int_{\partial M} \psi_\alpha\vec{\nabla}\psi^* d\vec{A} + \int_M \psi_\alpha \left(k^2\epsilon_R - \frac{2ik}{c}\partial_t\epsilon_R + \frac{1}{c^2}\partial_t^2\epsilon_R\right)\psi^* d^3x. \tag{26}$$

Thereby we assumed, that the wavevector k depends not on α and ϵ_R is real valued. Through subtraction of these both equations, one gets the modified GWS-Relation,

$$-\int_{\partial M} \psi_\alpha\vec{\nabla}\psi^* - \psi^*\vec{\nabla}\psi_\alpha d\vec{A} + \int_M k^2\partial_\alpha\epsilon_R|\psi|^2 d^3x = \tag{27}$$

$$-\frac{4ik}{c}\int_M \partial_t\epsilon_R\psi^*\psi_\alpha d^3x - \int_M \left(\frac{2ik}{c}\partial_\alpha\partial_t\epsilon_R + \frac{1}{c^2}\partial_\alpha\partial_t^2\epsilon_R\right)|\psi|^2 d^3x. \tag{28}$$

The additional terms are on the right hand side of the equal sign, they must be neglectable in the quasi-stationary regime, so that eq. (2.24) holds. We look at the behaviour for $\alpha = t$ and receive

$$2i\mathbf{c}^\dagger S^\dagger \frac{dS}{dt}\mathbf{c} + \int_M k^2\partial_t\epsilon_R|\psi|^2 d^3x = \tag{29}$$

$$-\frac{4ik}{c}\int_M \partial_t\epsilon_R\psi^*\psi_t d^3x - \int_M \left(\frac{2ik}{c}\partial_t^2\epsilon_R + \frac{1}{c^2}\partial_t^3\epsilon_R\right)|\psi|^2 d^3x. \tag{30}$$

Therefore, in non-stationary conditions, the GWS-Time-relation is more complicated. However one should also keep in mind, that this might be already a relativistic regime, then the forces on the particles are also different and a measuring of the scattering matrix S might be pointless.

If we compare eq. (2.9) with eq. (2.25), we might want to express the derivative of the scattering matrix with S itself,

$$\frac{dS}{dt} \approx i\frac{w}{4}\left(S - (S^t)^{-1}\right). \tag{31}$$

However, eq. (31) hinges on the non-unitary of the scattering matrix, caused by the small intern gains and losses due to the particle movement (energy conversion). The equation is only valid approximately, furthermore in realistic systems the small, relevant contributions might be overshadowed by other losses. In our simulations we work anyway with a unitary scattering matrix.

A.3 Notes force-density derivation

Here we document some notes regarding the derivation of the force-density (1.25), which might be helpful.

Since we describe the system with a non continuous dielectric function ϵ_R (34) (scattering landscape), we are able to formulate a force density f^i for the whole system. The force density is then anyway zero on areas, where no particle is present. Thus the electric force on a particle can be calculated, via integration of f^i over a volume, where (only) one particle is contained. f^i itself can be seen as an auxiliary function, the only physical quantities of our interest are the resulting force F^i and torque M^i on the whole particles.

In this context it is clear, that we are allowed to simplify f^i like in eq. (1.22). The resulting force density holds not only for the force generation, but also for the torque, as

$$\epsilon_{ijk}\partial_k R^j = \epsilon_{ijk}\delta_{jk} = 0, \tag{32}$$

$$\epsilon_{ijk}R^j\partial_k|\psi|^2 = \partial_k(\epsilon_{ijk}R^j|\psi|^2). \tag{33}$$

That means, the cross product with the lever R^i (a torque density) will not be changed by simplifications like eq. (1.22). With the same trick we can shift the differential operator from the fields to the dielectric function, furthermore as $\epsilon_R = 1 + \chi$ changes only at the boundary of the particles, one can differentiate with respect to the particle position, see eq. (1.23). In addition, in the quasi-stationary case the field depends not on the particle velocities, which enables us to define a stationary energy change, eq. (1.27).

A.4 Separation of the kinetic energy change

Here we want to bring the kinetic energy change of the particle system, see eq. (1.27), in a more usual form, where the contributions of translation (force F^i) and rotation (torque M^i) are separated, see eq. (3.3).

For N_p arbitrary shaped particles we write the piecewise constant dielectric function ϵ_R as

$$\epsilon_R = 1 + \sum_{s=1}^{N_p} (\epsilon_s - 1) H\left(|x_O^i(t) - x_M^i(t)| - |x^i - x_M^i(t)|\right), \tag{34}$$

$$\partial_t \epsilon_R = \sum_{s=1}^{N_p} (\epsilon_s - 1) \delta\left(|x_O^i(t) - x_M^i(t)| - |x^i - x_M^i(t)|\right) \left[e_R^i \partial_t (x_O^i - x_M^i) + e_r^i \partial_t x_M^i\right], \tag{35}$$

with the radius of the scatterers $R = |x_O^i(t) - x_M^i(t)|$ (the distance from the center of mass x_M^i to the boundary x_O^i of the respective particle), Heaviside-function H and delta-distribution δ. The macroscopic energy change might be written as

$$\begin{aligned}
\partial_t E_{\text{kin}} &= \frac{1}{4}\epsilon_0 \int_M \partial_t \epsilon_R |\psi|^2 d^3x && (36)\\
&= \frac{1}{4}\epsilon_0 \sum_s (\epsilon_s - 1) \int_{V_s} \delta(R - r) \left[e_R^i \partial_t (x_O^i - x_M^i) + e_r^i \partial_t x_M^i\right] |\psi|^2 d^3x && (37)\\
&= \frac{1}{4}\epsilon_0 \sum_s (\epsilon_s - 1) \int_{\partial V_s} \partial_t x_O^i |\psi|^2 e_R^i dA && (38)\\
&= \frac{1}{4}\epsilon_0 \sum_s (\epsilon_s - 1) \left[\int_{\partial V_s} \partial_t x_M^i |\psi|^2 e_R^i dA + \int_{\partial V_s} \partial_t (R e_R^i) |\psi|^2 e_R^i dA\right] && (39)\\
&= \frac{1}{4}\epsilon_0 \sum_s (\epsilon_s - 1) \left[\int_{\partial V_s} \partial_t x_M^i |\psi|^2 e_R^i dA + \int_{\partial V_s} \partial_t R |\psi|^2 dA\right] && (40)\\
&= \frac{1}{4}\epsilon_0 \sum_s (\epsilon_s - 1) \left[v_M^i \int_{\partial V_s} |\psi|^2 n^i dA \pm \int_{\partial V_s} v_R^i e_v^i |\psi|^2 dA\right] && (41)\\
&= \frac{1}{4}\epsilon_0 \sum_s (\epsilon_s - 1) \left[v_M^i \int_{\partial V_s} |\psi|^2 dA^i \pm \int_{\partial V_s} \epsilon_{ijk} \omega^j R^k e_v^i |\psi|^2 dA\right] && (42)\\
&= \frac{1}{4}\epsilon_0 \sum_s (\epsilon_s - 1) \left[v_M^i \int_{\partial V_s} |\psi|^2 dA^i \pm \omega^i \int_{\partial V_s} \epsilon_{ijk} e_R^j e_v^k R |\psi|^2 dA\right] && (43)\\
&= \frac{1}{4}\epsilon_0 \sum_s (\epsilon_s - 1) \left[v_M^i \int_{\partial V_s} |\psi|^2 dA^i \pm \omega^i \int_{\partial V_s} \epsilon_{ijk} t^j n^k R |\psi|^2 dA\right] && (44)\\
&= \frac{1}{4}\epsilon_0 \sum_s (\epsilon_s - 1) \left[v_M^i \int_{\partial V_s} |\psi|^2 dA^i + \omega^i \int_{\partial V_s} \epsilon_{ijk} R_\perp^j |\psi|^2 dA^k\right]. && (45)
\end{aligned}$$

Where we switched from the spherical unit vectors e_R^i, $e_v^i = ae_\varphi^i + be_\vartheta^i$ to the surface normal vector n^i and the tangential vector (alongside the path) t^i. Regarding the sign, if $\partial_t R > 0$, the lever $R_\perp^i$ is anti-parallel to the tangential vector t^i. Otherwise the vectors are parallel. The remaining integrals reach over the surface of the respective particle, $dA^i = n^i dA$, and equate to the field force (1.28) and torque (1.29).

For instance, for a $2D$-system in the xy-plane, the angular speed ω^i shows in z-direction. All other unit vectors lie in the plane and $e_v^i = \pm e_\varphi^i$, $v_R^i = R\omega e_v^i$ is the rotation velocity on the surface. $R_\perp^i$ is the lever according to the normal force $|\psi|^2 n^i$, see also figure 1.2.

As usual, the kinetic energy of the system contains translation and rotation parts,

$$E_{\text{kin}} = \sum_s \frac{1}{2} m v^2 + \frac{1}{2} I w^2, \tag{46}$$

$$\partial_t E_{\text{kin}} = \sum_s m v^i \partial_t v^i + I w^i \partial_t w^i = \sum_s v^i F^i + w^i M^i. \tag{47}$$

A.5 GWS-relations for second order derivatives

By analogy to the GWS-relations for the first derivatives of the scattering matrix, we can determine relations for multiple derivatives, leading in general to more complex expressions. Here we want to shortly formulate the relations for double derivatives of the Helmholtz equation.

We consider mixed derivatives of the wave equation (1.14) with respect to two system parameters α and β. After multiplying with ψ^* and applying the inverse product rule, we get

$$\vec{\nabla}\left(\psi^* \vec{\nabla}\psi_{\alpha\beta}\right) - \vec{\nabla}\psi^* \vec{\nabla}\psi_{\alpha\beta} + \psi^* \partial_\alpha \partial_\beta (U\psi) = 0, \tag{48}$$

with $U = k^2 \epsilon_R$, the indices mark the differentiation with regards to the respective quantity. The wave equation is still relevant on its own, multiplying it with $\psi_{\alpha\beta}$ and complex conjugation leads to

$$\vec{\nabla}\left(\psi_{\alpha\beta} \vec{\nabla}\psi^*\right) - \vec{\nabla}\psi_{\alpha\beta} \vec{\nabla}\psi^* + U\psi_{\alpha\beta}\psi^* = 0. \tag{49}$$

Subtraction of the both equations and integration over the scattering area M gives again a macroscopic system quantity, which is solely determinable through changes in the scattering matrix S,

$$\vec{\nabla}\left(\psi^*\vec{\nabla}\psi_{\alpha\beta} - \psi_{\alpha\beta}\vec{\nabla}\psi^*\right) + U_\alpha\psi^*\psi_\beta + U_\beta\psi^*\psi_\alpha + U_{\alpha\beta}\psi^*\psi = 0, \tag{50}$$

$$\mathbf{c}^\dagger Q_{\alpha\beta}\mathbf{c} := -i\mathbf{c}^\dagger S^\dagger S_{\alpha\beta}\mathbf{c} = -\frac{1}{2}\int_M \left(U_\alpha\psi^*\psi_\beta + U_\beta\psi^*\psi_\alpha + U_{\alpha\beta}\psi^*\psi\right) d^3x. \tag{51}$$

Where we have assumed, that the injected field is independent of the parameters, $\mathbf{c}_\alpha = \mathbf{c}_\beta = 0$. We compare the relation above with the direct derivative of the GWS-relation,

$$\vec{\nabla}\left(\psi^*\vec{\nabla}\psi_{\alpha\beta} - \psi_{\alpha\beta}\vec{\nabla}\psi^*\right) + \vec{\nabla}\left(\psi^*_\beta\vec{\nabla}\psi_\alpha - \psi_\alpha\vec{\nabla}\psi^*_\beta\right) + \partial_\beta(U_\alpha\psi^*\psi) = 0, \tag{52}$$

and receive a second relation,

$$\vec{\nabla}\left(\psi^*_\beta\vec{\nabla}\psi_\alpha - \psi_\alpha\vec{\nabla}\psi^*_\beta\right) = U_\beta\psi^*\psi_\alpha - U_\alpha\psi^*_\beta\psi, \tag{53}$$

$$\mathbf{c}^\dagger Q_\beta Q_\alpha\mathbf{c} = \mathbf{c}^t S^\dagger_\beta S_\alpha\mathbf{c} = \frac{i}{2}\int_M (U_\beta\psi^*\psi_\alpha - U_\alpha\psi^*_\beta\psi)d^3x, \tag{54}$$

since for the unitary scattering matrix S holds

$$S^\dagger S = 1, \quad S^\dagger_\beta S = -S^\dagger S_\beta \tag{55}$$

$$S^\dagger_\beta S_\alpha = S^\dagger_\beta S S^\dagger S_\alpha = -S^\dagger S_\beta S^\dagger S_\alpha = Q_\beta Q_\alpha. \tag{56}$$

The two relations (51) and (54) include derivatives of the field ψ, which make them hard to interpret. We would expect, that such a formulation is possible for any desired number of differentiations.

We consider the case of $\alpha = \beta = t$ and get

$$\mathbf{c}^\dagger Q_t^2\mathbf{c} = \int_M U_t\Im(\psi^*_t\psi)d^3x = -\int_M U_t\Im(\psi^*\psi_t)d^3x. \tag{57}$$

Thus a questionable relation holds for input states proportional to the eigenvectors $\mathbf{c}_i = |\mathbf{c}|u_i$ of the GWS-time-operator Q_t,

$$\frac{1}{|\mathbf{c}|^2}\left[\mathbf{c}_i^\dagger Q_t\mathbf{c}_i\right]^2 = \mathbf{c}_i^\dagger Q_t^2\mathbf{c}_i, \tag{58}$$

$$\frac{1}{4|\mathbf{c}|^2}\left[\int_M U_t|\psi|^2d^3x\right]^2 = \int_M U_t\Im(\psi^*_t\psi)d^3x. \tag{59}$$

A.6 Video links

Here are the links for some videos of the simulated waveguide system. If the video files are included in a separate document, they can be opened by clicking on the respective case.

Realistic values from chapter 7:

One particle heating: The field follows the movement of the particle, the field intensity change is nearly continuous.

Two particle heating: Only at the beginning both particles get accelerated. Since the circular particle get accelerated stronger, the field focus at some point only upon the faster particle.

Ten particle cooling and Ten particle planewave: In accordance to the comparison visualised in figures 7.1 and 7.2.

Arbitrary units from chapter 4 and 6:

Ten particle cooling: In accordance to figures 6.1 and 6.2.

Ten particle randomfield: In accordance to figures 4.8 and 4.10a.

Ten particle planewave: In accordance to figures 4.9 and 4.10b.

Fourty particle cooling: Without collisions in accordance to figures 6.10 and 6.11.

Fourty particle cooling: With some collisions due to reduced input power.